Hydrological Modelling of Ethiopian Watersheds:

The Application of Hydrological Models for Flow Forecasting and Analysis of Sensitivity to Climate and Landuse Changes

Dereje Tesfahun Mengistu

Thesis for the degree of Philosophiae Doctor (PhD)
University of Bergen, Norway
2019

UNIVERSITY OF BERGEN

Hydrological Modelling of Ethiopian Watersheds:

The Application of Hydrological Models for Flow Forecasting and Analysis of Sensitivity to Climate and Landuse Changes

Dereje Tesfahun Mengistu

Thesis for the degree of Philosophiae Doctor (PhD)

at the University of Bergen

Date of defense: 15.10.2019

Year: 2019

Title: Hydrological Modelling of Ethiopian Watersheds:

Name: Dereje Tesfahun Mengistu

Print: Skipnes Kommunikasjon / University of Bergen

Preface

The Ethiopian Malaria Prediction Systems (EMaPS) project is a collaborative multi-disciplinary research project (http://emaps.uib.no) aimed at developing and validating models for predicting malaria transmission and setting up an early-warning system by combining information on climate, water, and epidemiological and entomological data. Eight PhD candidates (six Ethiopians and two Norwegians) take part in the project. I am from Ethiopia and within this project focus mainly on the hydrological significance of water availability and flow forecasting.

I would like to extend my heartfelt thanks to Professor Bernt for managing and leading the project, and for giving me the opportunity to be involved in this remarkable research, which is consequential for my future career opportunities and scientific output. I owe special and sincere thanks to my supervisor Professor Asgeir for his dedication, insightful guidance and professional expertise, which have benefitted the overall success of my education and this study. I am deeply grateful for his tireless support in the various challenges I encountered during this study. He also deserves many thanks for his genuine and endless help in completing this study. Finally, I would like to thank all employees at the University of Bergen (staff at the registration office and IT department, as well as the institute's professors), my classmate, my office mate and the PhD candidates of the EMaPS project (Ellen Viste, Torlief Lunde, Diriba Korecha, Abebe Animut and Adugna Woyessa) for their kind support in all challenges I encountered during the project.

Bergen, 2019

Dereje Tesfahun Mengistu

Abstract

Hydrological modelling studies vary depending on the purpose, data availability and number of outputs required. Quantifying the hydrological responses to various human- and climate-induced changes requires different modelling schemes than those used for simple flow estimation. Based on these fundamental principles of model use, this research examines three major model applications. In **part I** of the research, a sensitivity analysis of Soil and Water Assessment Tool (SWAT)-simulated streamflow to hypothetical and Global Climate Model (GCM)-generated climate change scenarios was conducted within Eastern Nile basins (Blue Nile, Tekeze and Baro Akobo), which contribute to about 70% of Ethiopia`s total annual surface water potential. In **part II**, the effects of climatic and/or land use changes on the hydrology of the highly forested Omo Gibe river basin in southern Ethiopia were investigated. The study area is selected because one-third of the country's power consumption is covered by this basin by means of constructed cascade hydroelectric power plants. In **part III**, simple and complex hydrological models were evaluated at a relatively smaller watershed (Gilgel Abbay) to revitalize systems-type black-box models for the purpose of flow forecasting.

In **Paper I**, the hydrological model SWAT was run with daily and monthly precipitation and temperature data for the three basins of the Eastern Nile: the Abbay (Blue Nile), Baro Akobo and Tekeze basins. The model was calibrated and validated for the daily and monthly streamflow, as presented in the research paper by Mengistu and Sorteberg (2012). Twenty hypothetical climate change scenarios (perturbed temperatures and precipitation) were used to test the sensitivity of SWAT-simulated annual streamflow. The results reveal that the annual streamflow sensitivity to changes in precipitation and temperature differed among the basins and that the dependence of the response to the strength of the changes was not linear. On average, the annual streamflow responses to a change in precipitation with no temperature change were 19%, 17% and 26% per 10% change in precipitation, while the average annual streamflow responses to a 10% change in temperature and no precipitation change were

−4.4% K−1, −6.4% K−1, and −1.3% K−1 for the Abbay, Baro Akobo and Tekeze river basins, respectively.

In addition, 47 temperature and precipitation scenarios from 19 AOGCMs participating in CMIP3 were used to understand future changes in streamflow due to climate changes (Mengistu & Sorteberg, 2012). The climate models were in disagreement regarding both the strength and direction of future precipitation changes. Thus, no clear conclusions could be made about future changes in the Eastern Nile streamflow. However, such types of assessment are important as they emphasize the need to use several ensembles of AOGCMs, as the results are strongly dependent on the choice of climate models.

In **Paper II**, the sensitivity of the Omo Gibe river basin in southern Ethiopia to both climatic and land use changes was investigated using the hydrological model SWAT. The model was calibrated and validated using observational data. Almost 60% of the average annual rainfall is lost through evaporation in the basin and the average runoff-rainfall coefficient was 0.26. Around two-thirds of the water yield was estimated to come from surface runoff, while groundwater was found to be responsible for the other third.

The sensitivity of streamflow to precipitation changes was found to be high compared to the sensitivity to land use. On average, there was a 25% change in streamflow for a 10% change in precipitation. On the other hand, the response of streamflow to changes in temperature while holding the precipitation fixed is modest. A linear regression analysis of streamflow responses to the different temperature scenarios indicates that a 1°C change in temperature produces a 1.4% change in annual streamflow.

The simulated effect of land use changes resulting from various hypothetical land use modifications was secondary to the effect of precipitation changes on the annual streamflow. However, the seasonal changes in streamflow were in some cases strongly affected by land use. For example, a deforestation scenario (entire forest-area coverage changed to bare lands) increased the January-April (dry season) streamflow by 38%. Results further indicate that the combined effects of land use and climate change may

differ from the sum of the individual land use and climate change simulations. For example, in an increased precipitation scenario, changing land use to more bare land areas would increase streamflow and water yield less than simple additions of the individual effects. This shows that according to the model, nonlinear interactions among the water-balance components may occur when simultaneous changes in land use and climate change are imposed. From these two applications, streamflow proves highly sensitive to climate change scenarios and particularly to precipitation. For a unit change in precipitation, the change in streamflow is nearly double.

Paper III evaluates the performance of different black-box rainfall-runoff models (simple single input-output models) and complex hydrological models for flow forecasting of the Gilgel Abbay catchment (upper Blue Nile river basin, Ethiopia). Seven black-box models embedded in the Galway River Flow Forecasting System **(**GFMFS) software packages, as well as HBV and SWAT models were applied.

The performance of the simple linear model (SLM) is inferior to that of all other models. However, in comparison to the complex hydrological models (SMAR, HBV and SWAT), the simple single input-output models of the artificial neural network (ANN) and the linear perturbation model (LPM) outperformed in both simulation and updated mode when evaluated based on the statistical criteria of Nash-Sutcliffe Efficiency (NSE) and R^2 at the Gilgel Abbay catchment. This indicates increasing model complexity (thereby increasing the number of tunable parameters), which does not necessarily enhance the model's performance. This is clearly reflected in HBV and SWAT, with the performances accounting 86% and 66% their variances, respectively. Therefore, insofar as flow forecasting is concerned with smaller catchments, simple models are efficient and can be used for water development planning and management, thereby avoiding the difficulty of the calibration/validation of complex hydrological models. Furthermore, these types of models can be applied in data-scarce areas within Africa, thereby avoiding multi-parameter complex hydrological models.

Acknowledgements

This work was carried out with support from the Ethiopian Malaria Prediction System (EMaPS) project, which was funded by the Norwegian Program for Development, Research and Education (NUFU) and the University of Bergen.

List of publications

Mengistu, D. T. and Sorteberg, A. (2012), Sensitivity of SWAT-Simulated Streamflow to Climatic Changes within the Eastern Nile River Basin, Hydrol. Earth Syst. Sci., 16, 391-407, doi: 10.5194/hess-16-391-2012.

Mengistu, D. T., and Sorteberg, A. (2015), Sensitivity Analysis of Omo Gibe River Basin to Climate and Land Use Changes, Southern Ethiopia.

Mengistu, D.T., and Sorteberg, A. (2016), Revisiting Systems Type Black-Box Rainfall-Runoff Models for Flow Forecasting Application.

Table of Contents

1 Intoduction

1.1 Outline

This thesis consists of three papers, preceded by an introduction and synthesis. The main purpose of the introduction and synthesis is to provide additional background information and present their mutual/combined relevance. Chapter 1 begins by introducing Ethiopia's socio-economical background, as well as its physiographical nature and different catchments and major river systems within the country and ends with the main aims of the thesis. Chapter 2 provides an overview of the three papers' main findings, while the input data used in the different studies are introduced in chapter 3. Chapter 4 explains the hydrological modelling hierarchy and the major hydrological processes calculated in the SWAT model that is used throughout the thesis. Chapter 5 presents the hydrology of Ethiopia, as well as the rainfall distribution, seasonality and regional differences among different catchment areas. Concluding remarks and future perspectives are described in chapter 6, while chapter 7 provides a list of references, after which the three scientific papers are attached.

1.2 Background

Ethiopia is located in East Africa and comprises a major portion of the Horn of Africa, covering a land mass of 1.13 million km^2. The vast majority of its landmass consists of a huge central plateau and lowland plains. The other part of the country consists of mountains with altitudes between 2,100 and 2,500 m and some peaks rising to 4,500 m, which are characterized by three climatic zones: tropical in the south and southwest, cold to temperate in the highlands and arid to semi-arid in the northeastern and southeastern lowlands (Figure 1).

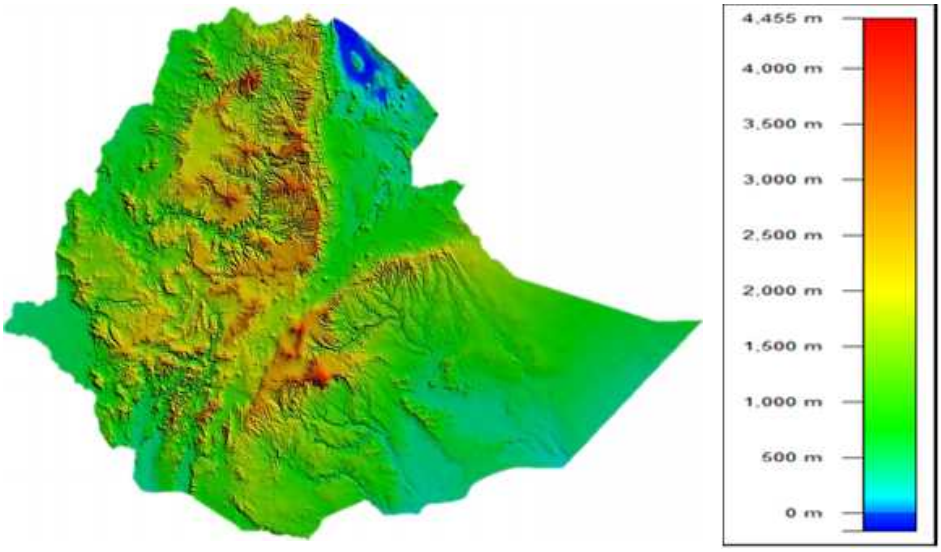

Figure 1: Digital elevation map of Ethiopia

Ethiopia is the second most populous country in Africa, with half of its population living at around 2,200 m above mean sea level (a.m.s.l), in the areas with cooler temperatures, higher rainfall and fewer cases of malaria. Another 40% lives in areas lying between 1,400 and 2,200 a.m.s.l, while the remaining population lives at heights below 1,400 a.m.s.l. Ethiopia`s population is unevenly distributed, with nearly 80% of its 83 million inhabitants living in only 37% of the total area of the country.

Ethiopia has 12 major river basins, of which eight drain about 75% of the annual runoff to neighboring countries (MOWR, 2001a) (Figure 2). The remaining basins are one lake and three dry basins, which comprise up to 7% of the country`s land mass and serve as a home for a number of pastoralists, whose livestock has no water.

The annual renewable freshwater potential is 122 billion m^3, but 3% of this amount remains within the country (MOWR, 2001a). It is estimated that 54.4 billion m^3 of surface runoff and 2.2 billion m^3 of groundwater can be developed for utilization (Birhane, 2003). Currently, less than 5% of the surface water potential has been used (MOWR, 2001a; MOWR, 2001b).

The total hydropower potential of the country is estimated at around 650 million TWH, of which about 160 million TWH is economically viable. At present, the production capacity is less than 450 MW and is expected to rise to 670 MW (McCornick P.G et al., 2003).

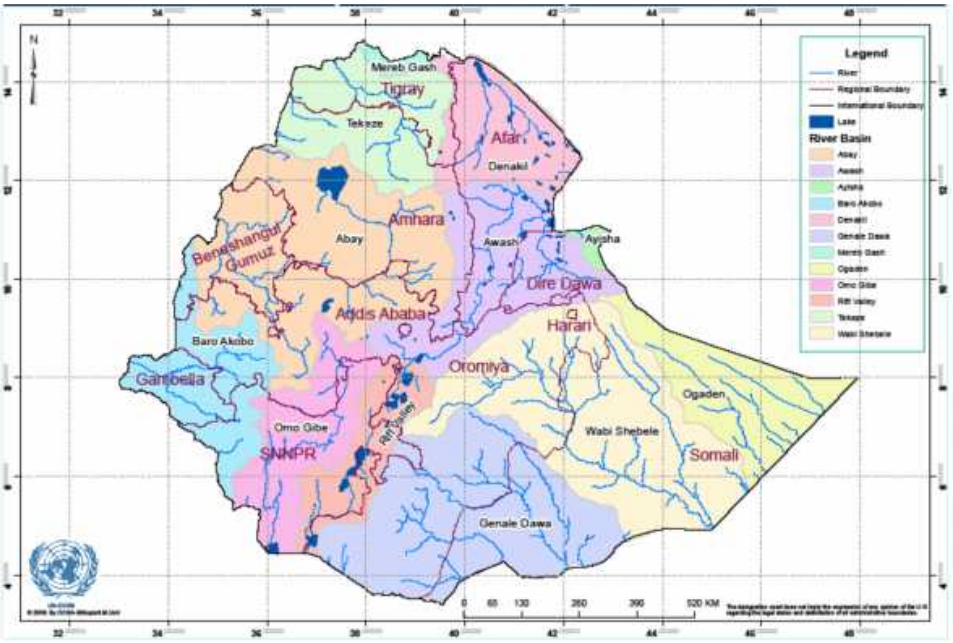

Figure 2: Major river basins of Ethiopia (MOWR, 2001a)

Ethiopia is largely dependent on the agricultural sector, which provides 86% of the country's employment and comprises 57% of its economy (McCornick P.G et al., 2003). Rainfed crop cultivation is the main activity and is practiced over an area of 27.9 million hectares (ha), which is approximately 23% of potentially arable land (World Bank, 2006).

The mean annual rainfall varies between 100 mm in the northeast arid and semi-arid climatic zone to 2,800 mm in the southwest cool and temperate zone (Lemma, 1996). Due to the uneven and irregular nature of the rainfall distribution across the country in terms of area and season, there is insufficient opportunity for the economy's sustainable growth. The production of food, fiber and other agricultural products cannot meet the

local demand. In addition, frequent drought and famine are life challenges for the country.

For Ethiopia, the economy of which is highly dependent on agriculture and population growth, it is wise to efficiently manage water resources and link them with research results. A comprehensive understanding of hydrological processes in watersheds is a prerequisite for successful watershed management and environmental restoration, which this study addresses. Due to the spatial and temporal heterogeneity of soil properties, vegetation and land use practices, hydrologic cycles become complex systems. Physically based distributed models can be applied to almost any type of hydrological problem. This dissertation attempts to investigate the extent to which the flow of the study area is influenced by climate and/or land use changes using a physically distributed model. Such models are based on understanding the physics of the hydrological processes that control catchment response and use physically based equations to describe these processes.

1.3 Aims

The overall aim of this study is to select and apply hydrological models for flow forecasting and the analysis of changes in water resources in response to climate and land use changes in Ethiopia's watersheds.

Objective 1: Test the applicability of the physically based SWAT model for the Eastern Nile and perform sensitivity studies to assess the potential impacts of climate change on water resources.

Objective 2: Quantify the impact of climate and/or land use changes on the water-balance components of the Omo Gibe river basin in Ethiopia.

Objective 3: Asses the usefulness of different rainfall-runoff models by comparing nine rainfall-runoff models with different complexities, ranging from simple to complex hydrological models.

2 Overview and Summary of Papers

The study area of this thesis includes water resources in the Eastern Nile region located in the western part of Ethiopia (consisting of three large river basins, namely Blue Nile, Tekeze and Baro Akobo), a forested large river basin in southern Ethiopia (Omo Gibe basin) and a relatively smaller catchment (Gilgel Abbay, located in the upper Blue Nile basin) (see Figure 1 in Papers I, II and III for details).

2.1 Paper I: Sensitivity of SWAT-Simulated Streamflow to Climatic Changes within the Eastern Nile River Basin

Mengistu, D. T. and Sorteberg, A. (2012), Sensitivity of SWAT-Simulated Streamflow to Climatic Changes within the Eastern Nile River Basin, Hydrol. Earth Syst. Sci., 16, 391-407, doi: 10.5194/hess-16-391-2012.

The River Nile is currently under great pressure from various competing applications, as well as social, political and legal conditions within the riparian countries (Taye et al., 2011). To understand and resolve the potential water-resource-management problems associated with water supply, power generation and agricultural practices, as well as to contribute to future water-resource planning, reservoir design and management, and protection of the natural environment, it is necessary to provide quantitative estimates of the hydrological effects of climate change.

The Eastern Nile on the Ethiopian plateau stretches between 5°N, 33°E and 15°N, 39°E, with altitudes ranging from 390 m in parts of Baro Akobo (Sobat) to over 4,500 m in the Tekeze (Atbara) river basin (MoWR, 2002). The total average annual flows are estimated to be 50, 23.6 and 8.2 billion m^3 for the Blue Nile (Abbay), Baro Akobo (Sobat) and Tekeze (Atbara) river basins, respectively (Arsano et al., 2004; MoWR, 2002). They provide 86% of the Nile's water [Blue Nile (Abbay) 59%, Baro-Akobo (Sobat) 14% and Tekeze 13% (Swain, 1997)]. Due to the high seasonal variability in rainfall on the Ethiopian plateau, the flow of the Blue Nile (Abbay) varies dramatically. The maximum runoff is recorded in August and is about 60 times greater than the minimum in the month of February (Arsano, 2005).

Climate-sensitivity scenarios were performed by perturbing the baseline simulation (the validated simulation forced with observed station data) as input. The climate perturbations are given as a percentage change in precipitation (precipitation is multiplied by a given factor). Thus, the number of wet and dry days was not perturbed; this was done only for the precipitation intensity and the temperature change in degrees Celsius (adding the prescribed change to the baseline simulation temperatures) (Varanou et al., 2002). Each scenario was then run for the same simulation period as the baseline simulation. The applied perturbations were temperature increases of 0, +2 and +4°C and precipitation changes of -20%, -10%, -5%, 0%, +5, +10% and +20%. A combination of the abovementioned temperature and precipitation perturbations served to examine the sensitivity of the SWAT streamflow to the meteorological parameters. Climatic variables such as relative humidity, wind speed, cloud cover and solar radiation were considered to be unchanged.

The CMIP3 global coupled climate models (AOGCMs) were also applied to calculate the annual mean temperature and precipitation changes from the base period 1980–2000 to the period 2080–2100 for the three subbasins. A total of 47 climate change simulations were assessed for each subbasin using three different emission scenarios (SRES A2, A1B and B1) and 19 models. Together with the aforementioned sensitivity tests and an assessment of the impact of the AOGCMs, temperature and precipitation changes were carried out on the annual flow of the various sub-basins.

The SWAT2005 adequately simulated the monthly variability in flows for the Eastern Nile basin. The total simulated monthly streamflow ranged from good ($0.65<E_{NS}<0.75$) to very good ($E_{NS}>0.75$). The average daily and monthly difference between the observed and simulated flow (PBIAS) was good (PBIAS $\leq \pm 20\%$) for the calibration period, with the exception of the Abbay subbasin where it was only satisfactory ($\pm 20\% < \text{PBIAS} \leq \pm 40\%$). In summary, the model's good performance in the validation period indicates that the fitted parameters during the calibration period listed in Table 4 of Paper I can be taken as a representative set of parameters for the Eastern Nile watershed and can be used for further simulation and evaluation of alternative scenario analysis for other periods using the SWAT model. The model simulated monthly flows better

than daily flows and is probably not adequate for studies of single severe events in small catchments.

Sixty percent of the average annual rainfall was estimated to be lost through evaporation. The simulations estimated the runoff coefficients to be 0.24, 0.30 and 0.18 for the Abbay, Baro Akobo and Tekeze subbasins, respectively. Surface runoff carried around 55% of the streamflow in the Abbay and Tekeze, while in Baro Akobo it carried about 72% of the streamflow. The remaining contribution was from groundwater.

The streamflow sensitivity to changes in precipitation and temperature differed among the basins and depended on the strength of the changes. The annual streamflow responses to a 10% change in precipitation with no temperature change were on average 19%, 17% and 26% for the Abbay, Baro Akobo and Tekeze river basin, respectively. However, the responses to a reduction and increase in precipitation were not the same. While Baro Akobo was more sensitive to a reduction in precipitation, Tekeze showed a larger sensitivity to precipitation increases.

The streamflow sensitivity to temperature was moderate. The average annual streamflow responses to a 1°C change in temperature and no precipitation change were -4.4%, -6.4% and -1.3% for the Abbay, Baro Akobo and Tekeze river basins, respectively. The very low sensitivity of the Tekeze basin indicated that flows were moisture limited for a large part of the year.

The overall assessment made by a sensitivity analysis for the 20-hypothetical climate-sensitivity scenarios revealed that the annual streamflow of the Eastern Nile was very sensitive to variations in precipitation and moderately sensitive to temperature changes. In addition, we showed that the modelled response to a combined temperature and precipitation change were very similar to simulations in which the responses from only the temperature change and only the precipitation change were added.

Applying the combined temperature-precipitation sensitivities and 47 temperature and precipitation scenarios from 19 AOGCMs participating in CMIP3, we estimated the future streamflow change to be very uncertain and strongly dependent on the choice of climate model. This is due to the disagreement between the different climate models

on both the strength and direction of future precipitation changes. Thus, based on state-of-the-art climate models, little can be said about future changes in the Eastern Nile's streamflow. However, our analysis emphasizes the need for performing ensemble runs using different climate models in this type of assessment. This uncertainty may have implications for long-term water-resource planning, estimation of future hydropower potential, reservoir design and determination of the extent to which the development of agriculture should utilize river- or groundwater-based irrigation systems.

2.2 Paper II: Sensitivity Analysis of Omo Gibe River Basin to Climate and Land Use Changes, Southern Ethiopia

Mengistu, D. T. and Sorteberg, A. (2015), Sensitivity Analysis of Omo Gibe River Basin to Climate and Land Use Changes, Southern Ethiopia.

The Omo Gibe river basin is a lifeline for hundreds of thousands of indigenous people in southwestern Ethiopia and northern Kenya, and the construction of hydroelectric power plants in the basin has been widely debated. According to a report made by Avery (2010), "Runoff patterns in the Omo River have changed in the last twenty years. Forests and vegetation have been cleared in the Omo Basin through human activity, and as a consequence, runoff has become more variable, with much more rapid response to rainfall. Without effective catchment management, the overall runoff volume can be expected to increase with catchment land use change." In addition, the key issue reported by international media is the "elimination of the riverine forest and woodland, due to the construction of hydroelectric power plant in the basin lead to at least a 50% to 60% reduction of river flow volume" (BBC, 2009; Avery, 2010).

Based on the controversy around the management of the basin, this paper focuses on four basic research questions that may be useful for basin-integrated management practices. 1) Does changing land use due to deforestation affect the streamflow volume in the amount specified in the abovementioned report (BBC, 2009; Avery, 2010)? 2) How sensitive is the annual streamflow to land use change compared to climate change? 3) How will the emerging hydropower development be affected by individual and combined changes of land use and/or climate change? 4) Are the combined effects

of land use and climate change on the streamflow-generation process the sum of the individual effects or are there nonlinearities in the system? Moreover, the paper is further aimed at quantifying the effect of climate and land use changes on the water-balance components of the Omo Gibe river basin.

Understanding the Omo Gibe river basin's sensitivity to climate and land use changes has become crucial for ongoing cascaded large-scale hydropower development and overall river basin management. This study attempts to understand the likely impact of climate and land use change using the SWAT simulation model, which was calibrated and validated using daily-discharge data series.

The results show that the sensitivity of streamflow to precipitation changes was high. A 10% change in the precipitation generally changes the annual or wet season streamflow more than twofold (22–23%). On the other hand, the response of streamflow to changes in local temperature between 2°C and 4°C is insignificant. In terms of land use change, the results of various hypothetical land use modifications indicate that a 10% change in the land use system affects the annual or wet season flow by less than 7% in both directions (either deforestation or afforestation). For example, keeping the precipitation unchanged while changing 10% of the forest land use to bare land would increase the annual water yield by 4.1% and during the wet season by 5.1%. This would not, however, offset the impact reduction resulting from a drier precipitation scenario. A possible nonlinear interaction among the water balance components or feedbacks may occur when simultaneous changes in land use and climate change occur. However, given the slow nature of land use change, a change in precipitation is more sensitive and impactful for water developments than a change in land use. Given Ethiopia's history of high precipitation variability, a fluctuation of 10% or more in precipitation is possible. Therefore, managing the emerging cascaded hydropower development requires careful consideration of implementing seasonal flow-forecasting models and reservoir-operation management for sustainable upstream-downstream interaction.

2.3 Paper III: Revisting Systems Type Black-Box Rainfall-Runoff Model for Flow Forecasting Application

Mengistu, D. T. and Sorteberg, A. (2015), Revisiting Systems Type Black-Box Rainfall-Runoff Model for Flow Forecasting Application.

We tend to spend huge amounts of time and resources to setup and use complex hydrological models for the simple goal of flow estimation. Running complex models becomes even more difficult when the amount of available data is scarce, which is a common problem in many parts of Africa. The aim of this paper is to evaluate and revitalize the systems type black-box model against complex hydrological models for easy flow estimation application. Six systems type black-box models, namely the simple linear model (SLM), the non-parametric simple linear model (NP-SLM), the linear perturbation model (LPM), the non-parametric linear perturbation model (NP-LPM), the linearly varying gain factor model (LVGFM) and the nonlinear black-box type artificial neural network model (ANN) are compared with the three complex hydrological models SMAR, HBV and SWAT. The models are compared based on daily rainfall and stream-flow data (1980–2000) on the Gilgel Abbay watershed. The Gilgel Abbay catchment (4,051km^2) is the largest among the four main sub-catchments in the Lake Tana basin in northern Ethiopia (Fig.1 in Paper III) and provides about 60% of the lake inflow.

A comparison of the systems type black-box and complex hydrological models in the study area indicates that the LPM and ANN models perform better than complex hydrological models such as SMARG, HBV and SWAT in terms of R^2 and the NSE criteria. This confirms that simpler models (which take only rainfall as input) can surpass their complex counterparts in performance regarding continuous simulation and the reproduction of hydrographs or flow estimations. There is a strong justification, therefore, for the claim that increasing a model's complexity and thereby the number of parameters does not necessarily enhance its performance. It is suggested that the simpler models may still play a significant role in practical hydrology as effective simulation tools and that countries with scarce hydrological data should revitalize the

application of systems type black-box modelling schemes that depend only on rainfall and runoff data sets, which could be readily available.

3 Data

This section attempts to describe the number and types of datasets used for the study basin. A range of spatially distributed data, for instance on topographic features, soil types, land use and stream networks (optional) are required for the model. Hydrometeorological data are also used as input for the model.

3.1 Precipitation and Temperature Observations

Table 1 summarizes precipitation and temperature observation data used in the study. The data source is obtained from National Meteorological Agency of Ethiopia (NMA). A total of 114 precipitation and 72 temperature gauged stations data were collected and carefully analyzed for the application of the model. The locations and distributions of these stations are shown in the Figure 5 in Paper I, and Figure 1 in Papers II and III.

Table 1: Precipitation and temperature observation data summary used in the study

Basin	Parameter	Number of stations	Temporal resolution	Period	Reference	Paper(s) where data is used
Eastern Nile	Precipitation	97	Daily	1987-2006	NMSA	Paper I
	Temperature	60				
Omo Gibe	Precipitation	17		1987-2007		Paper II
	Temperature	12				
Gilgel Abbay	Precipitation	7		1980-2000		Paper III
	Temperature	4				

3.2 Hydrological data

Hydrological discharge data were collected from the Ministry of Water Resources of Ethiopia for the purpose of calibrating and validating the model simulation. As shown in Table 3, six and two stations were selected for the calibration and validation of the Eastern Nile and Omo Gibe river basins, respectively.

Table 2: Number of stream gauges used to calibrate and validate the model simulation of the study basin

Basin	Parameter	Number of stations	Temporal resolution	Period	Reference	Paper(s) where data is used
Eastern Nile basin • Abbay • Baro • Tekeze	Stream flow	3 2 1	Daily	1991-2000 1990-2004 1994-2003	MOWR	Paper I
Omo Gibe basin		2		1987-2007		Paper II
Gilgel Abbay		1		1980-2000		Paper III

3.3 DEM

Digital elevation models (DEMs) were created using a topographic database of 1km^2 and 90 m^2 resolution for the Eastern Nile, the Omo Gibe and the Gilgel Abbay basins (Papers I, II and III, respectively). These data were sourced from the Ministry of Water Resources, Ethiopia. The DEMs (see Figure 2 in Paper I) were used to delineate the watershed and the drainage patterns of the surface analysis. Subbasin parameters such

as slope gradient and slope length of the terrain, and stream network characteristics such as channel slope, length and width were derived from the DEMs.

3.4 Land Use and Soil Data

Land use is one of the main factors affecting surface erosion and evapotranspiration in a watershed. The source of the land use map in this study is the Ministry of Water Resources, Ethiopia and the land use/land cover map is sourced from the global Hydro1K dataset (Hansen, 1998) and adapted to correspond with the SWAT-predefined land use classification (see Figure 3 in Paper I, Figure 2 in Paper II and Figure 1 for Gilgel Abbay in paper III). About 50% of the Eastern Nile (Paper I) and 69% of the Gilgel Abbay basins (Paper II) are used for agricultural purposes, while the Omo Gibe basin is covered with mixed forest, which comprises over 40% of its total catchment area (Table 3).

Table 3: Summary of the most dominant land uses for the three study areas

Basin	Dominant land use		Second most dominant land use		Reference	Spatial resolution
	Name	%	Name	%		
Eastern Nile	Agriculture	50	Pastoral	28.8	MOWR and global Hydro 1k dataset (Hansen,1998)	1km*1km
Omo Gibe	Mixed forest	48.1	agriculture	36.6		
Gilgel Abbay	Agriculture	65	Agro-pastoral	33		

Different types of soil texture and physical-chemical properties are required for the SWAT model. These data were obtained from various sources. The soil map was obtained from the Water Resources Information and Metadata Base Centre Department at the Ministry of Water Resources, Ethiopia. However, several properties such as

moisture-bulk density and saturated hydraulic conductivity, as well as percentages of clay content, silt content and sand content in the soil, which are required by SWAT model, were not incorporated. These additional data were extracted from Wambeke (2003), USDA (1999) and FAO (1995). Table 4 shows the most dominat soil-type percentage cover and resoultion of the map (Figure 4 in Paper I, Figure 2 in Paper II and Figure 1 in Paper III).

Table 4: Dominant soil types of the three study basins

Basin	Dominant soil type		Second most dominant soil type		Reference	Spatial resolution
	Name	%	Name	%		
Eastern Nile	Chrome Luvisols	21	EutricVertisol	17.3	MOWR and modified using FAO	10*10km
Omo Gibe	Dystric Cambisols	32.6	Orthic Acrisols	17.6		
GIlgel Abbay	Haplic Luvisols	69.7	Chromic Luvisols	15.4		

4 Models

4.1 General

Hydrological models can be a tool for better understanding changes in climate and land use that affect components of the hydrological cycle, as well as evapotranspiration, stream flow, recharge to sub-surface storage, and so forth.

For the proper management and integration of issues around water resources in the management plans of irrigation, hydropower, health and other sectors, attaining a better understanding of the hydrologic processes in a watershed is beneficial. As many of the basins only have a few observational points regarding a few parameters, these hydrologic processes need to be modeled with appropriate hydrological models.

The two classical types of hydrological models are the deterministic and stochastic models.

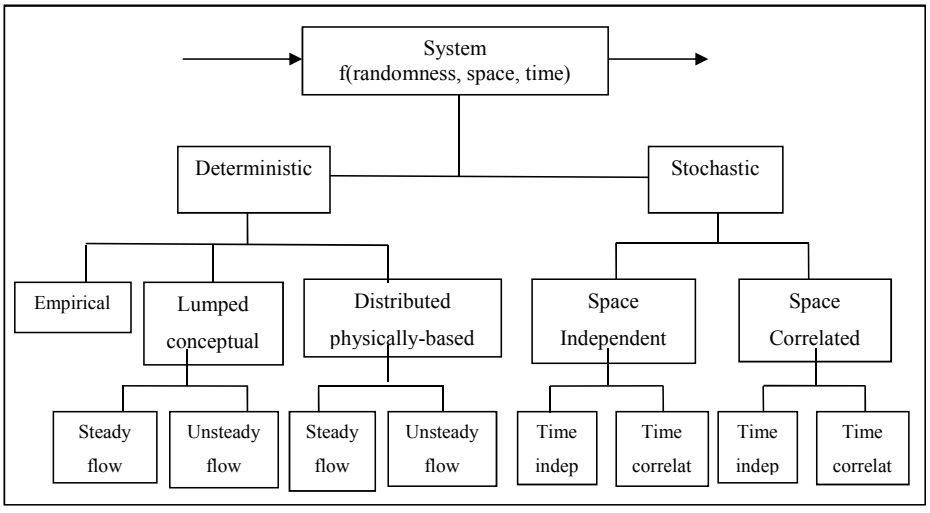

Figure 3: Classification of hydrological models according to process description (Chow et al., 1988).

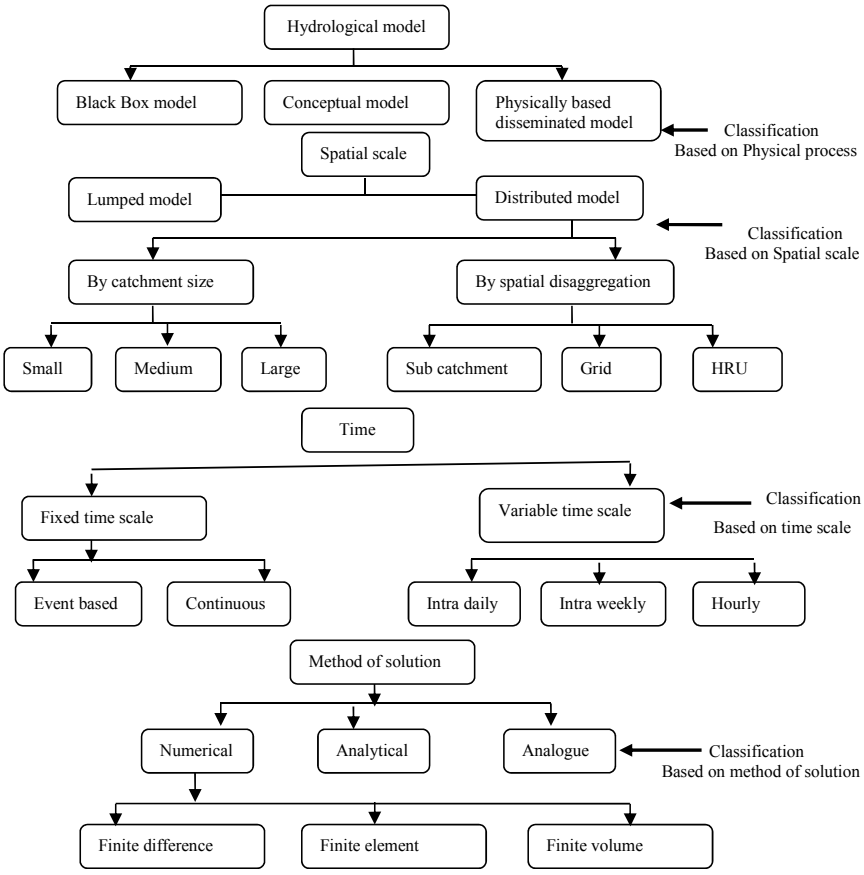

Figure 4: Classification of hydrological models according to process description, spatial scale, time scale and method of solution (Chow et al., 1988).

Deterministic Hydrological Models

Deterministic models permit only one outcome from a simulation with one set of inputs and parameter values. Deterministic models can be classified depending on whether the model offers a lumped or distributed description of the considered area and whether the description of the hydrological processes is empirical, conceptual or physically

based (Figures 3 and 4). Most conceptual models are lumped and most physically based models are distributed. The three main groups of deterministic models are as follows:

• Empirical models (black box)
• Lumped conceptual models (grey box)
• Distributed process (physical) description-based models (white box)

Empirical (Black-Box) Models

Black-box models are empirical, involving mathematical equations that have been assessed not from the physical processes in the catchment but from analyses of concurrent input and output time series.

The first of this type of model is the ***rational method*** published by the Irish engineer Thomas James Mulvaney (1822–1892) in 1851. The model was a single simple equation often used for drainage design in small suburban and urban watersheds. The equation assumes the proportionality between peak discharge, *qpk,* and the maximum average rainfall intensity, *ieff:*

$$qpk = CR \times ieff \times AD$$

Where *AD* is the drainage area and *CR* is the runoff coefficient, which depends on watershed land use.

The equation was derived from a simplified conceptual model of travel times on basins with negligible surface storage. The model reflects how discharges are expected to increase with area, land use and rainfall intensity in a rational way, hence its name: the rational method.

The scaling parameter C reflects the fact that not all rainfall becomes discharge. The method does not attempt to separate the different effects of runoff production and runoff routing that control the relationship between the volume of rainfall falling on the catchment in a storm and the discharge at the hydrograph peak. In addition, the constant C is required to take account of the nonlinear relationship between antecedent conditions and the profile of storm rainfall, and the resulting runoff production. Thus,

C is not a constant parameter, but varies from storm to storm on the same catchment and from catchment to catchment for similar storms.

The other well-known model among the black-box models is the unit hydrograph model published by Sherman (1932), who used the idea that the various time delays for runoff produced on the catchment to reach the outlet could be represented as a time distribution without any direct link to the areas involved.

Because the routing procedure was linear, this distribution could be normalized to represent the response to a unit of runoff production or the effective rainfall generated over the catchment in a one-time step (Figure 4). The method is one of the most commonly used hydrograph modeling techniques in hydrology and is simple to understand and easy to apply. The unit hydrograph represents a discrete transfer function for effective rainfall to reach the basin outlet, lumped to the scale of the catchment.

Other empirical models were developed using linear regression and correlation methods used to determine functional relationships between different data sets. The relationships are characterized by correlation coefficients and standard deviation, and the parameter estimation is carried out using rigorous statistical methods involving tests for the significance and validity of the chosen model.

Lumped Conceptual Models

Lumped models treat the catchment as a single unit, with state variables that represent average values over the catchment area, such as storage in the saturated zone. Due to the lumped description, the description of the hydrological processes cannot be based directly on the equations intended to be valid for the individual soil columns. Hence, the equations are semi-empirical, but still have a physical basis. Therefore, the model parameters usually cannot be assessed from field data alone but have to be obtained with the help of calibration.

One of the first and most successful lumped digital computer models was the Stanford watershed model developed by Linsley et al. in 1960 at Stanford University. The Stanford model has up to 35 parameters, although it was suggested that many of them

could be fixed on the basis of the catchment's physical characteristics and only a far smaller number needed to be calibrated.

Distributed Process Description-Based Models

Another approach to hydrological process modeling is the attempt to produce models based on the governing equations describing all the surface and subsurface flow processes in a catchment. Freeze and Harlan (1969) made a first attempt to outline the potentials and some of the elements in a distributed process description-based model on the scale of a catchment. The calculations require large computers to solve the flow domain and the points at the elements of the catchment.

Distributed models of this type have the possibility of defining parameter values for every element in the solution mesh. They provide a detailed and potentially more correct description of the hydrological processes in a catchment than the other model types. The process equations require that many different parameters are specified for each element and make the calibration difficult in comparison with the observed responses of a catchment.

In principle, parameter adjustment for this type of model is not necessary if the process equations are valid and the parameters are strongly related to the physical characteristics of the surface, soil and rock. In practice, the model requires effective values at the scale of the elements. Because of the heterogeneity of the soil and surface vegetation, establishing a link between measurements and element values is difficult.

Distributed process description-based models can in principle be applied to almost any kind of hydrological problem. Their development increased in recent years due to the increase in computer power, programming tools and digital databases, and the need to handle processes and predictions of runoff, sediment transport and/or contaminants.

Another reason for this increase in interest is that the models are needed for impact assessment. Changes in land use such as deforestation and urbanization often affect only part of a catchment area. With a distributed model, it is possible to examine the effects of such land use changes in their correct spatial context by understanding the physical meaning between the parameter values and the land use changes.

Recent examples of distributed process-based models include SHE (Abbott et al., 1986), MIKE SHE (Refsgaard & Storm, 1995), IHDM (Institute of Hydrology Distributed Model; Calver & Wood 1995), THALES (Grayson et al.1992) and SWAT (Arnold and Allen, 1996).

Stochastic Time-Series Model

Stochastic models allow for some randomness or uncertainty in the possible outcomes resulting from uncertainty in the input variables, boundary conditions or model parameters. Traditionally, a stochastic model is derived from a time-series analysis of a historical record. The stochastic model can then be used for the generation of long hypothetical sequences of events with the same statistical properties as the historical record. In this technique, several synthetic series with identical statistical properties are generated. These generated sequences of data can then be used in the analysis of design variables and their uncertainties, for example in estimating reservoir storage requirements.

With regard to process description, the classical stochastic simulation models are comparable to the empirical, black-box models. Hence, stochastic time-series models are composed of a simple deterministic core (the black-box model), which is contained within a comprehensive stochastic methodology. Hence, these form the broad generic classes of rainfall-runoff models, be they lumped or distributed, i.e., deterministic or stochastic. The vast majority of models used in rainfall-runoff modeling are deterministic, though simpler models still offer wide applicability and flexibility. If the interest lies in simulating and predicting a one-time series, for instance run-off prediction, simple lumped-parameter models can provide just as good a simulation as complex process description-based models.

4.2 Use of SWAT and its Comparison with other Models

Borah and Bera (2003, 2004) compared SWAT with several other watershed scale models. In their 2003 study, they report that the dynamic watershed simulation model

(DWSM) (Borah et al., 2004), the Hydrologic Simulation Program - Fortran (HSPF) model (Bicknell et al., 1997), SWAT and other models have hydrology, sediment, and chemical routines that are applicable to watershed-scale catchments. They conclude that SWAT is a promising model for continuous simulations in predominantly agricultural watersheds. In their 2004 study, they found that SWAT and HSPF could predict yearly flow volumes and pollutant losses, were adequate for monthly predictions, with the exception of months with extreme storm events and hydrologic conditions, and were poor in simulating daily extreme flow events. Gosain et al. (2005) used SWAT to estimate the return flows on account of introducing an irrigation project in a subbasin of the Krishna River in southern India. The assessment of return flow is a very challenging task and very often the used estimates are erroneous. Gosain et al. (2006) also used SWAT to evaluate the climate change impact on 12 Indian river systems using data from the HadRM2 regional climate model.

Van Liew et al. (2003a) compared the streamflow predictions of SWAT and HSPF in eight nested agricultural watersheds within the Little Washita river basin in southwestern Oklahoma. They conclude that SWAT is more consistent than HSPF in estimating streamflow for different climatic conditions and may thus be better suited for investigating the long-term impacts of climate variability on surface water resources. Saleh and Du (2004) found that the average daily flow, sediment loads and nutrient loads simulated by SWAT came closer than HSPF to the measured values that were collected at five sites during both the calibration and verification periods for the upper North Bosque River watershed in Texas. Singh et al. (2005) found that SWAT flow predictions were slightly better than the corresponding HSPF estimates for the 5,568 km^2 Iroquois River watershed in eastern Illinois and western Indiana, primarily due to SWAT's superior simulation of low flows. Nasr et al. (2007) found that both SWAT and the MIKESHE model (Refsgaard & Storm, 1995) simulated the hydrology of Belgium's Jeker River basin in an acceptable way. However, MIKESHE predicted the overall variation of river flow slightly better.

Srinivasan et al. (2005) found that SWAT estimated flow more accurately than the soil moisture distribution and routing (SMDR) model (for the 39.5 ha FD36 experimental

watershed in east central Pennsylvania) and that SWAT was also more accurate on a seasonal basis.

Recently, climate change impact assessment has become a very pertinent concern for the water and agriculture sectors. The Soil and Water Assessment Tool has been modified in response to a widely acknowledged need for tools and information that can help water and land managers assess and manage the impacts of climate variability and change. The users can conduct watershed-based studies of the potential implications of climate variability and changes in water and land resources. Specifically, SWAT provides flexible capabilities for creating climate change scenarios, allowing users to quickly assess a wide range of "what if" questions about how weather and climate could affect their systems. The existing capabilities of SWAT for assessing the effects of land use change and management practices have been enhanced to assess the coupled effects of climate and land use change.

In summary, the wide range of SWAT applications described above underscores that the model is a very flexible and robust tool that can be used to simulate a variety of watershed problems.

4.3 Major Hydrological Processes Calculated in SWAT

This section is adopted directly from SWAT theoretical document which is available at http://www.scribd.com/doc/48374721/swat2000.

4.3.1 Surface Runoff

The two methods used in SWAT for estimating surface runoff are the SCS (soil conservation service) curve number procedure and the Green & Ampt infiltration method.

In this study, the SCS curve number method was used to estimate surface runoff volumes due to the unavailability of sub daily rainfall data needed for the Green & Ampt method. The SCS runoff equation is given by: -

$$Q_{surf} = \frac{(R_{day} - I_a)^2}{(R_{day} - I_a + S)} \qquad (4.1)$$

where Q_{surf} is depth of direct runoff, mm R_{day} depth of 24-hour precipitation, mm, I_a is the initial abstraction which includes surface storage, interception and infiltration prior to runoff (mm), and S is retention, mm. Empirical studies found that S is related to soil type, land use, and the antecedent moisture condition of the basin. These are represented by the runoff curve number, CN, which is used to estimate S with the following equation:

$$S = 25.4\left(\frac{1000}{CN} - 10\right) \qquad (4.2)$$

Where CN is the curve number for the day. The Curve Numbers are assigned based on soil type (hydrologic soil group) and land use, and are modified depending on soil moisture content at the time of rainfall (Ponce and Hawkins, 1996). CN_1, CN2 and CN_3 represent the three types of soil moisture conditions I, II and III for the day of the given study area.

By analyzing rainfall and runoff data for many small watersheds, the following empirical relation between I_a and S was developed: $I_a = 0.2S$ and substituting it in equation 4.1 becomes

$$Q_{surf} = \frac{(R_{day} - 0.2S)^2}{(R_{day} + 0.8S)} \qquad (4.3)$$

NB! Surface runoff (Q_{surf}) will only occur during $R_{day} > I_a$ *(=0.2S)*. S (The retention parameter) is a function of soil water content and calculated as:

$$S = S_{\max} \cdot \left(1 - \frac{SW}{[SW + \exp(w_1 - w_2 . SW)]}\right) \qquad (4.4)$$

where, S_{max} is the maximum value the retention parameter, mm, SW is the soil water content, mm, and w_1 and w_2 are shape coefficients. The maximum retention parameter value, S_{max}, is calculated by solving equation 4.2 using CN_1.

$$S_{\max} = 25.4\left(\frac{1000}{CN_1} - 10\right) \qquad (4.5)$$

Where CN_1 is moisture condition *I* at wilting point.

The shape coefficients (w1 and w2) are calculated in SWAT as:

$$w_1 = \ln\left[\frac{FC}{1 - S_3 \cdot S_{\max}^{-1}} - Fc\right] + w_2 \cdot FC \qquad (4.6)$$

$$w_2 = \frac{\left(\ln\left[\frac{FC}{1 - S_3 \cdot S_{\max}^{-1}} - Fc\right] - \ln\left[\frac{SAT}{1 - 2.54 \cdot S_{\max}^{-1}} - SAT\right]\right)}{(SAT - FC)} \qquad (4.7)$$

where w_1, w_2 and w_2 are the first and second shape coefficients, respectively, FC is the amount of water in the soil profile at field capacity (mm of water), S_3 is the retention parameter at, S_{max} is the retention parameter at CN_1, SAT is the amount of water in the soil profile when completely saturated (mm of water), and 2.54 is the value of the retention parameter value at CN=99 where the number refers saturation condition.

By rearranging equation 4.2, it is possible to calculate the daily curve number as:

$$CN = \frac{25400}{(S + 254)} \qquad (4.8)$$

The moisture condition II and III curve numbers are calculated from equation 4.9 and 4.10.

$$CN_1 = CN_2 - \frac{20.(100 - CN_2)}{(100 - CN_2 + \exp[2.533 - 0.0636.(100 - CN_2)])} \qquad (4.9)$$

$$CN_3 = CN_2.\exp[0.00673(100 - CN_2)] \qquad (4.10)$$

Where CN_2 is moisture condition *II* which is the average value that the daily curve number can assume in average moisture condition and CN_3 is moisture condition *III* that the daily curve number can assume in wet moisture (field capacity) condition.

The moisture condition II curve number provided in the tables of SWAT manual are assumed to be appropriate for 5% slopes. Equation 4.11 is developed by Williams, (1995) to calculate the curve number which is adjusted for various slopes and given by.

$$CN_{2s} = \frac{(CN_3 - CN_2)}{3} \cdot [1 - 2 \cdot \exp(-13.86 \cdot slp)] + CN_2 \qquad (4.11)$$

Where CN_{2s} is adjusted curve number for the moisture condition II, CN_3 and CN2 are the moisture condition III and II curve numbers for the default 5% slope, respectively, and *slp* is the average percent slope of the sub basin.

4.3.2 Evapotranspiration

Evapotranspiration is the process by which water from land, plant and water surface on the earth is converted to water vapor and transferred into the atmosphere. The combined loss of water from the land to the atmosphere is usually called the loss. It is generally quite a large fraction of total precipitation over a long period of time. Among the three methods; the Penman-Monteith method, the Priestley-Taylor method and the Hargreaves method incorporated in SWAT, we use the Hargreaves method to estimate potential evapotranspiration (PET). The method was selected due to the fact that it requires only air temperature. The form used in SWAT was published is (Hargreaves et al.., 1985);

$$\lambda E_0 = 0.0023 H_0 (T_{mx} - T_{mn})^{0.5} \cdot (\overline{T}_{av} + 17.8) \qquad (4.12)$$

After SWAT computed the PET, then actual evapotranspiration is calculated from canopy interception, transpiration from plants and evaporation from soil and/or sublimation. The following section is discussing about how SWAT treats all these possible losses.

i) Evaporation of intercepted Rainfall

Interception storage is that portion of the rainfall that is intercepted by trees, plants, obstacles, and vegetation before it can reach the ground. Interception occurs in the initial part of the storm and eventually the intercepting surfaces become wet (maximum holding capacity). Empirical relationships are developed and depend on Density, Vegetation type and given by:

$$E_a = E_{can} = E_0 \qquad (4.13)$$

$$R_{INT(f)} = R_{INT(i)} - E_{can} \qquad (4.14)$$

Where E_a is the actual evapotranspiration(AET),mm, E_{can} is the volume of water stored in the canopy, mm, E_0 is the potential evapotranspiration, mm, $R_{INT(i)}$ is the initial volume water held in the canopy, mm, and $R_{INT(f)}$ is the final volume of water held in the canopy, mm. If the potential evapotranspiration, E_0 is greater than the amount of free water held in the canopy, RINT, then

$$E_{can} = R_{INT(i)} \qquad (4.15)$$

$$R_{INT(f)} = 0 \qquad (4.16)$$

Once any free water in the canopy has been evaporated, the remaining evaporative water demand ($E'_0 = E_0 - E_{can}$) is portioned between the vegetation.

ii) Transpiration

Transpiration is loss of water through small openings (stomata) of the leaves and calculated for the methods of Hargreaves and Priestley Talyor methods of estimating potential evapotranspiration as:

$$E_t = \frac{E'_0 . LAI}{3.0} \qquad (4.17)$$

$$E_t = E'_0 \qquad (4.18)$$

iii) Sublimation and Evaporation from the soil

Water lost from soil to atmosphere controlled by surface wetness and replenishment of wetness. The maximum amount of sublimation/evaporation on a given day is calculated as:

$$E_s = E'_0 . \mathrm{cov}_{sol} \qquad (4.19)$$

Where E_s is the maximum sublimation/evaporation on a given day, mm, E'_0 is the PET adjusted for evaporation of free water in the canopy, mm, and cov_{sol} is the soil cover index and calculated as:

$$Cov_{sol} = \exp\left(-5.0\times10^{-5}.CV\right) \qquad (4.20)$$

Where CV is the above ground biomass and residue (kg ha^{-1}). If the snow water content is greater than 0.5mm H_2O, the soil cover index is set to 0.5.

As soil/sublimation is related with the efficiency of water use of plants, the computation of evaporation is adjusted as:

$$E'_s = \min\left[E_s, \frac{E_s.E'_0}{E_s + E_t}\right] \qquad (4.21)$$

Where E'_s is the maximum evaporation adjusted for plant water use, E_s is the maximum sublimation/soil evaporation, E'_0 is the PET for evaporation of free water in the canopy, and E_t is the transpiration. When E_t is low $E'_s \rightarrow E_s$ However, as E_t approach E'_o,

$$E'_s \rightarrow \frac{E_s}{1+\mathrm{cov}_{sol}} \qquad (4.22)$$

Once the maximum amount of sublimation/soil evaporation for the day is calculated, SWAT will first remove water from the snow pack to meet the evaporative demand. If the water content of the snowpack is greater than the maximum sublimation/soil evaporation demand, then

$$E_{sub} = E'_s \qquad (4.23)$$

$$SNO_{(f)} = SNO_{(i)} - E'_s \qquad (4.24)$$

$$E''_s = 0 \qquad (4.25)$$

Where E_{sub} is the amount of sublimation, E'_s is the maximum sublimation/soil evaporation adjusted for plant water use on a given day prior to accounting for

sublimation (mm H_2O), $SNO_{(i)}$ and $SNO_{(f)}$ are the amount of water in the snow pack on a given day prior to and after accounting for sublimation, mm ,respectively., and E''_s is the maximum soil water evaporation.

If the water content of the snowpack (*SNO*) is less than the maximum sublimation/soil evaporation demand (E`s), then

$$E_{sub} = SNO_{(i)} \qquad (4.26)$$

$$SNO_{(f)} = 0, \qquad (4.27)$$

$$E''_s = E'_s - E_{sub} \qquad (4.28)$$

Regarding to soil water evaporation, SWAT used to initially portion the evaporation demand for each layer according to the following equation:

$$E_{soil,Z} = E''_s \cdot \frac{Z}{Z + \exp(2.374 - 0.00713z)} \qquad (4.29)$$

Where $E_{soil,Z}$ is the evaporative demand at depth z (mm H_2O), E''_s is the maximum soil water evaporative on a given day (mm H_2O), and z is the depth below the surface.

4.3.3 Percolation

Percolation is the downward movement of water through the soil. In SWAT, percolation is calculated for each soil layer in the profile. Upward flow may occur when a lower layer exceeds field capacity. If the water content exceeds the field capacity water content, then the available water is allowed to percolate for that layer. The soil water to field capacity ratios of the two layers regulates movement from a lower layer to an adjoining upper layer. Percolation is also affected by soil temperature. Percolation will not allow in the soil at a particular layer, if the temperature in the layer is 0°C or below.

Equation 4:30 and 4:31 are used to calculate the amount of water available for percolation in the soil layer:

$$\mathrm{SW}_{\mathrm{ly.excess}} = \mathrm{SW}_{\mathrm{ly}} - \mathrm{FC}_{\mathrm{ly}} \quad if \quad SW_{ly} > FC_{ly} \qquad (4.30)$$

$$SW_{ly,excess} = 0 \quad if \quad SW_{ly} \leq FC_{ly} \qquad (4.31)$$

where $SW_{ly,\ excess}$ is the drainable volume of water in the soil layer on a given day (mm of water), SW_{ly} is the water content of the soil layer on a given day (mm of water) and FC_{ly} is the water content of the soil layer at field capacity (mm of water).

Once the volume of drainable water ($\mathrm{SW}_{\mathrm{ly,\ excess}}$) is estimated, the percolating water amount ($\mathrm{W}_{\mathrm{perc,\ ly}}$) is calculated as:

$$w_{perc,ly} = SW_{ly,excess} \cdot \left(1 - \exp\left[\frac{-\Delta t}{TT_{perc}}\right]\right) \qquad (4.32)$$

where Δt is the length of the time step (hrs), and TT_{perc} is the travel time for percolation (hrs).

The total volume of water ($\mathrm{W}_{\mathrm{seep}}$) leaving from the bottom of the soil profile on day i is calculated:

$$w_{seep} = w_{perc,ly=n} + w_{crk,btm} \qquad (4.33)$$

Where $\mathrm{wperc}_{,\ ly=n}$ is the volume of water percolating out of the lowest layer, n, in the soil profile on day i (mm), and $w_{crk,\ btm}$ is the volume of water flow past the lower boundary of the soil profile due to bypass flow on day i (mm).

4.3.4 Groundwater flow

Groundwater balance in SWAT model is calculated by assuming two layers of aquifers. SWAT partitions groundwater into a shallow, unconfined aquifer and a deep-confined aquifer. Groundwater flow contribution to total stream flow is simulated by creating shallow aquifer storage (Arnold et al., 1993). Percolate from the bottom of the root

zone is recharge to the shallow aquifer. A recession constant, derived from daily stream flow records, is used to lag flow from the aquifer to the stream.

The summary of different formulae used in SWAT for computing shallow and deep aquifers is summarized in the following table 5:

Table 5: Summary of ground water computation adopted from SWAT theoretical document which is available at http://www.scribd.com/doc/48374721/swat2000.

No	Formulae used for ground water computation in SWAT	Remark
1	$aq_{sh,i} = aq_{sh,i-1} + w_{rchrg} - Q_{gw} - w_{revap} - w_{deep} - w_{pump,sh}$	Shallow aquifer water balance
2	$aq_{dp,i} = aq_{dp,i-1} + w_{deep} - w_{pump,dp}$	Deep aquifer water balance equ
3	$Q_{gw} = \frac{800 \cdot K_{sat}}{L_{gw}^2} \cdot h_{wtbl}$	The volume of ground water ur steady state condition
4	$\frac{dh_{wtbl}}{dt} = \frac{w_{rchrg} - Q_{gw}}{800 \cdot \mu}$	The volume of ground water u steady condition due to water t fluctuation
5	$\frac{dQ_{gw}}{dt} = 10 \cdot \frac{K_{sat}}{\mu \cdot L_{gw}^2} \cdot \left(w_{rchrg} - Q_{gw}\right) = \alpha_{gw} \cdot \left(w_{rchrg} - Q_{gw}\right)$	General equation for groundwa volume calculation under stead non-steady state condition
6	$Q_{gw,i} = Q_{gw,i-1} \cdot \exp\left[-\alpha_{gw} \cdot \Delta t\right] + w_{rchrg} \cdot \left(1 - \exp\left[-\alpha_{gw} \cdot \Delta t\right]\right)$ $Q_{gw} = Q_{gw,0} \cdot \exp\left[-\alpha_{gw} \cdot t\right]$ $\alpha_{gw} = \frac{1}{N} \cdot \ln\left[\frac{Q_{gw,N}}{Q_{gw,o}}\right]$	Integrating the above general e Shallow aquifer with no recha The base flow recession consta
7	$\alpha_{gw} = \frac{1}{N} \cdot \ln\left[\frac{Q_{gw,N}}{Q_{gw,o}}\right] = \frac{1}{BFD} \cdot \ln[10] = \frac{2.3}{BFD}$	Base flow days computation
8	$w_{deep,mx} = \beta_{deep} \cdot w_{rchrg}$ $w_{deep} = 0$ $w_{deep} = w_{deep,mx} - aq_{shthr,rvp}$ $w_{deep} = w_{deep,mx}$	The volume of water percolate deep aquifer if $aq_{sh} \le aq_{shthr,rvp}$ if $aq_{shthr,rvp} < aq_{sh} < \left(aq_{shthr,rvp} +$ if $aq_{sh} \ge \left(aq_{shthr,rvp} + w_{revap,mx}$

Note:

$aq_{sh,\ i}$: the volume of water stored in shallow aquifer at time step i, mm

W_{revap}: the volume of water flowing into soil zone at time step, i, mm

w_{deep}: the volume of water percolating from shallow aquifer to deep aquifer at time step I, mm

$aq_{sh,\ i-1}$: the volume of water stored in shallow aquifer at time step i-1, mm

$w_{pump,\ sh}$: the volume of water lost during pumping from shallow aquifer in time step I, mm

Q_{gw}: ground water or base flow into the main channel

w_{rchrg}: the volume of water entering in the aquifer in time step I, mm

h_{wtbl}: Water table height (m)

L_{gw}: subbasin divide for the groundwater system to the main channel, m

K_{sat}: hydraulic conductivity of the aquifer, mm/day

gw: base flow recession constant

$Q_{gw,\ o}$: the groundwater flow at the start of the recession, mm

$Q_{gw,\ N}$: the groundwater flow on day N, mm

β_{deep}: the aqifer percolation coefficient

BFD: baseflow days

aq_{sh}: the volume of water stored at the beginning of day i, mm

$w_{deep,\ mx}$: the max amount of water percolating into deep aquifer on day, mm

$aq_{shthr,\ rvp}$: the threshold water level in the shallow aquifer for evap.

dhwthi/dt: the rate of change of water table height

μ: specific yield of the shallow aquifer(m/m)

N: the time elapsed since the start of the recession, day

4.4 Previous Work Using SWAT to Estimate the Effect of Climatic Changes

The effects of climate change on hydrological systems have been assessed by inserting the climate-model output (mainly temperature and precipitation) into the hydrological model. Additionally, numerous studies have been conducted at scales ranging from small watersheds to the entire globe to assess the impacts of climate change on hydrologic systems (Jha et al., 2006). As Jha et al. (2006) note with reference to Arnell et al.'s (2001) survey, nearly 80 studies were published in the late 1990s in which climate change impacts for one or more watersheds were analyzed using a climate model - hydrological model approach. These studies represent different sub-regions of the world, with more than half of them being carried out for river basins in Europe (Jha et al., 2006). Relatively fewer studies have been conducted in the tropical regions of

Africa, where one of the longest rivers is found, namely the Nile. The River Nile is already under great pressure due to various competing applications as well as social, political and legal conditions within the riparian countries (Taye et al., 2011). To understand and resolve the potential water-resource-management problems associated with water supply, power generation and agricultural practices, as well as for future water-resource planning, reservoir design and management, and protection of the natural environment, it is necessary to quantitatively estimate the hydrological effects of climate and land use change. In this regard, as Taye et al. (2011) state, several studies have been conducted on the sensitivity of stream flow to climate change for many parts of the Nile. Among these studies, Elshamy et al. (2009) ran an ensemble of climate change scenarios using the Nile forecasting model with bias-corrected precipitation and temperatures from 17 AOGCMs for the period of 2081–2098. This served to assess the effects on the stream flow of the Blue Nile at Diem, which belongs to the Eastern Nile basin. One of the conclusions drawn by Elshamy et al. (2009) is that the uncertainty in future precipitation change due to increased greenhouse gas emissions is large, which makes future changes in stream flow very uncertain. Recently, Taye et al. (2011) simulated the climate change impact on hydrological extremes in two regions (the Nyando basin located in the White Nile and Lake Tana catchment located in the upper Blue Nile subbasin). They note that the unclear results for the Lake Tana catchment imply that the GCM uncertainty was more important for the unclear trend than the hydrological models' uncertainty.

Like climate change, researchers are recently becoming more interested in looking at the spatial-temporal effects of land use and climate change on stream flow responses, which are crucial for sustainable water-resource planning and management. Several investigations have been conducted on the question of the impacts of these changes on stream-flow response. For example, Pikounis et al. (2003) examined the hydrological effects of specific land use changes in a catchment of the River Pinios in Greece using SWAT and made an analysis based on the SWAT's monthly outputs. They developed three land-use-change scenarios: expansion of agriculture, complete deforestation and expansion of urban areas. All of these three scenarios resulted in an increase in discharge during the wet months and a reduction in dry periods (Pikounis et.al, 2003).

Similarly, Fohrer et al. (2001) studied land use changes in Germany. In their study, the total annual water budget was significantly affected if the land use changes affected more than 20% of the basin area. The above two studies mainly focus on land use changes and do not consider the consequences of climate change. Guo et al. (2008) mention several studies that show a certain degree of interdependence between climate and land use changes on different aspects of the water cycle. A major finding of their study is that the climate effect is dominant in the annual stream flow (Guo et. al, 2008). While land-cover changes had a moderate impact on annual stream flow, they strongly influenced the seasonal stream flow and altered the annual hydrograph of the basin (Guo et al., 2008). In a study of the upper Mara river basin in Kenya, Mango et al., (2011) show that a conversion of forests to agriculture and grassland in the basin reduced the dry season flows and increased peak flows, thereby leading to greater scarcity of water at a critical time of the year. In the same paper, the simulated runoff responses to climate change scenarios were nonlinear and suggest that the basin was very vulnerable under low (-3%) and high (+25%) extremes of projected rainfall changes. However, the impacts of land use are more evident in seasonal stream-flow change than in climate change effects, which are influenced mainly during extreme storm events. The two studies discussed above show that various catchments behave differently due to the effects of climate and land use change on annual and seasonal scales.

4.5 Previous Work on Systems Type Black-Box Rainfall-Runoff Models

Several hydrological models have been developed to simulate rainfall-runoff relationships across the world (Rajurkar et al., 2004). These can be classified as empirical black-box models, and conceptual and physically based distributed models (Rajurkar et al., 2004). Black-box models are empirical, involving mathematical equations that are assessed not from the physical processes in the catchment, but from an analysis of concurrent input and output time series. Conceptual (lumped) models treat the catchment as a single unit, with state variables that represent average values over the catchment area, such as storage in the saturated zone. Another approach to

hydrological process modeling is the attempt to construct models based on the governing equations describing all the surface and subsurface flow processes in a catchment. These are called physically distributed models. Each of the models in this group has particular advantages and limitations (Rajurkar et al., 2004). For instance, in areas where obtaining sufficient hydro-meteorological data is problematic or where the purpose of hydrological modeling is limited to flow estimation, applications of linear-system theoretic models (black-box models) are inevitably important for water-related development. However, choosing between the various available hydrological models to suit a practical demand and finding the most appropriate model for a specified basin is challenging. Many models are in practice simple linear-system theoretic models (black-box models) (Rajurkar et al., 2003), which do often not represent the nonlinear dynamics that are inherent in the process of rainfall-runoff transformation.

Minns and Hall (1996), and Campolo et al., (1999) observe that rainfall information alone is not sufficient to calculate the runoff from a catchment, as the initial state (such as the amount of soil moisture and orographic features) of a catchment plays an important role in determining the runoff-rate behavior. The rainfall-runoff relationship in mountainous regions is influenced by the steep-gradient profiles (i.e., inter flow and sheet flow) and less influenced by soil composition (Markewich et al., 1990). Nevertheless, soil composition in less steep environments plays a major role in runoff generation due to the presence of very to moderately drained soils (Markewich et al., 1990; Skaggs et al., 1991; Amatya et al., 1999, 2002; Slatyery et al., 2006). Therefore, higher streamflows and runoff coefficients (R/P, where R is runoff and P is precipitation) are usually associated with mountainous areas (Sun et al., 2002), while smaller R/P ratios are expected for low-topographic gradient watersheds (Amatya et al., 1997, 2000). Sun et al. (2008a, b) argue that runoff in lower-land-plain watersheds have a far larger variability than upland watersheds due to the wider range of variable source areas, including ephemeral water storage in depressions on low gradient terrains.

Evapotranspiration is another factor that affects the hydrological processes of the watershed in shallow water tables (Torres et al., 2011). Evapotranspiration is mainly influenced by humidity gradients, solar energy, wind speed, soil properties and

vegetation type (Amatya & Trettin, 2007; Sun et al., 2010). Other studies found that, depending on the soil-moisture status, lowland watersheds were highly responsive to rainfall by producing more frequent and greater amounts of runoff, with peak-flow rates also depending on the surface depressional storage (Amatya et al., 1997). Furthermore, some rainfall-runoff simulation models demonstrate that the degree of water saturation in the soil prior to a precipitation event [the antecedent soil moisture condition (AMSC)] correlates with the portioning of the event rainfall into infiltration and stream flow (Ye et al., 1997; Wei et al., 2007; Tramblay et al., 2010).

Seasonal climate variability affects both the soil moisture and the characteristics of storm events, which in turn affect the runoff-generation pattern (Torres et al., 2011). These characteristics include rainfall intensity, frequency, duration and direction (Singh, 19970). Although the antecedent soil-moisture condition of a watershed influences the water available for runoff, as well as evapotranspiration and infiltration via soil-water storage, it is highly variable and difficult to measure (Sun et al., 2002).

5 The Hydrology of Ethiopia

The study areas of this thesis include three river catchments: 1) the Eastern Nile (**Paper I**), 2) Omo Gibe (**Paper II**) and 3) Gilgel Abbay (**Paper III**). The Eastern Nile and its tributaries all originate on the Ethiopian plateau and its three subbasins lie between 5ºN, 33ºE and 15ºN, 39ºE, with altitudes ranging from 390 m in parts of Baro Akobo (Sobat) to over 4,500 m in the Tekeze (Atbara) river basin (MoWR, 2002). The Blue Nile has a total length of 1,450 km, of which 800 km are inside Ethiopia. The Blue Nile flows south from Lake Tana and then west across Ethiopia and northwest into Sudan. Although there are several feeder streams that flow into Lake Tana, the source of the river is generally considered to be a small spring at Gish Abbay (Lesser Abbay), which lies north of Lake Tana at an altitude of approximately 2,744 m. Other affluent streams of this lake include the Gorgora, Magech, Gumara, Ribb and Kilti rivers. Lake Tana's outflow then flows for 30 km before plunging into Tis Issat Falls. The river then loops across north-west Ethiopia through a series of deep valleys and canyons and joins the Rahad and Dinder rivers downstream of Roseires in Sudan, after which it is known as the Blue Nile.

There are numerous tributaries of Abbay between Lake Tana and the Sudanese border. They include the Bashilo, Walaka, Jamma, Muger, Guder, Anger, Didessa, and Dabus rivers from the left bank and the Muga, Temcha, Lah, Chamoga, Fettam and Beles rivers from the right bank of the main Abbay River. After flowing past Roseires in Sudan, the Blue Nile joins the White Nile at Khartoum and flows through Egypt to the Mediterranean Sea at Alexandria. Due to the high seasonal variability in rainfall over the Ethiopian plateau, the seasonal variation of the flow of the Abbay is large with maximum runoff in August, when it is about 60 times greater than its minimum in the month of February (Arsano, 2005).

The Baro-Akobo (Sobat) river system marks a 380 km frontier between Ethiopia and Sudan, and originates in the Western Ethiopian Highlands. The Baro River is created by the confluence of the Birbir and Gebba rivers, east of Metu in the Illubabor Zone of the Oromia region in Ethiopia. It then flows west through the Gambela region to join

with the Pibor River from Sudan as well as rivers from northern Uganda to form the Sobat. Other tributaries of the Baro include the Alwero and Gilo rivers. Of the Sobat River tributaries, the Baro River is the largest, contributing 83% of the total water flowing into the Sobat. During the rainy season, between June and October, the Baro River alone provides about 14% of the Nile's water at Aswan in Egypt. In contrast, these rivers have very low flow during the dry season.

The Tekeze (Atbara) rises in the Northern Ethiopia Highlands, has the Angereb and Guang as its major tributaries and replenishes the main Nile north of Khartoum. The Tekeze joins the Atbara River after entering northeastern Sudan. The climatic pattern and the physical environment of the Tekeze sub-system are very similar to those of the Abbay subbasin (Figure 5).

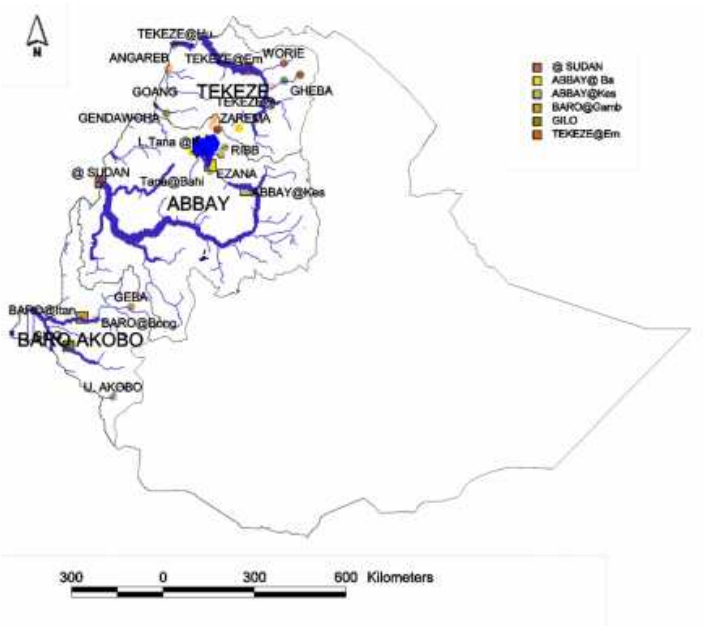

Figure 5: Map showing an outline of Ethiopia and the water sources of the Eastern Nile basin, including stream gauges at the major tributaries (dots) and stream gauges for the calibration and validation of the model (boxes).

The total average annual flows are estimated to be 50, 23.6 and 8.2 billion m^3 from the Blue Nile (Abbay), Baro Akobo (Sobat) and Tekeze (Atbara) river basins, respectively

(Arsano et al., 2004; MoWR, 2002). They provide 86% of the water of the Nile (Blue Nile (Abbay) 59%, Baro-Akobo (Sobat) 14%, Tekeze 13%) (Swain, 1997). Due to the high seasonal variability in rainfall over the Ethiopian plateau, the flow of the Blue Nile (Abbay) varies dramatically. The maximum runoff is in August, when it is about 60 times greater than its minimum in the month of February (Arsano, 2005). The climate varies from warm, desert-like climate at the Sudan border, to wet in the Ethiopian highlands. The annual rainfall ranges from 800 mm to 2200 mm with an average of about 1,420 mm for Blue Nile (Abbay). The annual rainfall reaches at maximum of 3,000 mm over the highlands and a minimum of 600 mm in the lowlands with an annual rainfall of about 1,419 mm in the case of the Baro Akobo basin. In contrast to the Blue Nile river basin (Abbay) and Baro Akobo, the annual rainfall for Tekeze (Atbara) is far lower, ranging from 600 mm to 1,200 mm, with an average of about 900 mm. Most of rainfall occurs from June to September for all three basins (MoWR, 2002). More than 50%, 23% and 15.7% of the Blue Nile, Tekeze and Baro Akobo subbasins respectively are used for agriculture, whereas the rest is covered by forest, grass, bush and shrubs. The major soil types are lithosols and eutric cambisols for the Tekeze subbasin; chrome acid luvisols, eutric vertisol, luvisols and lithic leptosols for the Blue Nile; and dystric cambisols and orthic acrisols for the Baro Akobo subbasin (Figure 4 in paper I).

The Omo Gibe basin is also one of the significant surface water resources of Ethiopia. It is drained by two major rivers from the highlands: the Gibe River flowing southwards and the Gojeb River flowing eastwards. Downstream of their confluence only minor tributaries join, as the river continues southwards where it empties into Lake Turkana at the border with Kenya (Avery, 2010) (See Figure 1 in Paper II). By volume, Lake Turkana is the 24th largest lake and the world's largest permanent desert lake. The Lake Turkana catchment area is situated in both Ethiopia and Kenya and has an area of 130,860 km^2, of which the Omo Gibe river basin covers 50% (74,300 km^2) of the total drainage area. Ninety percent of the inflow to Lake Turkana is contributed by the Omo Gibe river basin. The Omo River has a total length of about 1,200 km, with an average slope of 3.1 m/km. The long-term mean flow is estimated to be 435m^3/s or 13.5 billion m^3 per annum (EEPCO, 2009) and seasonal variations are substantial, with a monthly

mean flow ranging from 60 m^3/s in March to over 1,500 m^3/s in August (EEPCO, 2009) (Figure 6).

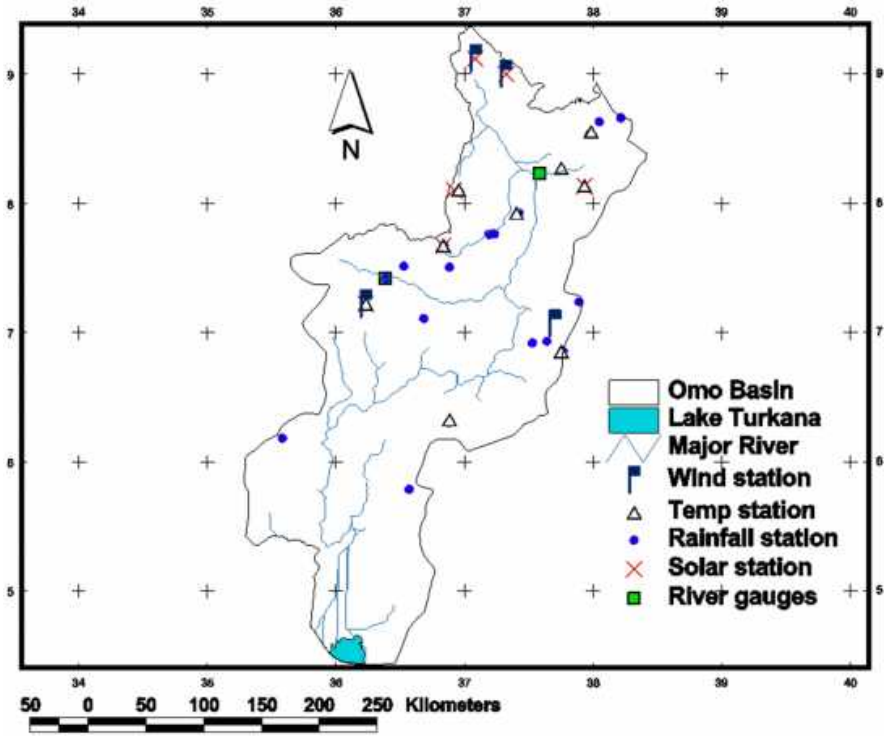

Figure 6: Map of the Omo Gibe river basin including major river networks, meteorological stations and stream gauges used for calibration.

The annual rainfall within the Omo Gibe catchment decreases from north to south and with its decrease in elevation. It varies from a minimum of 1,200 mm in the lowlands to a maximum of about 1,900 mm in the highland areas (EEPCO, 2009). The average annual rainfall calculated over the entire basin is 1,426 mm, with a mean annual temperature of 20.4°C. Seventy-five to 80% of the annual rainfall occurs during a five-month period from May to September (EEPCO, 2009). Over 40% of the Omo Gibe river basin is covered by mixed forest, whereas the rest is covered by agriculture, pasture, grass, bush and shrubs. The major soil types of the Omo Gibe basin are dystric cambisols and lithosols.

The Gilgel Abbay catchment (4,051 km^2) is the largest among the four main sub-catchments in the Lake Tana basin in northern Ethiopia (Figure 7) and provides about 60% of the lake inflow. It is located at 10° 44'N latitude and 37° 23'E longitude (Figure 5). The catchment includes the two gauged subbasins: Upper Gilgel Abbay (1,664 km^2), which is the focus of this study, and Koga (307 km^2) (Figure 6), with elevations ranging from 1,787 m to 3518 m (see Figure 2 in paper I). The topography is rugged in the southern part of the catchment and in the periphery to the west and southeast, while the remaining part is a typical plateau with gentle slopes. The soil is dominated by clays and clay loams. The dominant land use units are agricultural (65%) and agro-pastoral land (33%) (BECOM, 1999).

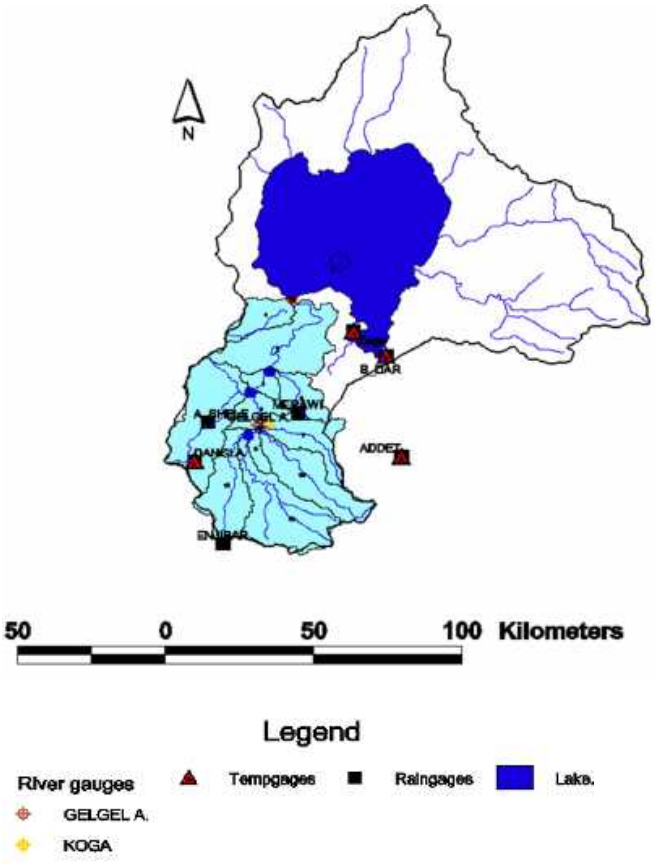

Figure 7: Map of Lake Tana including the four major rivers (the Megeche, Gumara, Rib and Gilgel Abbay rivers), the drain to Lake Tana, the Upper Blue

Nile river basin and the precipitation, temperature and stream-gauging station located in the Gilgel Abbay subbasin.

Long-term (1980–2000) annual air-temperature values recorded at Merawi and Dangla stations ranged from 11°C to 37.7°C, with an average daily temperature of 18.4°C. The rainfall in Upper Gilgel Abbay has one main rainy season between June and September, receiving about 70–90% of the annual rainfall (Kebede et al., 2006; Tarekegn & Tadege, 2005; Abdo et al., 2009). Long-term rainfall data (1964–2005) also range between 834 and 2,106 mm, with July representing the wettest month (356 mm) and January representing the driest month (3.1 mm) on average. The rainfall data from meteorological stations indicate significant spatial variability of rainfall following the topography, with a decreasing trend from south to north. The temperature variations are small throughout the year (BCEOM, 1999).

6 Concluding remarks and perspectives

This chapter attempts to present the main findings and conclusions of the study based on the main objectives. The main objectives of this study are synthesized into three groups. The first goal is to test the applicability of a physically distributed hydrological model (SWAT) that is forced by daily station-based precipitation and temperature data and calibrated with the daily streamflow to simulate two major river basins (Eastern Nile, Paper I and Omo Gibe basin, Paper II). The second main objective of this study is to analyze the impact of climate and/or land use change on streamflow and other water-balance components to the assumed hypothetically synthesized scenarios. The third goal is to test the usefulness of simpler models compared to complex hydrological models for flow forecasting purposes.

6.1 Main Findings

The Soil and Water Assessment Tool 2005 adequately simulated the monthly variability in flows for the Eastern Nile basin. The total simulated monthly streamflow ranges from good ($0.65 < E_{NS} < 0.75$) to very good ($E_{NS} > 0.75$). The average daily and monthly difference between the observed and simulated flow (PBIAS) was good (PBIAS $\leq \pm 20\%$) for the calibration period, with the exception of the Blue Nile subbasin, where it was only satisfactory ($\pm 20\% <$ PBIAS $\leq \pm 40\%$) (**Paper I**).

The streamflow sensitivity to changes in precipitation and temperature differed among the basins within the Eastern Nile and depended on the strength of the changes. The general assessment, which is made by a relative sensitivity analysis for the 20 hypothetical climate change scenarios, is that the Eastern Nile's annual streamflow is very sensitive to variations in precipitation and moderately sensitive to temperature changes (**Paper I**).

The annual streamflow responses to a 10% change in precipitation with no temperature change were on average 19%, 17% and 26% for the Abbay, Baro Akobo and Tekeze river basins, respectively. However, the responses to a reduction and increase in precipitation were not the same. While Baro Akobo was more sensitive to a reduction

in precipitation, Tekeze showed a larger sensitivity to an increase. The streamflow sensitivity to temperature was moderate. The average annual streamflow responses to a 1°C change in temperature and no precipitation change were -4.4%, -6.4%, and -1.3% for the Abbay, Baro Akobo and Tekeze river basins, respectively. The very low sensitivity of the Tekeze basin indicates that flows were moisture limited for a large part of the year **(Paper I).**

Applying the combined temperature-precipitation sensitivities and 47 temperature and precipitation scenarios from 19 AOGCMs participating in CMIP3, we estimated the future streamflow change to be very uncertain and strongly dependent on the choice of climate model. The reason for this is the disagreement between the different climate models on both the strength and direction of future precipitation changes.

In **Paper II,** the sensitivity of the Omo Gibe river basin to climate and/or land use change was also modeled using SWAT. The model was successfully calibrated and validated at the Great Gibe and Gojeb river gauges, with good agreement between the observed and simulated monthly streamflow. The monthly bias during the validation period was -14% and 7% for the Great Gibe and Gojeb rivers, respectively, while the Nash-Sutcliffe efficiency factor was 0.75 and 0.88, respectively.

The simulated effect of land use changes resulting from various hypothetical land use modifications is secondary to the effect of precipitation changes on the annual streamflow. However, the seasonal changes in streamflow were in some cases strongly affected by land use. As an example, a deforestation scenario (entire forest-area coverage changed to bare lands) increased the January-April (dry season) streamflow by 38% (**Paper II**).

The results indicate that modeling various changes in land use renders a change in streamflow that generally lies below 10% per 10% change in land use. Deforestation of the entire region, through the change of the entire forest-area coverage (48% of the basin) to bare lands, increased the annual streamflow by 19.9% compared to the

reference simulation. This result deviates from the report by Avery (2010), which states that the streamflow may decrease by 50–60%.

Streamflow sensitivity to land use change was largest when agricultural land was converted to either forest or bare lands. In the AAG to BRLNDS scenario, there is strongly reduced evapotranspiration due to less transpiration and more soil moisture retained in the soil due to plant cover, which later led to increased streamflow. In contrast, in the case of AAG to FRST, the soil moisture contributes significantly to reducing evaporation but there is strong transpiration due to plant cover. The overall effect results in decreased streamflow.

For many of the simulations, the relative streamflow sensitivity was largest in the dry period of JFMA due to changes in evapotranspiration, as transpiration (a component of evapotranspiration) was altered when land use was altered. In addition, many of the simulations show the weakest streamflow response in the period of October–December. This is because this period follows the wet period (MJJAS), as well as because evapotranspiration is dominated by evaporation and the soil moisture is large. Thus, changes in transpiration due to land use changes are less important.

The results on the sensitivity of streamflow to temperature and precipitation (14 hypothetical climate change scenarios) show that the basin streamflow is very sensitive to precipitation changes and moderately sensitive to temperature changes. The annual streamflow response to a 10% change in precipitation with no temperature change was 25% on average, while the streamflow sensitivity to temperature was relatively low. The average annual streamflow responses to a 1°C change in temperature and no precipitation change was -1.4%.

The highest sensitivity to precipitation change was observed during the dry period (JFMA), with a 31% change in streamflow from a 10% precipitation increase. This is because of the relatively decreased evapotranspiration due to minimum transpiration from less vegetation cover during this period.

For all seasons except JFMA, the combined effect of a precipitation change and temperature increase was linear (the sum of the changes to precipitation and temperature individually). The nonlinear behavior during JFMA was due to the interaction among various factors that are more pronounced in this season than in other periods of the simulation. These factors include the soil's physical properties (in relation to limited soil moisture), less vegetation cover, minimum precipitation amount and high temperatures during this period.
The JFMA season is far more sensitive to temperature change than the other two seasons (-3.5%/K). This is due to moisture constraint and an increased temperature to dry out moisture from the soil via evapotranspiration in the season, which in turn results in a reduction of streamflow. The large sensitivity of streamflow in JFMA may have serious implications for the management of water supply for domestic and industrial use, and for power generation and agriculture, because a number of small streams which are currently perennial may be altered to become intermittent.

In addition to describing the effects of individual land use or climate change on seasonal and annual streamflow, the effect of simultaneous changes in both land use and climate on the water cycle was investigated. The results indicate that the combined effects differ only slightly from the effect resulting from the sum of the individual land use and climate changes. For example, in a wet scenario, changing land use to increase bare land areas would increase streamflow by 58.41%, which is slightly less than the 63.4% from simple additions of the individual effects from changes in land use (16.8%) and climate (46.6%). However, there are exceptions to this linear response, showing that the model simulates some effects leading to nonlinear interactions among water-balance components when simultaneous changes in land use and climate change would take place in the same basin.

Among the nine hydrological models that were tested (**Paper III**), the performance of the naïve SLM is inferior to that of all other models. As the study catchment is characterized by seasonality, the LPM outperforms the LVGFM and even the SMAR model. However, the ANN, which is characterized by a large number of weights

(parameters), generally performs better than the simpler models. The SMAR model variants, having either nine or ten parameters, fail to adequately simulate the hydrological behaviour of the Gilgel Abbay catchment.

Therefore, this study confirms that simpler models (which take only rainfall as input) can surpass their complex counterparts in performance for continuous simulation and in reproducing hydrographs or flow estimations.

6.2 Conclusion and Future Perspectives

In summary, the good performance of SWAT in the validation period indicates that the fitted parameters during the calibration period can be taken as a representative set of parameters for the Eastern Nile and Omo Gibe watersheds, and that further simulation and evaluation of alternative-scenario analysis can be carried out for other periods using this tool. The tool simulates monthly flows better than daily flows and is probably not adequate for studies of single severe events in small catchments.

The overall assessment made by a sensitivity analysis for the hypothetical climate-sensitivity scenarios reveals that the annual streamflow of the study areas was very sensitive to variations in precipitation and moderately sensitive to temperature changes. In addition, we show that the modelled response of a combined temperature and precipitation change was very similar to the simulations that resulted from adding the responses from the temperature change only and the precipitation change only (**Papers I and II**).

Using the combined temperature-precipitation scenarios from 19 AOGCMs participating in IPCC AR4, we estimated that the streamflow change varied strongly, as the climate models disagree on both the strength and direction of future precipitation changes. Thus, based on the state-of-the-art climate models, little can be said about future changes in the Eastern Nile's streamflow. This finding is similar to that in the study of Elsahmay et al. (2009). However, our analysis emphasizes the need for performing ensemble runs using different climate models in this type of assessment. This uncertainty may have implications for long-term water-resource planning,

estimation of future hydropower potential, reservoir design and determination of the extent to which the development of agriculture should utilize river- or groundwater-based irrigation systems (**Paper I**).

Paper II proposes that the management of the emerging cascaded hydropower development promises to be a daunting task, given the high sensitivity of precipitation. This requires careful consideration in implementing seasonal flow-forecasting models and reservoir-operation management for sustainable upstream-downstream interaction.

In conclusion, **Paper III** confirms that in cases where the river is well gauged, simpler models for continuous river-flow simulation can surpass their complex counterparts in performance. There is a justification for the claim that increasing the model complexity, thereby increasing the number of parameters, does not necessarily enhance the model performance as long as the additional parameters are not well constrained. It is suggested that, in practical hydrological applications, the simpler models may still play a significant role as effective simulation tools and that performance enhancement is not guaranteed by the adoption of complex model structures.

Finally, we note several weaknesses of the above analysis. The first is that it attempts to address climate change impact with only one hydrological model and two forcing variables (precipitation and temperature), thereby neglecting all other variables (such as vegetation or radiation changes), which may affect runoff generation. The second limitation is that we multiplied the precipitation with a fraction, which entails that we assumed that the wet-day frequency remained unchanged and that the whole precipitation change was given as a change in intensity. For temperature, we added a constant for the entire year, thereby assuming that the changes were not dependent on the season. We also used a simple linear estimate to link the CMIP3 climate change scenarios to changes in streamflow. These were all crude assumptions. However, we feel that the substantial uncertainty about future precipitation changes partly justifies our crude treatment of the parameters.

7 References

Abbott B, Bathurst, J C, Cunge, J A, O'Connell, P E and Rasmussen, J,1986, An introduction to the European Hydrological System-Systeme Hydeologique Europeen (SHE), J. Hydrol.87,45-59.

Abdo, K. S., Fiseha, B. M., Rientjes, T. H. M., Gieske, A. S. M., and Haile, A. T.: Assessment of climate change impacts on the hydrology of Gilgel Abbay catchment in Lake Tana basin, Ethiopia, Hydrol. Process., 23(26), 3661–3669, 2009.

Arnell, N. W., Liu, C., Compagnucci, R., da Cunha, L., Hanaki, K., Howe, C., Mailu, G., Shiklo manov, I., and Stakhiv, E.: Impacts, Adaptation, and Vulnerability, in: Climate Change 2001, edited by: McCarthy, J. J., Canziani, O., Leary, N. A., Dokken, D. J., and White, K. S., Cambridge University Press, Cambridge, United Kingdom, Hydrol. Water Resour., Chapter 4, 191–233, 2001.

Arnold, J. G. and Allen, P. M.: Estimating hydrologic budgets for three Illinois watersheds, J. Hydrol., 176(1–4), 57–77, 1996.

Arnold, J. G., Allen, P. M., and Bernhardt, G.: A comprehensive surface groundwater flow model, J. Hydrol., 142, 47–69, 1993.

Arsano, Y.: Ethiopia and the Eastern Nile basin, Aquat. Sci., 67, 16–17, doi: 10.1007/s00027-004-0766-x, 2005.

Arsano, Y.: Ethiopia and the Nile: The Dilemma of National and Regional Hydro-politics, PhD dissertation, Zurich, Switzerland, University of Zurich, 2004.

BCEOM: Abbay River Basin integrated master plan, main report, MoWR, Addis Ababa, Ethiopia, 1999.

Bicknell, B. R., J. C. Imhoff, A. S. Donigian, and R. C. Johanson. 1997. Hydrological simulation program - FORTRAN (HSPF): User's manual for release 11. EPA-600/R-97/080. Athens, Ga.: U.S. Environmental Protection Agency.

Borah, D. K., and M. Bera. 2003. Watershed-scale hydrologic and nonpoint-source pollution models: Review of a thematical bases. Trans. ASAE 46(6): 1553-1566.

Borah, D. K., and M. Bera. 2004. Watershed-scale hydrologic and nonpoint-source pollution models: Review of applications. Trans. ASAE 47(3): 789-803.

Borah, D. K., M. Bera, M. and R. Xia. 2004. Storm event flow and sediment simulations in agricultural watersheds using DWSM. Trans. ASAE 47(5): 1539-1559.

Calver, A and Wood, W L,1995, The Institute of Hydrology Distributed Model, in V P Singh(Ed.), *Computer models of watershed Hydrology*, Water Resource Publications, Colorado,595-626.

Chow, V.T., Maidment, D.R., and Mays, L.W. (1988) *Applied hydrology*. McGraw-Hill, Singapore.

Crawford, N. H., and R. K. Linsley, 1966. Digital simulation in hydrology, Stanford Watershed Model IV. Tech. Rep. N. 39, Dept. Civil. Eng. Stanford University, Stanford, CA.

Gulilat Birhane, 2003, Present and future water resources development in Ethiopia related to research and capacity building, Ministry of Water Resources, Addis Abeba, Ethiopia.

Elshamy, M. E., Seierstad, I. A., and Sorteberg, A.: Impacts of climate change on Blue Nile flows using bias-corrected GCM scenarios, Hydrol. Earth Syst. Sci., 13, 551–565, doi: 10.5194/hess-13-551-2009, 2009.

Fohrer N, Eckhardt K, Haverkamp S, Frede H-G, 2001. Applying the SWAT model as decision supporting tool for land use concepts in peripheral regions in Germany. 994 -999. In: Stott D-E, Mohtar R-H, Steinhardt C-G (eds). Sustaining the Global Farm. 10th International Soil Conservation Organization Meeting, May 24-29, 1999, West Lafayette. http://topsoil.nserl.purdue.edu/nserlweb/isco99/pdf/isco99pdf.htm.

Fohrer N, Haverkamp S, Eckhardt K, Frede H-G, 2001. Hydrologic response to land use changes on the catchment scale. Phys Chem Earth B. 26: 577-582.

Freeze, R. A. and R. L. Harlan, 1969. Blueprint for a physically based digitally simulated hydrologic response modal, Journal of Hydrology, 9, 237-258.

Gosain, A. K., S. Rao, and D. Basuray. 2006. Climate change impact assessment on hydrology of Indian River basins. Current Sci. 90(3): 346-353.

Gosain, A. K., S. Rao, R. Srinivasan, and N. Gopal Reddy. 2005. Return-flow assessment for irrigation command in the Palleru River basin using SWAT model. Hydrol. Process. 19(3): 673-682.

Grayson, R B, Moore, I D and McMahon, T A, 1992, Physically-based hydrologic modelling. 2. Is the concept realistic? *Wat. Resour. Res*., 28(10), 2659-2666.

Green, W. H. and Ampt, G. A.: Studies on soil physics. 1. The flow of air and water through soils, J. Agric. Sci., 4, 11–24, 1911.

Griensven, V. (2002). Sensitivity analysis and auto-calibration of an integral dynamic model for river water quality. *Water Science and Technology* , 321-328.

Guo, H., Hu, Q., and Jiang, T.: Annual and seasonal streamflow responses to climate and land-cover changes in the Poygan Lake basin, China, J. Hydrol., 355, 106–122, 2008.

Hargreaves, G. H. and Samani, Z. A.: Agricultural benefits for Senegal River basin, J. Irrigat. Drain. Engin., 111, 113–124, doi:10.1061/(ASCE)0733-9437(1985)111:2(113) 1985.

Hooghoudt, S. B.: Bijdrage tot de kennis van enige natuurkundige grootheden van de grond, Versl. Landbouwkd. Onderz, 46, 515–707, 1940.

Jha, M., Arnold, J. G., Gassman, P. W., Giorgi, F., and Gu, R.R.: Climate change sensitivity assessment on Upper Mississippi River Basin Streamflows using SWAT, J. Am. Water Res. Ass.,42, 997–1015, doi:10.1111/j.1752-1688. 2006. Tb04510.x, 2006.

Kebede, S., Travi, Y., Alemayehu, T., and Ayenew, T.: Water balance of Lake Tana and its sensitivity to fluctuations in rainfall, Blue Nile Basin, Ethiopia, J. Hydrol., 316, 233–247, 2006.

Lemma Gonfa.1996: Climate Classification of Ethiopia, Bulletin 3; NMSA, Addis Abeba, Ethiopia

Linsley, R. K. and N. H. Crawford, 1960. Computation of synthetic storm flow record on a digital computer, Int. Assoc. Sci. Hydrol. Pub., 51, 526-538.

Linsley, R. K., M. A. Kohler and J. L. H. Paulhus, 1982. Hydrology for Engineers. McGraw Hill, New York, NY.

Mango l.M., Melesse A.M., McClain M.E., Gann D., and Setegn S.G.: Land use & climate change impacts on the hydrology of the upper Mara River Basin, Kenya: results of modeling study to support better resource management, Hydrol. Earth Syst. Sci., 15, 2245–2258, doi: 10.519/hess-15-2245-2011, 2011.

McCoenick P.G., Kamara, AB.and Girma Tadesse. (eds): 2003; Integrated water and land management research and capacity building priorities for Ethiopia, Proceedings of MoWR/EARO/IWMI/ILRI, International workshop held at ILRI, Addis Abeba, Ethiopia, 2-4 December 2002.Monteith, J. L.: Evaporation and the Environment. The State and Movement of Water in Living Organisms, Cambridge University Press, Sawnsea, 205–234, 1965.

MoWR: Ethiopian water sector strategy, Ministry of Water Resources, Addis Abeba, 2002.MoWR: Data collected from different river basin development master plan studies. Planning and projects department, Ministry of Water Resources, Addis Abeba, Ethiopia, 2001a.

MoWR: Water Sector Development program-Methodological Framework, Addis Abeba , Ethiopia 2001b.

Mulvaney, T. J., 1851. On the use of self-registering rain and flood gauges in making observations of the relations of rainfall and flood discharges in a given catchment. Trans. of the institution of Civil Engineers, Ireland, 4(2), 18.

Nasr, A., M. Bruen, P. Jordan, R. Moles, G. Kiely, and P. Byrne. 2007. A comparison of SWAT, HSPF, and SHETRAN/GOPC for modeling phosphorus export from three catchments in Ireland. Water Res. 41(5):65-1073.

Pikounis M., Varanou E., Baltas E., Dassaklis A., Mimikou M., (2003). Application of the SWAT model in the Pinios River Basin under different land-use scenarios, Global Nest: the int.J.Vol.5, No.2, pp 71-79.

Ponce, V. M. and Hawkins, R. H.: Runoff curve number: has it reached maturity? J. Hydrol. Engin., 1(1), 11–19, 1996.

Refsgaard, J. C., and B. Storm. 1995. MIKE-SHE. In Computer Models in Watershed Hydrology, 809-846. V. J. Singh, ed. Highland Ranch, Colo.: Water Resources Publications.

Ritchie, J. T.: Model for predicting evaporation from a row crop with incomplete cover, Water Resour., 1204–1213, 1972.

Saleh, A., and B. Du. 2004. Evaluation of SWAT and HSPF within BASINS program for the upper North Bosque River watershed in central Texas. Trans. ASAE 47(4): 1039-1049.

Sherman, L. K., 1932. Streamflow from rainfall by the unit graph method, Engineering News Record, No. 108, 501-505.

Singh, J., H. V. Knapp, J. G. Arnold, and M. Demissie. 2005. Hydrological modeling of the Iroquois River watershed using HSPF and SWAT. J. American Water Resour. Assoc. 41(2): 343-360.

Smedema, L. K. and Rycroft, D. W.: Land Drainage. Planning and Design of Agricultural Drainage Systems, Cornell Uinersity, New York, 1983.

Srinivasan, M. S., P. Gerald-Marchant, T. L. Veith, W. J. Gburek, and T. S. Steenhuis. 2005. Watershed-scale modeling of critical source areas of runoff generation and phosphorus transport. *J. American Water Resour. Assoc.* 41(2): 361-375.

Swain, A.: Ethiopia, the Sudan, and Eygpt: the Nile River dispute, J. Mod. African Stud., 35, 20 675–694, 1997.

Tarekegn, D. and Tadege, A.: Assessing the impact of climate change on the water resources of the Lake Tana sub-basin using the WATBAL model, CEEPA, Republic of South Africa, 2005.

Taye, M. T., Ntegeka, V., Ogiramoi, N. P., and Willems, P.: Assessment of climate change impact on hydrological extremes in two source regions of the Nile River Basin, Hydrol. Earth Syst. Sci., 15, 209–222, doi: 10.5194/hess-15-209-2011, 2011.

Taylor, P. A.: On the assessment of surface heat flux and evaporation using large-scale parameters, Weather, 100, 8192, doi: 10.1175/15200493(1972)100<0081: OTAOSH>2.3.co; 2 1972.

USDA-SCS. (1972). Hydrology. In *National Engineering Hand book section 4* . Washington ,Dc: USDA-SCS.

USDA-SCS: Hydrology (Revised), in: Engineering Handbook Sect. 4, Washington, DC, 1985.

Van Liew, M. W., J. G. Arnold, and J. D. Garbrecht. 2003a. Hydrologic simulation on agricultural watersheds: choosing between two models. Trans. ASAE 46(6): 1539-1551.

Williams, J. R.: The EPIC model, in: Computer Models of Watershed Hydrology, Water Resources Publications, Highlands Ranch, CO, 909–1000, 1995.

World Bank (2006): Ethiopia, Managing Water Resources to maximize Sustainable growth, Washington, DC

Official documents, Media and independent Resources

Avery S. (2010): Hydrological impacts of Ethiopian Omo Basin on Kenya`s Lake Turkana water levels and Fisheries Final Report prepared for the African Development Bank Tunis.

EEPCo, "Gibe 3 Environmental and Social Impact Assessment," 2009. Available at: http://www.eepco.gov.et/.(http: www.gisdevelopment.net)

8 Scientific Results

9 Paper I: Sensitivity of SWAT simulated streamflow to climatic changes within the Eastern Nile River

D. T. Mengistu[1, 2] **and A. Sorteberg**[2, 3]

[1]Arba Minch Institute of Technology, Arba Minch University, Ethiopia
[2]Geophysical Institute, University of Bergen, Norway
[3]Bjerknes Centre for Climate Research, University of Bergen, Norway

Correspondence to: D. T. Mengistu (dertes 24@yahoo.com, dme061@uib.no)

Received: 6 September 2011 – Published in Hydrol. Earth Syst. Sci. Discuss.: 5 October 2011
Revised: 12 January 2012 – Accepted: 26 January 2012 – Published: 9 February 2012

Abstract. The hydrological model SWAT was run with daily station-based precipitation and temperature data for the whole Eastern Nile basin including the three subbasins: - The Abbay (Blue Nile), Baro Akobo and Tekeze. The daily and monthly streamflows were calibrated and validated at six outlets with station-based streamflow data in the three different subbasins. The model performed very well in simulating the monthly variability while the validation against daily data revealed a more diverse performance. The simulations indicated that around 60 % of the average annual rainfall of the subbasins was lost through evaporation while the estimated runoff coefficients were 0.24, 0.30 and 0.18 for Abbay, Baro Akobo and Tekeze subbasins, respectively. About half to two-thirds of the runoff could be attributed to surface runoff while the other contributions came from groundwater. Twenty hypothetical climate change scenarios (perturbed temperatures and precipitation) were conducted to test the sensitivity of SWAT simulated annual streamflow. The result revealed that the annual streamflow sensitivity to changes in precipitation and temperature differed among the basins and the dependence of the response on the strength of the changes was not linear. On average the annual streamflow responses to a change in precipitation with no temperature change were 19 %, 17 %, and 26 % per 10 % change in precipitation while the average annual streamflow responses to a change in temperature and no precipitation change were −4.4 % K−1, −6.4 % K−1, and −1.3 % K−1 for Abbay, Baro Akobo and Tekeze river basins, respectively.

47 temperature and precipitation scenarios from 19 AOGCMs participating inCMIP3 were used to estimate future changes in streamflow due to climate changes. The climate models disagreed on both the strength and the direction of future precipitation changes. Thus, no clear conclusions could be made about future changes in the Eastern Nile streamflow. However, such types of assessment are important as they emphasis the need to use several an ensemble of AOGCMs as the results strongly dependent on the choice of climate models.

1 Introduction

Numerous studies have been conducted at different scales ranging from small watersheds to the entire globe to assess the impacts of climate change on hydrologic systems (Jha et al., 2006). As Jha et al. (2006) noted with reference Arnell et al. (2001), nearly 80 studies were published in the late 1990s in which climate change impacts for one or more watersheds were analyzed using a coupled climate model hydrologic model approach. However, more than half of the studies were carried out for river basins in Europe (Jha et al., 2006) and relatively few studies have been conducted in tropical region in Africa. The River Nile is already under great pressure from various competing applications as well as social, political and legal conditions within the riparian countries (Taye et al., 2011). To understand and resolve the potential water resource management problems associated with water supply, power generation, and agricultural practices as well as for future water resource planning, reservoir design and management, and protection of the natural environment, it is necessary to provide quantitative estimates of the hydrological effects of climate change. In this regard as Taye et al. (2011) stated several studies have been con- ducted on the sensitivity of streamflow to climate changes for many parts of the Nile. Among these studies, Elsahmay et al. (2009) run an ensemble of climate change scenarios using the Nile Forecasting Model with bias corrected precipitation and temperatures from 17 coupled general circulation models (AOGCMs) for the 2081–2098 period to assess the effects on the streamflow of the Blue Nile at Diem which belongs to Eastern Nile basin. One of the conclusions in Elshamy et al. (2009) was that the uncertainty in future

precipitation change due to increased greenhouse gas emissions are large, making the future changes in streamflow very uncertain. Recently Taye et al. (2011) simulated the climate change impact on hydrological extremes in two regions (Nyando basin found in White Nile and Lake Tana catchment located in upper Blue Nile subbasin) and noted that for Lake Tana catchment the GCM uncertainty was more important than the hydrological models' uncertainty.

Abbay (Blue Nile), Baro Akobo (Sobat) and Tekeze (Atbara) are the three major river basins in the Eastern Nile which all originated from the Ethiopian Highlands. 86 % (or 82 $km^{3)}$ of the total average flow of the Nile at Aswan is estimated to origin from these three river basins (Arsano, 2005). Several attempts have been made to implement hydrological models for the Blue Nile basin. Sutcliffe et al. (1989) and Dugale et al. (1991) used a simple daily hydrological model calibrated by METOSAT derived rainfall estimates and the National Oceanic and Atmospheric Administration, USA in collaboration with the Egyptian Ministry of Public Works has developed a comprehensive model of the Nile to predict the inflow to the Aswan Dam (Barrett et al., 1993; Schaake et al., 1993; Johanson and Curtis, 1994; Todd et al., 1995). However, as Conway (1997) stated, both of these investigations suffered by the lack of in situ data, in particular subbasin discharge data to calibrate the hydrological models and gauge estimates of daily rainfall to calibrate the METEOSAT derived estimates of rainfall. Conway (1997) applied a grid based water balance model with limited meteorological and hydrological data inputs on a monthly time step for the Blue Nile catchment. According to Conway (1997) the correlation between observed and simulated annual flows was 0.74 for a 76-yr data period and the mean error was 14 %, although relatively large errors occurred in individual years. Furthermore, Mohamed et al. (2005) focused on the interaction between the climatic processes and the hydrological processes on the land surface in the subbasins of Nile (White, Blue Nile, Atbara and the main Nile) using a regional atmospheric model to show that the model could reproduce runoff reasonably well over the subbasins of the Nile. The above studies except the latter, have all been investigating the upper Blue Nile basin but there are still very few published studies on the two other basins (Tekeze and Baro Akobo). Recently, Setegen et al. (2008) investigated the Lake Tana Basin (part of the Blue Nile) using the hydrological model

(SWAT) and studies applying the same model have also been conducted for the Meki basin (Central Ethiopia) and the upper Awash basin (western catchment of the Awash basin in Ethiopia) by Zeray et al. (2007) and Checkol (2006), respectively. These three studies showed that the SWAT model was able to describe the study areas with a quality that makes it suitable for water resource management use.

The aim of this paper is to test the applicability of the Soil and Water Assessment Tool (SWAT) physically distributed model over the three major subbasins in Eastern Nile at larger watershed scale and thereby complementing other older studies that have simulated parts of the catchment. Sensitivity studies to assess the potential impacts of climate change on the annual streamflow is performed using twenty hypothetical climate change perturbations in temperature, precipitation or both. In addition, the sensitivities found above together with 47 temperature-precipitation scenarios from 19AOGCMs which were participating inpahse 3 of the Coupled Model Inercomparison Project (CMIP3) are used to assess the uncertainty in future streamflow changes for the Eastern Nile.

2 Description of the study area

The Eastern Nile and their tributaries all originate on the Ethiopian plateau and the three subbasins of the Eastern Nile lies between 5° N 33^{0} E and 15° N 39^{0} E with altitude ranges from 390 m in part of Baro Akobo to over 4500 m in the Tekeze river basin (MoWR, 2002). The total average annual flows are estimated to be 50.0, 23.6 and 8.2 billion cubic meters from the Abbay, Baro Akobo and Tekeze river basins, respectively (Arsano et al., 2004; MoWR, 2002). They provide 86 % of the waters of the Nile (Abbay 59 %, Baro Akobo 14 %, Tekeze 13 %, Swain, 1997).

According to materials published by the Ethiopian Central Statistical Agency, the Blue Nile has a total length of 1450 kilometer, of which 800 km are inside Ethiopia. The Blue Nile flows south from Lake Tana and then west across Ethiopia and northwest into Sudan. Although there are several feeder streams that flow into Lake Tana, the source of the river is generally considered to be a small spring at Gish Abbay (Lesser Abbay) north of Lake Tana at an altitude of approximately 2744 m. Other

affluent streams of this lake include, from Gorgora, Magech, Gumara, Ribb, and Kilti Rivers. Lake Tana's outflow then flows 30 km before plunging over the Tis Issat Falls. The river then loops across north- west Ethiopia through a series of deep valleys and canyons and join Rahad and Dinder rivers downstream of Roseires in Sudan, after which it is known as the Blue Nile.

There are numerous tributaries of Abbay between Lake Tana and the Sudanese border. Some of these are Bashilo, Walaka, Jamma, Muger, Guder, Anger, Didessa, and Dabus Rivers from the left bank, and Muga, Temcha, Lah, Chamoga, Fettam and Beles Rivers from right bank of the main Abbay River. After flowing past Roseires inside Sudan, the Blue Nile joins the White Nile at Khartoum and, as the River Nile, flows through Egypt to the Mediterranean Sea at Alexandria. Due to the high seasonal variability in rainfall over the Ethiopian plateau, the seasonal variation of the flow of the Abbay is large with maximum runoff is in August when it is about 60 times greater than its minimum in the month of February (Arsano, 2005).

The Baro-Akobo (Sobat) river system marks a 380km frontier between Ethiopia and Sudan and originates in the Western Ethiopian Highlands. The Baro River is created by the confluence of the Birbir and Gebba Rivers, east of Metu in the Illubabor Zone of the Oromia Region, Ethiopia. It then flows west through the Gambela Region to join with the Pibor River from Sudan and Rivers from Northern Uganda to form the Sobat. Other notable tributaries of the Baro include the Alwero and Gilo Rivers. Of the Sobat River tributaries, the Baro River is the largest, contributing 83 % of the total water flowing into the Sobat. During the rainy season, between June and October, the Baro River alone contributes about 14 % of the Nile's water at Aswan, Egypt. In contrast, these rivers have very low flow during the dry season.

The Tekeze (Atbara), rises in Northern Ethiopia Highlands and have the Angereb and Guang as its major tributaries, it replenishes the main Nile north of Khartoum. The Tekeze joins the Atbara River after entering northeastern Sudan. The climatic pattern and physical environment of the Tekeze sub- system are very similar to those of the Abbay subbasin.

The climate varies from warm, desert-like climate at the Sudan border, to wet in the Ethiopian Highlands. The annual rainfall ranges from 800 mm to 2200 mm with an

average of about 1420 mm for the Abbay river basin. The annual rainfall reaches at maximum of 3000 mm over the highlands and a minimum of 600 mm in the lowlands with annual average rainfall of about 1419 for the case of Baro Akobo Basin. In contrast to the Abbay and Baro Akobo river basins, the annual rainfall for Tekeze is much lower, ranging from 600 mm to 1200 mm with an average of about 900 mm. Most of rainfall occurs from June to September for all the three subbasins (MoWR, 2002).

3 Methods and materials

3.1 Model description

We used the physically based, distributed parameter model- SWAT (Soil and Water Assessment tool, version SWAT2005) which operates on daily time step and uses physiographical data such as elevation, land use and soil properties as well as meteorological data and, river discharge data for calibration (Arnold and Allen, 1996).

3.2 Hydrological processes

The hydrological processes included in the model are evapotranspiration (ET), surface runoff, infiltration, percolation, shallow and deep aquifers flow, and channel routing (Arnold et al., 1998). The effects of spatial variations in topography, land use, soil and other characteristics of watershed hydrology are incorporated by dividing a basin into several subbasins based on drainage areas of tributaries and is further divided the subbasins into a number of hydrological response unit (HRUs) within each subbasin, based on land cover and soils. Each HRU is assumed spatially uniform in terms of land use, soil, topography and climate. The subdivision of the watershed enables the model to reflect differences in evapotranspiration for various crops and soils. All model computations are performed at the HRUs level.

The fundamental hydrology of a watershed in SWAT is based on the following water balance equation

$$\frac{\partial SW}{\partial t} = R_{day} - Q_{surf} - ET_a - W_{seep} - Q_{gw} \quad (3.1)$$

Where SW is the soil water content (mm), R_{day} is the amount of precipitation on (mm), Q_{surf} is the amount of surface runoff (mm), E_a is the amount of evapotranspiration (mm), W_{seep} is the amount of water entering the vadose zone from the soil profile (mm), and Q_{gw} is the amount of ground flow (mm). Detail descriptions of the different model components can be found in Arnold et al. (1998) and Neitsch et al. (2002a).

3.3 Physiographical data for the three subbasins

A range of spatially distributed data such as topographic features, soil types, land use and the stream network (optional) are needed for the model. Table 1 summarizes the input data use in the AVSWAT-X interface.

3.3.1 Digital elevation model

A DEM was created using a 1 km^2 resolution topographic database obtained from the Ethiopian Ministry of Water Resources. The DEM (see Fig. 2) was used to delineate the watershed and the drainage patterns of the surface area analysis. Subbasin parameters such as slope gradient, slope length of the terrain, and the stream network characteristics such as channel slope, length, and width were derived from DEM.

Table 1: Data sources for the Eastern Nile basin.

Data Type	***Scale***	***Data Descriptions***
DEM (Topographical data)	1km*1km	Elevation data from Ethiopia ministry of water resources
Soil	10km*10km	Soil texture data from ministry of water resources supplemented by the FAO soil data base

Land use	1km*1km	Land classification and their attributes from Ethiopia ministry of water resources

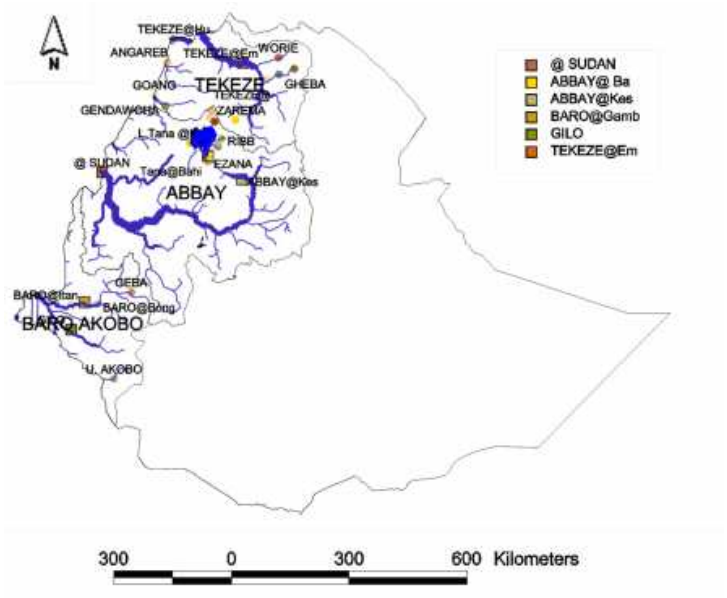

Figure 1: Map showing an outline of Ethiopia and the water sources of Eastern Nile basin including stream gauges at the major tributaries (dots) and stream gauges for calibration and validation of the model (boxes)

3.3.2 Land use and soil maps

Land use is one of the main factors affecting surface erosion, and evapotranspiration in a watershed. The source of land use map of the study is the Ministry of Water Resources Ethiopia and land use/land cover map was taken from the global Hydro1K dataset (Hansen, 1998) and modified to correspond with the SWAT predefined land uses classification (Fig. 3).

More than 50 %, 23 % and 15.7 % of Abbay, Tekeze and Baro Akobo subbasin, respectively, are used for agriculture whereas forest, grass, bush and shrubs cover the

rest. For detail see Fig. 3. Land use of the study area has changed over time (Rientjes et al., 2011) due to over increasing population density, changing agricultural practices, urbanization and water related infrastructure such as irrigation and hydropower production. As no detailed mapping of these changes exists for the whole region it is not taken into account.

Figure 2: Topography (m) of the eastern Nile basin based on a 1 × 1 km digital elevation model.

Different types of soil texture and physical chemical properties are required for SWAT simulations. These data were obtained from various sources. The soil map obtained from Ministry of Water Resources of Ethiopian at Water Resources Information and Metadata Base Centre department. However, several properties like moisture bulk

density, saturated hydraulic conductivity, percent clay content, percent silt content and percentage sand content of the soil which are required by SWAT model were not incorporated. These additional data were substantiated from various sources such as Wambeke (2003); USDA (1999) and FAO (1995). As it is shown in Fig. 4, the major soil types are lithosols and Eutric Cambisols for Tekeze subbasin: Chrome Acid Luvisols, Eutric Vertisol, Luvisols and lithic Leptosols for Abbay and Dystric cambisols and orthic Acrisols for Baro.

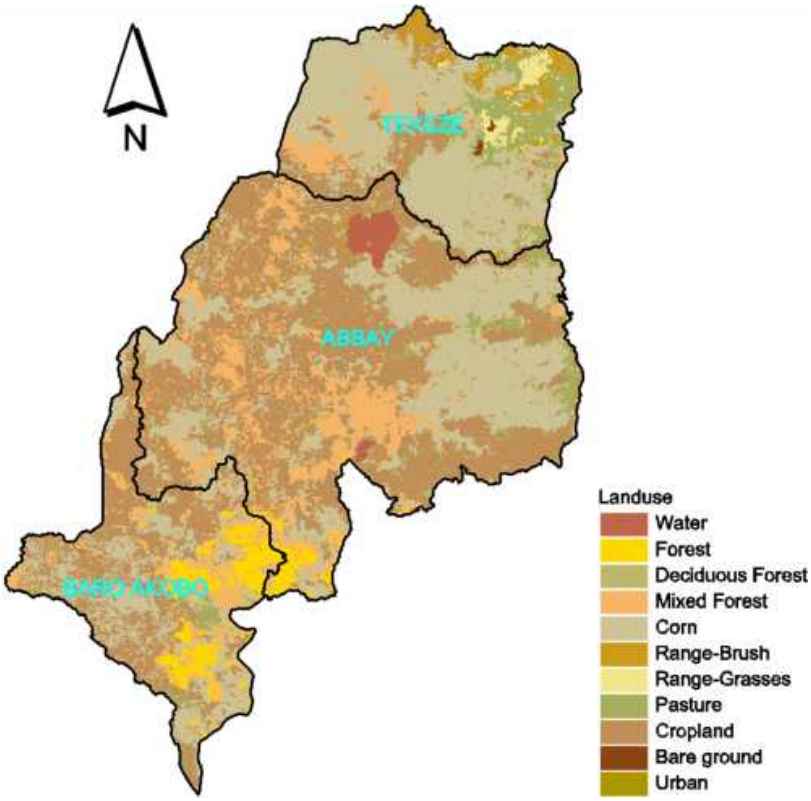

Figure 3: Map of land use of the three sub-basins of the Eastern Nile (Tekeze, Abbay and Baro Akobo)

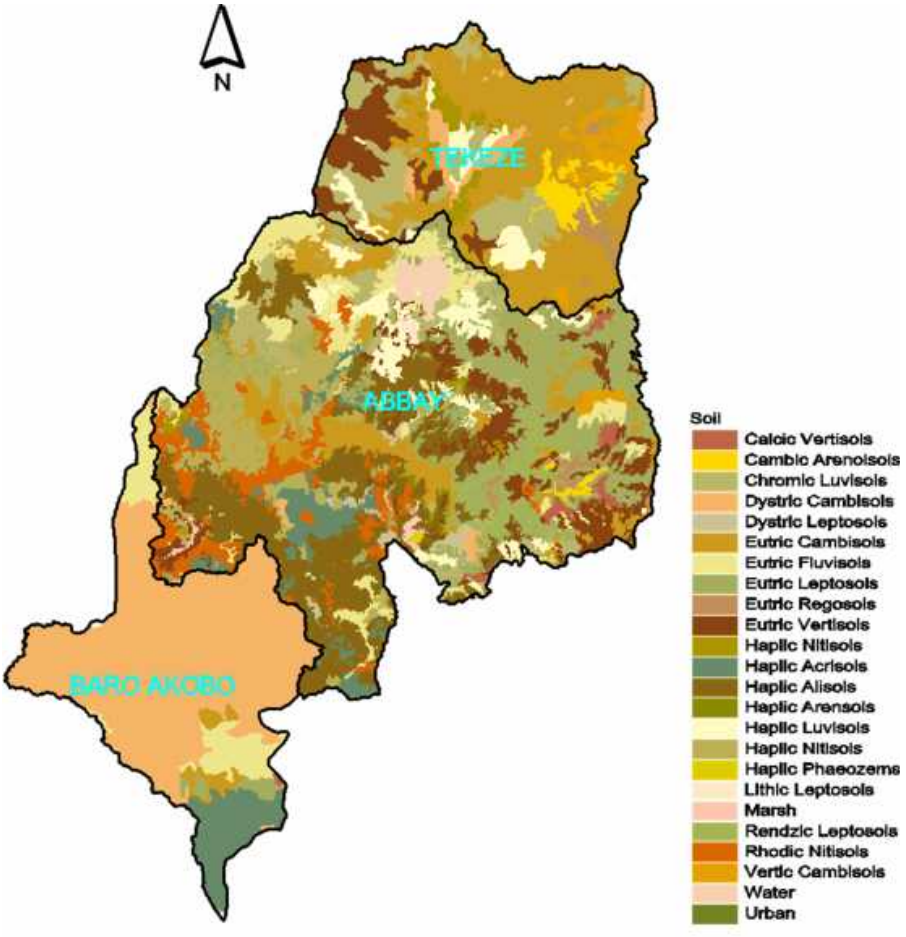

Figure 4: Map of soil types of the three sub-basins of the Eastern Nile (Tekeze, Abbay and Baro Akobo)

3.3.3 Meteorological Data

SWAT requires daily meteorological data, which were collected from the Ethiopian National Meteorological Agency (NMA) for the period 1987-2006. Figure 5 shows the stations used in this study and Table 2 summarize the number of stations in each subbasin. Missing values were filled using the SWAT built-in weather generator developed by Nicks, (1974). The weather generator used a first-order Markov chain

model. For each subbasin input to the weather generator was observed precipitation data for the weather station that was nearest the centroid of the subbasin and having a record length from 1967-2006. Given the observed wet and dry days frequencies, the model determines stochastically if precipitation occurs or not. When precipitation event occurs, the amount is determined by generating values from a skewed normal daily precipitation distribution or a modified exponential distribution which is calculated based on the observed data. The amount of daily precipitation is partitioned between rainfall and snowfall using average daily air temperature. The average percentage of missing data in the observed datasets was less than 10% and 5% of precipitation and temperature recorded data set respectively.

3.3.4 River Discharge

Hydrological discharge data were collected from the Ministry of Water Resources of Ethiopia. Table 3 summarizes the number of stream gauges with the date of the record length used for calibration and validation. All the flow data were daily except at Diem (Abbay, Sudan Border) where only monthly data was available.

3.5 Model Setup

The Abbay, Baro Akobo and Tekeze stream network and sub watersheds were delineated using ARCSAWT-X, following specification of the threshold drainage areas. The threshold area is the SWAT suggested drainage area required to form the origin of the stream. 24, 29, 25 sub watersheds; and 309, 128 and 313 HRUs of Abbay, Baro Akobo and Tekeze river basin-

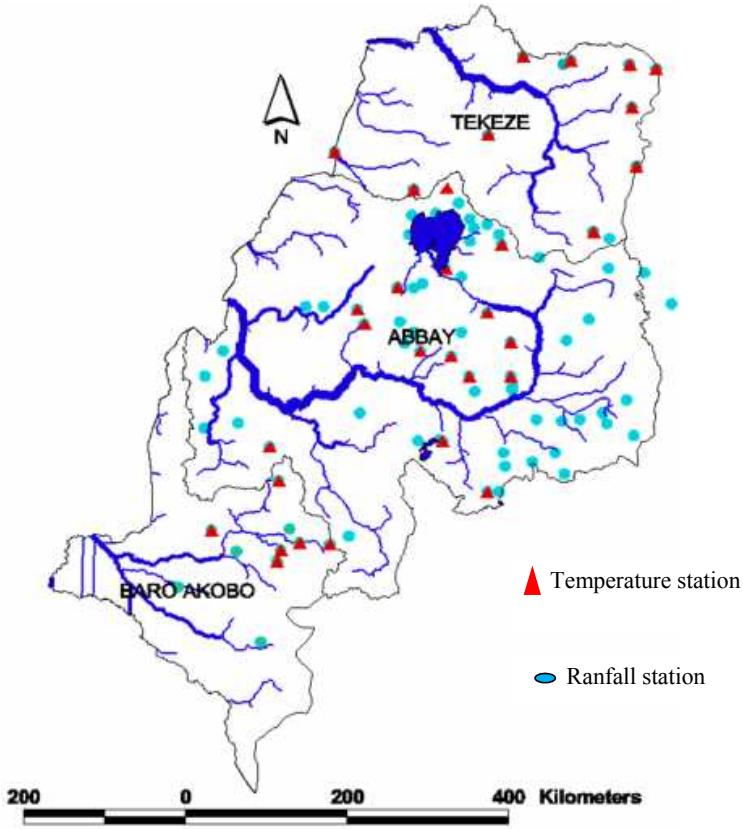

Figure 5: Main Rivers and meteorological stations in the eastern Nile basin.

Table 2: Meteorological data sources for Eastern Nile basin.

Data Type	***Number of stations***	***Data Descriptions***
Temperature (Tmax and Tmin)	Abbay 42stations Baro Akobo 8 stations Tekeze 10 stations	Daily data from the Ethiopian National Meteorological Agency (NMSA)
Precipitation	Abbay; 74 stations BaroAkobo 12 stations Tekeze 11stations	Daily data the Ethiopian National Meteorological Agency (NMSA)

Table 3: Streams gauges and their corresponding drainage area with calibration and validation dates used for model simulation

Stream gauge	Drainage Area(km2)	Calibration date[1]	Validation date
Tana outlet (Abbay)	15321	1/1/1991-12/31/1996	1/1/1997-12/31/2000
Kessie (Abbay)	65784	1/1/1991-12/31/1996	1/1/1997-12/31/2000
Diem (Abbay)	17400	1/1/1991-12/31/1996	1/1/1997-12/31/2000
Embamadre (Tekeze)	45694	1/1/1994-12/31/1999	1/1/2000-1/31/2003
Gambella (Baro Akobo)	23461	1/1/1990-12/31/1998	1/1/1999-12/31/2004
Gilo (Baro Akobo)	10137	1/1/1990-12/31/1998	No recorded data

as a function of 2% land use and 5% soil types within a given watershed, respectively were delineated up to the point of outlets for each subbasin. These points constituents of a drainage area of 174,000, 43,906, and 76,343 km^2 that drain about 86%, 60% and 93% of the entire Abbay (201,340km^2), Baro Akobo (74,102km^2) and Tekeze (82,350 km^2) subbasins, respectively which all are found in Ethiopia.

The SCS (Soil conservation service) curve number procedure (USDA-SCS,1972) was applied to estimate surface runoff volumes due to the unavailability of sub daily rainfall data required for the Green and Ampt method that SWAT offers a different option to estimate surface runoff. The potential evapotranspiration (PET) estimates and channel routing were performed using Hargreaves and Muskingum of the model option of SWAT, respectively.

[1] Time period variation were due to differences in readily available measured flow data records

3.6 Sensitivity Analysis

Table 4: List of adjusted parameters with calibrated values after manual and automatic calibration at the selected outlets for three subbasins of Eastern Nile using SWAT 2005 model.

Id	Parameter	Description	Range[2]	Initial values	Calibrated values	
				Abbay	Baro	Tekeze
1	CN_2	Initial SCS CN II value	±25%	*	-10%	-12%	-24%
2	Sol_K	Saturated Hydraulic conductivity [mm/mm]	±25%	**	-4%	1.3%	19%
3	ESCO	Soil evaporation compensation factor	0.0-1.0	0.95	0.7	0.58	0.8
4	SOL_AWC	Available water capacity [mm water/mm soil]	±25%	**	+25%	7%	9.4%
5	SOL_Z	Soil depth[mm]	±25%	**	-4%	25%	13%
6	GWQMN	Threshold water depth in the shallow aquifer for flow[mm]	0.0-5000	0.0	200	319	53
7	CANMX	Maximum canopy storage	0-10	0.0	9.7	2.4	0.31
8	ALPHA_BF	Base flow alpha factor	0.0-1.0	0.048	0.048	0.018	0.002

After pre-processing of the data and SWAT model set up, simulation was done for the periods indicated in Table 3 for the three sub basins. The built-in SWAT sensitivity analysis tool that uses the Latin Hypercube One- factor-AT-a –Time (LH-OAT) (Van Griensvenet al., 2002: Van Griensvenet,2005) was used. Six outlets (Figure 1) were selected for the sensitivity analysis; Three of them (Tana outlet, Kessie and Diem) in

- [2] The ranges are based primarily on recommendations given in the *SWAT User's Manual* (Neitsch et al. 2002a).
- * SWAT default parameters and SWAT driven parameters were used.
- ** Field measured and from literature collected parameters.

the Abbay, and two in Baro Akobo (Gambella and Gilo) and one in Tekeze (Embamadre).

According to Lenhart et al.(2002) the sensitivity of a flow to a parameter can be categorized into four classes. If the relative sensitivity lies between 0-0.05 and 0.05-0.2, then the parameter is classified as negligible and medium, respectively, whereas if it is varying between 0.2-1.0 and greater than 1 then categorized as high and very high class, respectively. Out of 28 selected parameters the curve number, available water capacity, average slope steepness, saturated hydraulic conductivity, soil evaporation compensation factor, soil depth, maximum canopy storage, threshold water depth in the shallow aquifer for flow, and base flow alpha factor were identified as being parameters to which the flow has medium, high or very high sensitivity. The ranking of the parameters was different at various outlets where sensitivity test was carried out. However, the curve number (CN_2) was the main sensitivity parameter for all outlets. This is due to the fact that the curve number depends on several factors including soil types, soil textures, soil permeability, land use properties etc. In addition, the relative sensitivity of the available water capacity (Sol-AWC), the soil evaporation compensation factor (ESCO) and the saturated hydraulic conductivity (Sol-K) were also high in all outlets. From the sensitivity test, eight parameters having a relative sensitivity greater than 0.05 (sensitivity of the flow to the parameter categorized as medium or higher) were selected for the calibration process.

The ranges are based primarily on recommendations given in the *SWAT User's Manual* (Neitsch et al. 2002a). SWAT default parameters and SWAT driven parameters were used. ** Field measured and from literature collected parameters.

3.7 Calibration and Validation

Watershed models contain many parameters; these parameters are classified into two groups: physical and process parameters**.** A physical parameter represents physically measurable properties of the watershed (e.g. areas of the catchment, fraction of impervious area and surface area of water bodies, surface slope etc) while process parameters represents properties of the watershed which are not directly measurable

e.g. average or effective depth of surface soil moisture storage, the effective lateral inflow rate, the coefficient of non-linearity controlling the rate of percolation to the groundwater (Sorooshian and Gupta, 1995). Thus, calibrations against available streamflow observations are often conducted to tune the model. Because automatic calibration relies heavily on the optimization algorithm and the specified objective function we follow the recommendations of Gan, (1998) to use both manual and automatic calibration procedures. We first conducted manual calibration of daily stream using the procedure developed by Santhi et al.(2001). Parameters identified from the sensitivity analysis were varied in sequence of their relative sensitivity within their ranges (Table 4) until the volume is adjusted to the required quantity (Zeray et al.,2007).This process continued till the volume simulated is within ±15% of the gauged volume.The surface runoff adjustment was then followed by that of the baseflow. Here,the same apporach was followed being the adjustment made to the most sensitivity parameters affecting the baseflow. Each time the baseflow calibration is finalized, the surface runoff volume was also checked as adjustment of the baseflow parameters can also affect the surface runoff volume. The same procedure was followed to calibrate the water balance of the monthly flows. After each calibartion, the coefficient of determintation (proportion of the variance in the observations explained by the model, R^2) and Nash-Sutcliffe effficeny value (E_{NS}) were checked ($R^2 > 0.6$ and $E_{NS} > 0.5$,Santhi et al.,2001). Finally, the automatic calibration algorithm in SWAT is used for fine tuning the calibration. This is based on the Shuffled Complex Evolution algorithm developed at the University of Arizona (SCE-UA) which is a global search algorithm that minimizes a single objective function for up to 16 model parameters (Duan et al., 1992).

The performance of SWAT was evaluated using the Nash-Sutcliffe efficiency value (E_{Ns}) and the coefficient of determination (R^2). The difference between the E_{Ns} and the R^2 is that the E_{Ns} can interpret the model performance in the replicating individually observed values while the R^2 does not (Rossi et al., 2008). It is only measuring the deviation from the best fit line. In addition, systematic difference between the model and observations in the percentage (PBias) and the ratio of the root mean square error between the simulated and observed values to the standard deviation of the

observations (RSR) was used. The equations and the interpretation of the values are given in Table 5. After manual and automatic calibration, the daily, monthly and annual streamflow were compared against the observed data.

3.8 Climate Sensitivity Scenarios

Climate sensitivity scenarios were performed by perturbing the baseline simulation (the validated simulation forced with observed station data) as input. The climate perturbations are given as a percentage change in precipitation (precipitation is multiplied with a given factor). Thus, the number of wet and dry days was not perturbed, only the precipitation intensity and degrees Celsius change for temperature (adding the prescribed change to the baseline simulation temperatures) (Varanou et al., 2002). Each scenario was then run for the same simulation period as the baseline simulation. The perturbations applied are with temperature increases of 0, +2 and +4°C and precipitation changes of -20%, -10%, -5%, 0%, +5%, +10% and +20% and combination of the above temperature and precipitation perturbations to examine the sensitivity of the SWAT streamflow to the meteorological parameters. Climatic variables such as relative humidity, wind speed, cloud cover and solar radiation were considered to be unchanged.

The CMIP3 global coupled climate models (AOGCMs) were also applied to calculate annual mean temperature and precipitation changes from the base period 1980-2000 to 2080-2100 for the three subbasins. A total of 47 climate change simulations were assessed for each subbasin using three different emission scenarios (SRES A2, A1B and B1) and 19 models. Together with the sensitivity tests mentioned above and estimate of the impact of the AOGCMs temperature and precipitation changes on the annual streamflow of the different sub basins were conducted.

Table 5: General reported ratings for Nash-Sutcliffe efficiency (E_{NS}), Mean relative bias (PBIAS), Root mean square error-standard deviation ratio (RSR) and Coefficient of determination (R^2) for calibration and validation process (adopted from Rossi et al., 2008).

Formulae	*Value*	*Rating*
$E_{NS} = 1 - \left[\frac{\sum_{i=1}^{n} (x_{obs}(i) - y_{mod\,el}(i))^2}{\sum_{i=1}^{n} (x_{obs}(i) - \overline{x_{obs}})^2} \right]$	>0.65 0.54to 0.65 >0.50	Very good Adequate Satisfactory
$PBIAS = \left[\frac{\sum_{i=1}^{n} (x_{obs}(i) - y_{mod\,el}(i))}{\sum_{i=1}^{n} (x_{obs}(i))} \cdot 100 \right]$	<±20% ±20% to 40% >±40%	Good Satisfactory Unsatisfactory
$RSR = \frac{\left[\sqrt{\sum_{i=1}^{n} (x_{obs}(i) - y_{mod\,el}(i))^2} \right]}{\sqrt{\sum_{i=1}^{n} (x_{obs}(i) - \overline{x_{obs}})^2}}$	0.0≤RSR≤0.5 0.5<RSR≤0.6 0.6<RSR≤0.7 RSR≥0.70	Very good Good satisfactory unsatisfactory
$R^2 = \frac{\left[\sum_{i}^{n} (x_{obs}(i) - \bar{x}_{obs})(y_{mod\,el}(i) - \bar{y}_{mod\,el}) \right]^2}{\sum_{i}^{n} (x_{obs}(i) - \bar{x}_{obs})^2 \sum_{i}^{n} (y_{mod\,el}(i) - \bar{y}_{mod\,el})^2}$	0.6	satisfactory

3.9 Sensitivity of annual streamflow to climate change

The relative sensitivity of the streamflow ($\Delta Q_{\Delta P, \Delta T}$) to either a precipitation (ΔP) or a temperature (ΔT) change or a combination of the two is calculated as:

$$\Delta Q_{\Delta P,\Delta T} = \frac{(Q_{\Delta P,\Delta T} - Q_{\Delta P=0,\Delta T=0})}{Q_{\Delta P=0,\Delta T=0}} \cdot 100 \qquad (3.2)$$

where Q is the annual or seasonal streamflow calculated using equation (3.1).

To be able to investigate if there is any nonlinearity in the streamflow change when both precipitation and temperature are changed we estimate the linear combination of the two.

$$\Delta Q_{\Delta T,\Delta P} = \left.\frac{\partial Q}{\partial P}\right|_{\Delta P,\Delta T=0} \Delta P + \left.\frac{\partial Q}{\partial T}\right|_{\Delta T,\Delta P=0} \Delta T \qquad (3.3)$$

where the local derivatives for each parameter is calculated as the sensitivity response when the other factor is kept unchanged. For example, $(\partial Q/\partial P)|_{\Delta P,\Delta T=0}$ are the responses in $m^3/\%$ of the simulations covering the precipitation perturbations ±5, 10 and 20% and no temperature perturbation. Any deviation from this will indicate nonlinear effects that may arise as precipitation and temperature is changed simultaneously.

4. Results and discussion

The result part starts with a validation of the SWAT model in the three different sub-basins, then estimates of the individual sensitivity of the streamflow to temperature and precipitation in conducted before we investigate if the combined effect of temperature and precipitation changes may provide any non-linearities in the streamflow response. Finally we combine the sensitivity simulations with temperature and precipitation

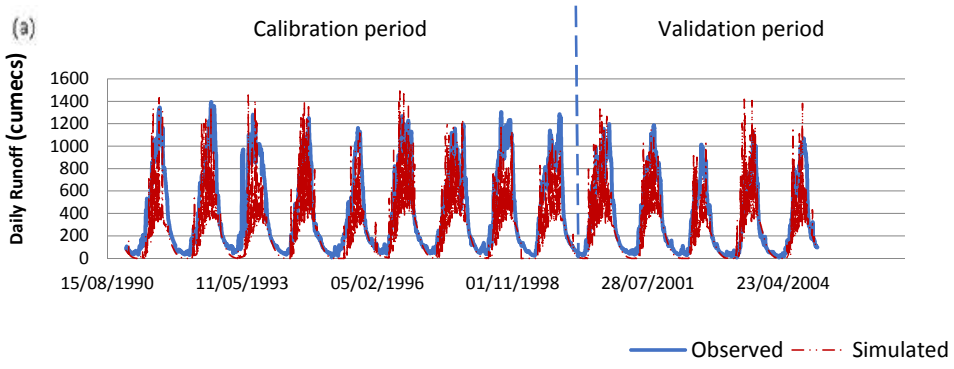

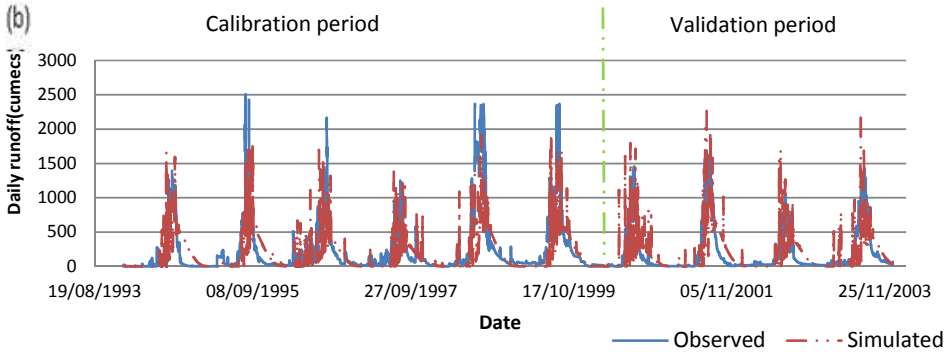

Figure 6: Daily calibration and validation (a) Baro Akobo at Gambella (b) Tekeze at Embamadre subbasins

changes from the CMIP3 coupled climate models to investigate the range of possible streamflow responses given the uncertainty in the global model's temperature and precipitation change.

4.1 Model calibration and validation

4.1.1 Abbay calibration and validation

The model was calibrated for the Abbay subbasin with one upstream (Tana), one mid-way (Kessie) and one downstream (at the Sudan Border) gauging station. It slightly overestimated the flow in the upper and middle part of the basin and underestimated it in the lower part (Table 6) during the calibration period (the calibration and validations periods are given in Table 3). The overestimation of these simulations was particularly pronounced during extreme events (not shown). However, there were good agreements between simulated and observed flows on both daily and monthly time scale (Figure 7a) for most of the years except 1995, when little rainfalls were recorded at Tana outlet. The E_{NS} and R^2 ranged from 0.62 to 0.90 and 0.90 to 0.97, respectively for the monthly calibration (see Table 7 for further details). The daily calibration statistics were lower ranging from 0.62 to 0.65 and 0.77 for E_{NS} and R^2, respectively (see Table 6).

In the validation period, the model similarly overestimated the flow at Tana outlet and at Kessie for the year 2000 giving slightly higher bias than the validation period. Thus, the daily and monthly E_{NS} simulation efficiency was between 0.55 to 0.57 and. 0.53 to 0.65, respectively.

4.1.2 Baro Akobo calibration and validation

Figure 6a and 7b show the time-series comparison of predicted and measured daily and monthly streamflows for the Baro Akobo subbasin at River Baro near Gambella over the 9-year (1990-1998) calibration period. In general, SWAT accurately tracked the measured streamflows for the time, although some peak flow months were over predicted. The time series comparison of predicted and measured cumulative daily and monthly streamflows for the 6-year (1999-2004) validation period is shown in the right side of the dashed line of Figure 6a and 7b, for the Baro Akobo subbasin at River Baro near Gambella. The predicted flows closely followed the corresponding measured flows, with less over prediction of peak flow months, as compared to the calibration period. Daily, and monthly, statistics computed for the calibration and validation periods (table 3 and 4) also show strong correlations between the simulated and measured flows. The validation period statistics were weaker than those computed for the calibration period (e.g. for daily data the Nash-Sutcliffe efficiency value (ENs) ranged from 0.70 to 0.81 for the calibration period and was 0.64 for the validation period (Table 6), whereas, the monthly values were higher than 0.80 for both of the periods).

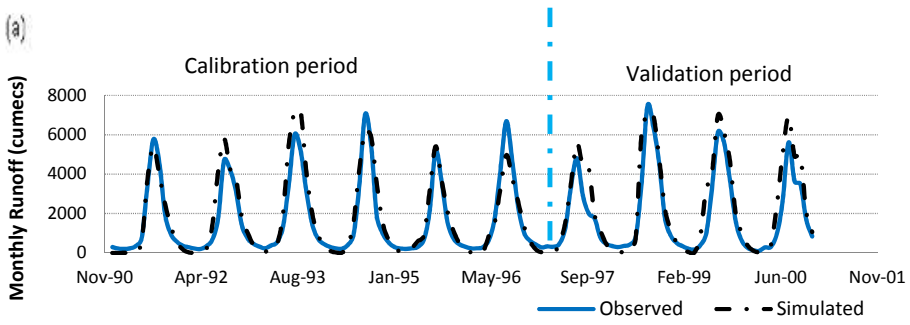

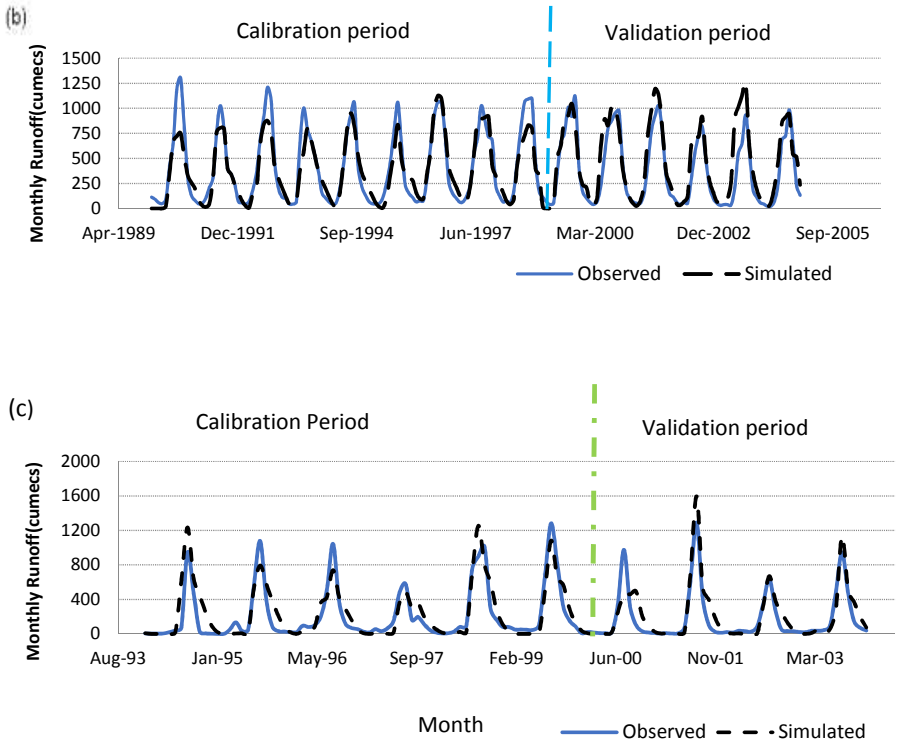

Figure 7: Monthly calibrations and validation at (a) Diem (Blue Nile), (b) Gambella (Baro Akobo and (C) Embamadre (Tekeze) subbasins

Table 6: Summary of daily streamflow statistics for the calibration and validation simulations for the Eastern Nile subbasins: Dates for calibration and validation period are given in Table 3.

Location	**Calibration**				**Validation**			
	E_{Ns}	**RSR**	**PBias**	**R^2**	**ENs**	**RSR**	**PBias**	**R^2**
Tana outlet (Abbay)	0.65	0.48	38	0.77	0.55	0.74	25	0.78
Kessie (Abbay)	0.62	0.57	14.2	0.77	0.57	0.66	9.9	0.71
Embamadre (Tekeze)	0.50	0.74	20	0.60	0.8	0.60	6.9	0.68
Gambella(Baro AKobo)	0.70	0.45	-10.9	0.65	0.64	0.40	-25.0	0.79
Gilo (Baro Akobo)	0.81	0.46	-11.1	0.86				

4.1.3 Tekeze calibration and validation

Calibration and validation of the Tekeze subbasin were carried out at Tekeze River near Embamadre and the predicted streamflows closely followed the corresponding measured flows, with a E_{NS} of 0.8 and 0.5, and with a R^2 of 0.81 and 0.60 for monthly and daily values during the calibration and validation periods (Table 7 and Table 6), respectively. Further, a bias of 2% in the calibration period also indicated a good agreement between measured and simulated monthly flows (Table 7).

Table 7: Summary of monthly streamflow statistics for the calibration and validation simulations for the Eastern Nile subbasins: Dates for calibration and validation period are given in Table 3.

Location	Calibration				Validation			
	E_{Ns}	RSR	PBias	R^2	ENs	RSR	PBias	R^2
Tana outlet	0.85	0.32	7.2	0.90	0.53	0.71	21	0.86
Kessie	0.62	0.58	28	0.90	0.54	0.80	37	0.86
Diem	0.90	0.31	-11.3	0.97	0.65	0.39	8.2	0.92
Embamadre	0.80	0.45	2.2	0.81	0.83	0.42	-13.9	0.88
Gambella	0.90	0.31	-3.8	0.92	0.81	0.44	-23.0	0.89
Gilo	0.93	0.40	-2.4	0.91				

4.2 The Annual Water Balance of the Eastern Nile

Table 8 illustrates the average annual water balance components of the Eastern Nile Basin during the calibration and validation periods. 58/57 percent, 56/58 percent and 62/64 percent of the average annual rainfalls were lost through evaporation in Abbay, Baro Akobo and Tekeze subbasin of the Eastern Nile during calibration and validation period, respectively. The average runoff coefficients were thus estimated to be 0.24, 0.30 and 0.18 for Abbay, Baro Akobo and Tekeze subbasins respectively. Surface runoff carried 55/58.5 percent, 71.6/74 percent and 51/54 percent of the water yield during the calibration and validation process for Abbay, Baro Akobo and Tekeze

Table 8: Annual averaged calibrated/validated hydrological balances and percent contribution of water balance components for the Eastern Nile basin SURQI: surface runoff, LATQ[II]: lateral flow into stream, GW_Q[III]: groundwater in the shallow aquifer, ET[IV]: evapotranspiration, PET[V]: potential evapotranspiration (Hargreaves method is used), PERC[VI]: percolation below root zone (groundwater recharge), TLOS[VII]: transmission losses.

Subbasin	Period	Rainfall (mm)	SURQ[I] (mm)	LATQ[II] (mm)	GW_Q[III] (mm)	ET[IV](mm)	PET[V] (mm)	PERC[VI] (mm)	TLOS[VII] (mm)
Abbay	Calibration/ validation	1422/1547	314.4/410	1.63/1.7	264.8/302	820.9/816	1585/1558	286/327	11/12
	%	100/100	22/26	0.1/0.1	19/20	58/57		20/21	0.8/0.8
Baro Akobo	Calibration/ validation	1774/1682	527/492	0.3/0.24	233/199	997/979	1519/1542	253/215	24/23
	%	100/100	30/29	0.2/0.1	13/12	56/58		14/13	1/1
Tekeze	Calibration/ validation	931/872	169/162	1.3/1.0	164/140	579/556	1396/1419	179/154	5/4
	%	100/100	18/19	0.1/0.1	18/16	62/64		19/18	0.5/0.5

subbasins respectively. While, the groundwater contributions were 46/43 percent for Abbay, 31.7/30 percent for Abbay and 50/47 percent for Tekeze during calibration and validation period respectively.

4.3 Sensitivity of annual Eastern Nile streamflow to climate change

The impact of the perturbed temperature and precipitation scenarios on annual streamflows in the three subbasins are shown in Table 9 and details are given in the sections below.

Table 9: Percentage change in simulated average annual Streamflow for each of twenty climate change scenarios compared with the baseline scenario

	Precipitation change (%)																				
Temp. Change	Abbay							Baro Akobo							Tekeze						
	-20	-10	-5	0	5	10	20	-20	-10	-5	0	5	10	20	-20	-10	-5	0	5	10	20
0	-34.9	-18.2	-9.3	0.0	9.8	19.6	40.3	-37.6	-22.5	-14.6	0.0	2.2	10.9	28.9	-42.1	-19.9	-10.8	0.0	12.6	33.0	62.7
+2	-38.6	-22.3	-13.5	-4.4	5.2	14.9	35.4	-43.0	-28.4	-20.6	-6.4	-5.3	4.2	21.8	-41.4	-19.1	-9.5	1.3	13.9	33.8	63.5
+4	-40.4	-24.4	-15.7	-6.6	2.9	12.5	32.8	-43.5	-29.1	-21.4	-7.3	-4.3	3.3	20.8	-44.9	-23.5	-14.0	-3.4	8.8	27.9	57.0

4.3.1 Sensitivity to precipitation changes

Sensitivity of annual streamflow to changes in precipitation, holding the temperatures fixed (equation 3.2) was different among the three subbasins. As a first approximation, a linear regression analysis of the streamflow responses for the various scenarios indicated that a 10% change in precipitation would produce a 19%, 17%, and 26% change in streamflow for Abbay, Baro Akobo and Tekeze river basin respectively (Figure 8). Table 9 and Figure 10 shows that the Abbay subbasin is equally sensitive to a reduction and increase in precipitation and the sensitivity is changing linearly with the precipitation change. This was not the case or Tekeze. The sensitivity to a precipitation increase was larger than to a decrease in precipitation (-42% and 63% change for a -20% and +20% precipitation changes, respectively). For the Baro Akobo subbasin, this was the opposite. Sensitivity was stronger to a decline in precipitation (-38% and 29% for -20 and +20% precipitation change, respectively). See Table 9 and Figure 10 for details. The change in sensitivity was likely due to the difference in topography and catchment characteristics of the subbasins. In the case of Tekeze basin, most of the region is categorized with a gentle slope, where sheet flow is dominating during an increase in precipitation. This is in contrast to Baro Akobo where 2/3 of the total drainage area is a plain. The land use and soil types of the two basins are also quite different. The depth of the soil in the Tekeze subbasin is shallower than Baro Akobo subbasin. Therefore, with an increase in precipitation, the response of the catchment generating direct streamflow will be smaller since more water infiltrated down to recharge the groundwater in the case of Baro Akobo subbasin. Thus, the sensitivity of Baro Akobo to an increase in precipitation will be smaller.

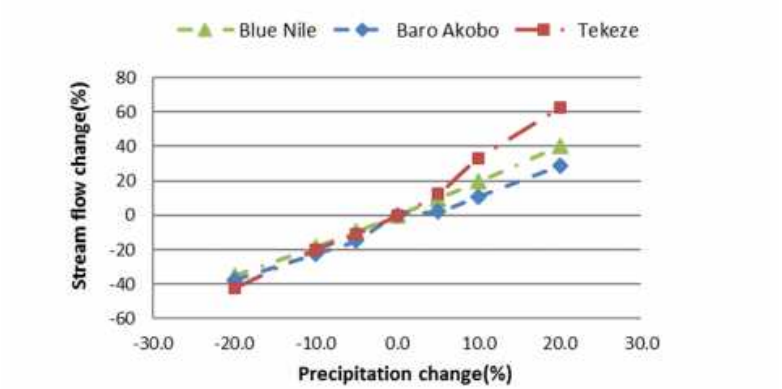

Figure 8: Annual streamflow changes to precipitation change holding temperature fixed for the three basins

4.3.2 Sensitivity to Temperature change

The relative sensitivity of streamflow to changes in temperature, holding the precipitation fixed (equation 3.2) was relatively modest in all the three subbasins (Figure 9). A linear regression analysis of the streamflow responses for the various temperature scenarios indicated that a 1˚C increase in temperature would produce a 4.4%, 6.4%, and 1.3% reduction in streamflow for Abbay, Baro Akobo and Tekeze

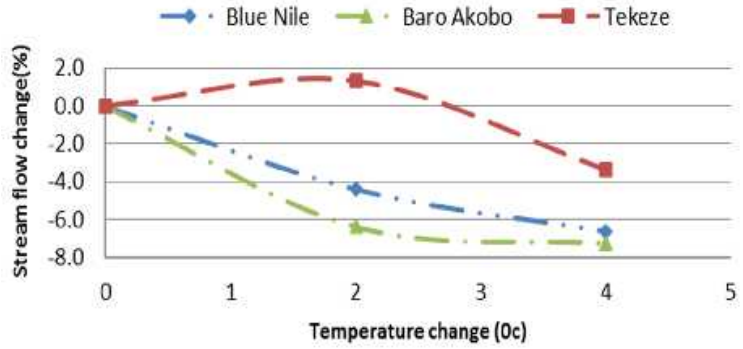

Figure 9: Annual streamflow changes to temperature change holding precipitation fixed for the three basins

river basin respectively (Figure 9). However, the sensitivity was not linear. Two of the subbasins (Abbay and Baro Akobo) showed a larger sensitivity from 0 to +2^{o}C than

from +2^{0}C to +4^{0}C. The reason was mainly due to the evaporation losses from the soil. When the temperature rises, the available water at the top surface of the soil gets lost easily whereas it is difficult to evaporate water from the deeper layers of the soil. Thus, a small change in temperature dries out the upper soil layer while a larger change will be less efficient in changing evaporation as the upper soil is already tried out. The Tekeze basin was less sensitive to temperature change compared to the other basins because the basin had limited moisture for approximately 2/3 of the year with today's temperatures.

4.3.3 Sensitivity to the combined effect of temperature and precipitation

Comparing the relative sensitivities of the streamflows when both temperature and precipitation were changed with the linear combination of sensitivities for the separate temperature and precipitation changes (equation 3.3) revealed that all regions shows a combined response that is very similar to the linear combination of the separate temperature and precipitation response (Figure 10). The only hint of a non-linear effect is in the Tekeze basin where combining a 4°C temperature increase with a positive precipitation increase gave a response that was around 2% smaller than the linear combination of the sensitivities (Figure 10c).

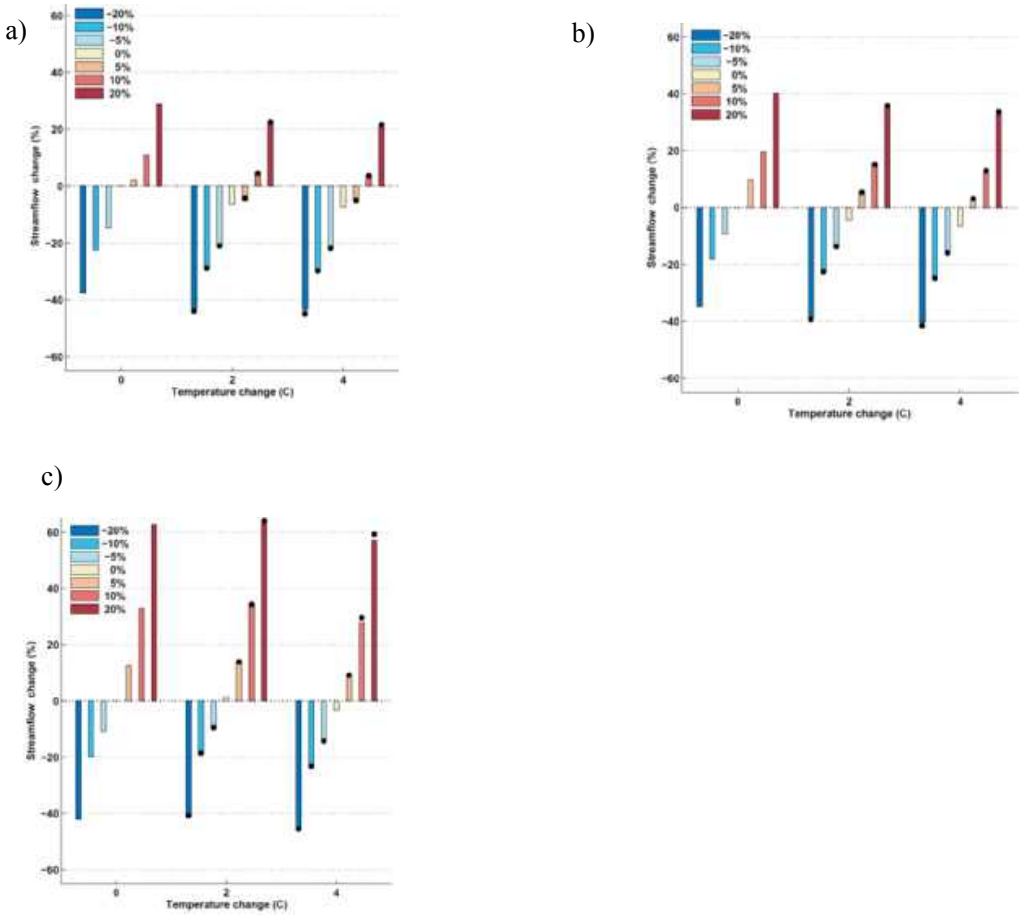

Figure 10: Change in annual streamflow (%) for different temperature and precipitation scenarios. a) Baro Akobo, b) Abbay and c) Tekeze. Black dots indicate the linear sensitivity estimate based on equation 3.3.

4.3.4 Estimation of future streamflow using CMIP3 simulations

To assess the uncertainty in future streamflow changes for the Eastern Nile we calculated the temperature and precipitation changes in the CMIP3, global coupled climate models (AOGCMs) with three different emission scenarios (SRES A2, A1B and B1). A total of 47 simulations with 19 different models were conducted. As the AOGCMs often have, large biases when it comes to reproducing the regional climatic

features, they are not well suited to force hydrological models without extensive bias corrections. An alternative approach is to use the combined temperature and precipitation changes of the AOGCMs, with the sensitivities of the above simulations $\Delta Q_{\Delta P,\Delta T}$ (equation 3.2), where ΔP and ΔT are taken from the AOGCMs and $\Delta Q_{\Delta P,\Delta T}$ is the linearly interpolated results of the sensitivity simulations. For example, if the temperature change

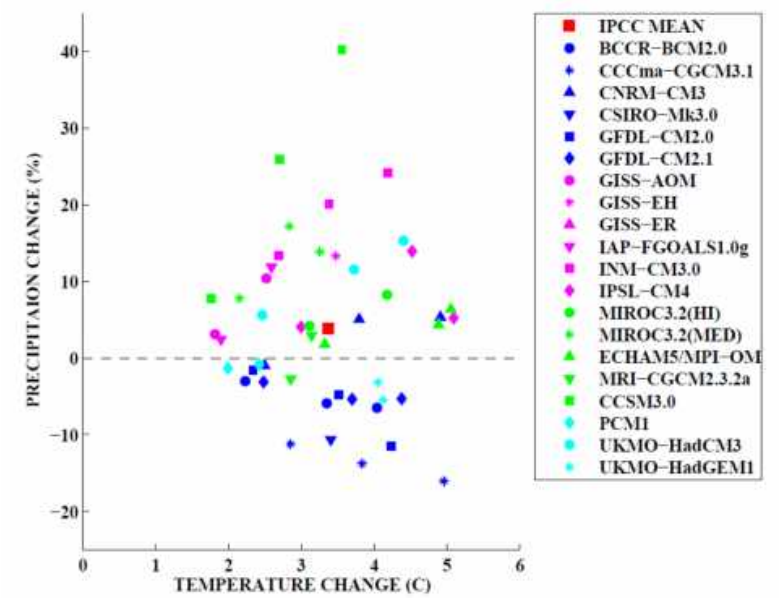

Figure 11: Change in temperature (°C) and precipitation (%) for the period 2081-2100 compared to 1981-2000 from 19 AOGCMs and three emission scenarios (totally 47 simulations). Red square indicates the mean change over all simulations.

is 3.1°C and precipitation change is 18%; $\Delta Q_{\Delta P,\Delta T}$ is the linear interpolation for the four sensitivity simulations +2. °C and +10%, +2. °C and +20%, +4. °C and +10% and +2. °C and +20%. tests. The results revealed that all models agreed on a temperature rise, but they disagreed on the direction of precipitation change (Figure 11). The large uncertainty in the models' precipitation change translated into large uncertainties in the

streamflow changes (Figure 12). Around 60%, 40% and 55% of the estimates indicated an increased annual flow in the Abbay, Baro Akobo and Tekeze, respectively and the ensemble mean changes were modest in all three basins (5%, -1%, and 12% the Abbay, Baro Akobo and Tekeze, respectively). However, the extremes ranged from a 152% increase in the Tekeze basin using the CCSM 3.0 SRES A2 scenario changes to a 55% reduction in the same basin using the same scenario, but the values were from the GFDL CM2.0 model (Figure 12c). This is in line with the large spread found for the Abbay in Elshamy et al. (2009).

5. Summary and Conclusion

This study report on a first attempt to use a physically based, distributed hydrological model (SWAT) forced with daily station based precipitation and temperature data and calibrated with daily streamflow measurements to simulate the Eastern Nile streamflow.

SWAT2005 adequately simulated monthly variability in flows for the Eastern Nile basin. The total simulated monthly streamflow ranged from good ($0.65<E_{NS}<0.75$ to very good ($E_{NS}>0.75$). The average daily and monthly difference between the observed and simulated flow (PBIAS) was good (PBIAS$\leq\pm$20%) for the calibration period with the exception of the Abbay subbasin where it was only satisfactory ($\pm$20 %< PBIAS$\leq\pm$40%). In summary, good performance of the model in the validation period indicate that the fitted parameters during calibration period listed in Table 4 can be taken as a representative set of parameters for the Eastern Nile watershed and further simulation and evaluation of alternative scenario analysis for other periods using the SWAT model. The model simulated monthly flows better than daily flows and the model was probably not adequate for studies of single sever events in small catchments. Sixty percent of the average annual rainfalls were estimated to be lost through evaporation. The simulations estimated the runoff coefficients to be 0.24, 0.30 and 0.18 for Abbay, Baro Akobo and Tekeze subbasin respectively. Surface runoff carried around 55% of the streamflow in the Abbay and Tekeze while in Baro Akobo the percentage was about 72. The remaining contribution was from groundwater.

The streamflow sensitivity to changes in precipitation and temperature differed among the basins and depended on the strength of the changes. The annual streamflow responses to a 10% change in precipitation with no temperature change were on average 19%, 17%, and 26% for Abbay, Baro Akobo and Tekeze river basin respectively. However, the responses to a reduction and increase in precipitation were not the same. While Baro Akobo was more sensitive to a reduction in precipitation, Tekeze showed a larger sensitivity to an increase. The streamflow sensitivity to temperature was moderate. The average annual streamflow responses to a 1°C change in temperature and no precipitation change were -4.4%, -6.4%, and -1.3% for the Abbay, Baro Akobo and Tekeze river basin respectively. The very low sensitivity of the Tekeze basin indicated that flows were moisture limited for a large part of the year.

a)

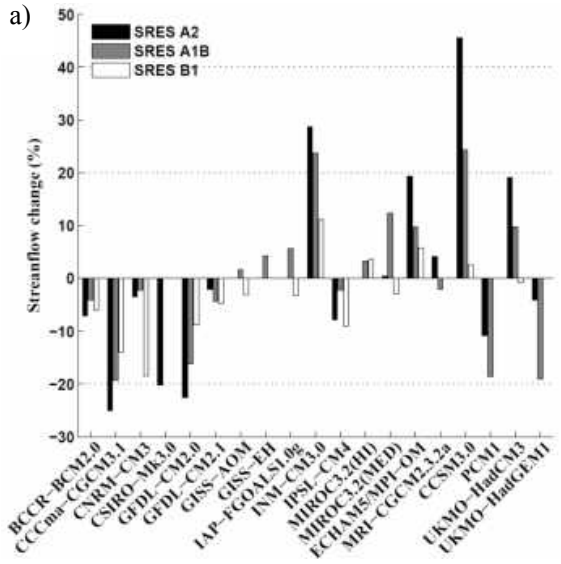

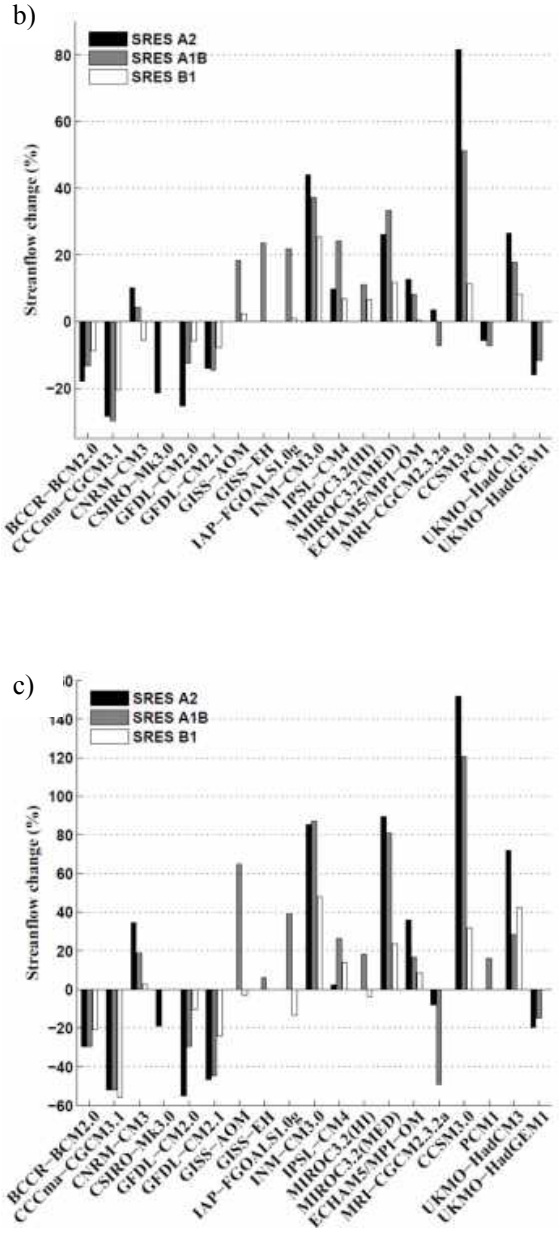

Figure 12: Change in annual streamflow (%) for the a) Baro Akobo, b) Abbay and c) Tekeze basins using the calculated combined temperature-precipitation sensitivities and precipitation and temperature changes (2081-2100 compared to 1981-2000) from 19 AOGCMs and three emission scenarios (totally 47 simulations for each sub-basin).

The overall assessment made by a sensitivity analysis for the 20 hypothetical climate sensitivity scenarios, revealed that the annual streamflow of the Eastern Nile was very sensitive to variations in precipitation and moderately sensitive to temperature changes. In addition, we showed that the modelled response of a combined temperature and precipitation change was very similar to adding the responses from the temperature change only and precipitation change only simulations.

Applying the combined temperature-precipitation sensitivities and 47 temperature and precipitation scenarios from 19 AOGCMs participating in CMIP3, we estimated the future streamflow change to be very uncertain and strongly dependent on the choice of climate model. The reason was the disagreement between the different climate models on both the strength and the direction of future precipitation changes. Thus, based on the state of the art climate models little can be said about future changes in Eastern Nile streamflow. However, our analysis emphasis the need for doing ensemble runs using different climate models in this type of assessment. This uncertainty may have implications for long-term water resource planning, estimation of the future hydropower potential, reservoir design and to which extent development of agriculture should utilize river or groundwater based irrigation systems.

Finally, we note a few of the weaknesses of this analysis. The first is that it tried to address the climate change impact with only one hydrological model and two forcing variables (precipitation and temperature), neglecting all other variables (such as vegetation or radiation changes) which might affect the runoff generation. In our sensitivity studies, we multiplied the precipitation with a fraction. This means that we assumed the wet-day frequency was unchanged and the whole precipitation change was given as a change in intensity. For temperature, we added a constant for the whole year and thereby assuming that the changes were not depending on season. Finally, we used a simple linear estimate to link the CMIP3 climate change scenarios to changes in streamflow. These were all crude assumptions. However, we feel that given the huge uncertainty in the future precipitation changes partly justifies this crude treatment.

Acknowledgements

This work has been carried out with support from the Ethiopian Malaria Prediction System (EMaPS) project funded by the Norwegian Program for Development, Research and Education (NUFU) and the University of Bergen.

References

Allen, R. G.: A penman for all seasons, J. Irrigat. Drain
Engin. ASCE, 12(4), 348–368, 1986.15

Arnold, J. G. and Allen, P. M.: Estimating hydrologic budgets for three Illinois watersheds, J. Hydrol., 176(1–4), 57–77, 1996.

Arnell, N.W., C. Liu, R. Compagnucci, L. da Cunha, K. Hanaki, C. Howe, G. Mailu, I. Shiklo-manov, and E. Stakhiv.:. Impacts, Adaptation, and Vulnerability. *In:* Climate Change 2001: JJ. McCarthy, O. Canziani, N.A. Leary, D.J. Dokken, and K.S. White (Editors). Cambridge University Press, Cambridge, United Kingdom, Hydrology and Water Resources, Chapter-4, pp. 191-233, 2001.

Arnold, J. G., Allen, P. M., and Bernhardt, G.: A comprehensive surface groundwater flow model, J. Hydrol., 142, 47–69, 1993.

Arnold, J. G., Sir invasion, R., Muttiah, R. S., and Williams, J. R.: Large area hydrologic mod-20elling and assessment, Par t 1: Model development, J. Am. Water Resour. Assoc., 7389, 1998.

Arsano, Y.: Ethiopia and the Nile: The Dilemma of National and Regional Hydro-politics, PhD dissertation, Zurich, Switzer land, University of Zurich, 2004.

Arsano, Y.: Ethiopia and the Easter n Nile basin, Aquat. Sci., 67, 16–17, doi: 10.1007/s00027-25004-0766-x, 2005.

Barrett, C. B.: The development of the Nile hydro meteorological forecast system, Hydrol. Process. 933–938, 1993.

Chiew, F. H. S.: Estimation of rainfall elasticity of streamflow in Australia, Hydrol. Sci. J., 51,613–625, 2006.

Checkol, D. A.: Modeling of Hydrology and Soil Erosion of Upper Awash River Basin, Cuvillier, Gottingen, 2006.

Conway, D.: A water balance model of the upper Blue Nile in Ethiopia, Hydrol. Sci. J., 42(2), 5265–286, 1997.

Duan, Q., Sorooshian, S., and Gupta, V.: Effective and efficient global optimization for conceptual rainfall-runoff models, Water Resour. Engin. 1015–1031, doi: 10.1029/91WR02985, 1992.

Dugale, G., Hardy, S., and Milford, J. R.: Daily catchment rainfall estimated from METEOSAT, Hydrol. Process, 5, 261–270, 1991.

Eckhardt, K. and Arnold, J. G.: Automatic calibration of a distributed catchment model, J. Hydro., 251, 103–109, 2001.

Elshamy, M. E., Seierstad, I. A., and Sorteberg, A.: Impacts of climate change on Blue Nile flows using bias-corrected GCM scenarios, Hydrol. Earth Syst. Sci., 13, 551–565, 15, doi: 10.5194/hess-13-551-2009, 2009.

FAO: Soils of EAST Africa, SEA, Food and Agriculture Organization of the United Nations, ACD-Rom Data, Rome, 1995.

FAO: The Soil and Terrain Database for Northeaster n Africa (CD-ROM), FAO, Rome, 1998.

Fu, G., Charles, S. P., and Chiew, F. H. S.: A two-parameter climate elasticity of stream-flow index to assess climate change effects on annual streamflow, Water Resour. Res., 43, W11419, doi: 10.1029/2007WR005890, 2007.

Gan, T. Y.: Application of scientific modelling of hydrological responses from hypothetical small Catchments to access a complex conceptual rainfall runoff model, Water Resources Series Tech. Rept. 111, University of Washington, Seattle, Washington, 1988.25.

Green, W. H. and Ampt, G. A.: Studies on soil physics. 1. The flow of air and water through soils, J. Agric. Sci., 4, 11–24, 1911.

Guo, H., Hu, Q., and Jiang, T.: Annual and seasonal streamflow responses to climate and land-cover changes in the Poygan Lake basin, China, J. Hydro., 355, 106–122, 2008.

Hamouda, M. A., Nour El-Din, M. M., and Moursy, F. I.: Vulnerability assessment of water resources system in the Easter n Nile basin, Water Resources Manage., 23, 2697–2725, 2009.

Hansen, M., Defries, R., Townshend, J. R. G., and Sohlberg, R.: UMD Global Land Cover Classification, Specify 1 Degree, 8 Kilometer, or 1 Kilometer (1.0), Department of Geography, University of Mar yland, College Par k, Mar yland, 1981–1994, 1998.

Hargreaves, G. H. and Samani, Z. A.: Agricultural benefits for Senegal River basin, J. Irrigat. Drain. Engin. 111, 113–124, doi: 10.1061/ (ASCE) 0733-9437(1985)111:2(113), 1985.

Johanson, P. A. and Curtis, P. D.: Water balance of Blue Nile River basin in Ethiopia, J. Irrigat. Drain. Engin, 120, 573–590, 1994.

Lenhart, T., Eckhardt, K., Fohrer, N., and Frede, H. G.: Comparison of two different approaches of sensitivity analysis, Phys. Chem. Earth, 27, 645–654, 2002.

Manoj Jha, Jeffrey G. Arnold, Philip W. Gassman, Filippo Giorgi, and Roy R. GU.: Climate change sensitivity assessment on upper Mississippi River Basin Streamflows using SWAT, J.the Amec.wat.Res.Ass., Center for Agricultural and Rural Development, Department of Economics, Iowa State University, Ames, Iowa, 50011-1070; Grassland, Soil and Water Research Laboratory, U.S. Department of Agriculture, Agricultural Research Service, 808 East Blackland Road, Temple, Texas 76502; Center for Agricultural and Rural Development, Department of Economics, Iowa State University, Ames, Iowa, 50011- 1070; Abdus Salam International Centre for Theoretical Physics, Physics of Weather and Climate Section, Strada Costeira 11, 34100 Trieste, Italy; Department of Civil Engineering, 494 Town Engineering, Iowa State University, Ames, Iowa 50011-3232,2007.

Mohamed, Y. A., van den Hur k, B. J. J. M., Savenije, H. H. G., and Bastiaanssen, W. G. M.: Hydroclimatology of the Nile: results from a regional climate model, Hydrol. Earth Syst. Sci., 9, 263–278, doi: 10.5194/hess-9-263-2005, 2005.
Monteith, J. L.: Evaporation and the Environment. The State and Movement of Water in Living15 Organisms, Cambridge University Press, Sawnsea, 205–234, 1965.
MoWR: Ethiopian water sector strategy, Ministry of Water Resources, Addis Abeba, 2002.
Neitsch, S. L., Arnold, J. G., Kinir y, J. R., Srinivasan, R., and Williams, J. R.: Soil and Water Assessment Tool User's Manual, Version 2000, Temple, Tx. USDA Agricultural Research Service and Texas A&M Blackland Research Center, 2002a.
Neitsch, S. L., Arnold, J. G., Kinir y, J. R., Srinivasan, R., and Williams, J. R.: Soil and Water Assessment Tool SWAT Theory, Version 2000, Temple, Tx. USDA Agricultural Research Service and Texas A&M Blackland Research Center, 2005.
Nicks, A. D.: Stochastic generation of the occurrence, patter n and location of maximum amount of daily rainfall. Statistical hydrology, US Governmental Print Office, Washington, DC, 154–25171, 1974.
Ponce, V. M. and Hawkins, R. H.: Runoff curve number: has it reached maturity? J. Hydrol. Engin., 1(1), 11–19, 1996.
Ritchie, J. T.: Model for predicting evaporation from a row crop with incomplete cover, Water Res., 1204–1213, 1972.
Rossi, C. G., Dybala, T. J., Mor iasi, D. N., Arnold, J. G., Amonett, C., and Marek, T.: Hydrologic calibration and validation of the soil and water assessment tool for the Leon River watershed. Soil Water Conserv., 533–541, and 2008.
Samani, H. A.: Reference crop evapotranspiration from temperature, Appl. Engin. Agric., 96–99, 1985.
Sankarasubramanian, A., Vogel, R. M., and Limbrunner, J. F.: Climate elasticity of streamflow in the United States, Water Resour. Res., 37, 1771–1781, 2001.
Santhi, C., Arnold, J. G., Williams, J. R., Dugas, W. A., Srinivasan, R., and Hauck, L. M.:5Validation of the SWAT Model on large River Basin with point and Nonpoint sources, J. Am. Wat. Res. Assoc., 37, 1169–1188, 2001.
Schaake, J. C.: GIS structure for the Nile River forecast project, in: Application of Geographic Information Systems in Hydrology and Water Resources Management, edited by: Kovar, K.and Nachtnebel, H. P., International Assoc. of Hydro. Sc. pub. No. 211, Wallingford, 1993.
Setegen, S. G., Srinivasan, R., and Dargahi, B.: Hydrological modelling in the Lake Tana basin, Ethiopia using SWAT model, Open Hydro. J., 2, 49–62, 2008.
Smedema, L. K. and Rycroft, D. W.: Land Drainage. Planning and Design of Agricultural Drainage Systems, Cornell University, New York, 1983.
Sorooshian, S. and Gupta, V. K.: Model calibration, in: Computer Models of Watershed Hydrology, edited by: Singh, V. P., Water Resources Publications, Colorado, USA, 1995.
Sutcliffe, J. V., Dug dale, G., and Milford, J. R.: The Sudan floods of 1988, Hydro. Sci. J., 31,355–364, 1989.
Swain, A.: Ethiopia, the Sudan, and Egypt: the Nile River dispute, J. Mod. African Stud., 35,675–694, 1997.
Taye, M. T., Ntegeka, V., Ogiramoi, N. P., and Willems, P.: Assessment of climate change impact on hydrological extremes in two source regions of the Nile River Basin, Hydrol. Earth Syst. Sci., 15, 209-222, doi: 10.5194/hess-15-209-2011, 2011.
Taylor, P. A.: On the assessment of surface heat flux and evaporation using large-scale parameters, Weather, 100, 81–92, doi: 10.1175/1520-0493(1972)100 <0081: OTAOSH>2.3.co; 21972.
Todd, M. C., Barrett, E. C., Beaumont, M. J., and Green, J. L.: Satellite identification of rain days over the upper Nile River basin using an optimum infrared rain/no-rain threshold temperature model, J. Appl. Meteor., 34,2600–2611, doi:10.1175/15200450(1995)034<2600: SIORDO>2.0.CO;2, 1995.
USDA: Soil Taxonomy, 2nd edn., US Agriculture, Edn., US Government Printing Office, Washington, DC, 1999.
USDA-SCS: Hydrology, in: National Engineering Hand Book Sect. 4, Washington, DC, USDA-SCS, 1972.
USDA-SCS: Hydrology (Revised), in: Engineering Handbook Sect. 4, Washington, DC, 1985.
Van Griensven, A., Francos, A., and Bauwens, W.: Sensitivity analysis and auto-calibration of an integral dynamic model for river water quality, Water Sci. Technol., 321–328, 2002.
Wambeke: Proper ties and management of soils of the tropics, FAO Land and Water Digital Media series, Rome, 2003.
Williams, J. R.: The EPIC model, in: Computer Models of Watershed Hydrology, Water Re-Sources Publications, Highlands Ranch, CO, 909–1000, 1995.
Zeray, L.: Calibration and Validation of SWAT Hydrologic Model for Meki Watershed, Ethiopia, Conference of Inter National Agricultural Research for Development, University of Kassel Wizenhausen and University of Gottingen, October 2007.

10 Paper II*:* Sensitivity of Omo-Gibe River Basin to Climate and Land use changes, Southern Ethiopia;

Sensitivity Analysis of Omo-Gibe River Basin to Climate and Land Use Changes, Southern Ethiopia

Dereje Tesfahun Mengistu[a*] and Asgeir Sorteberg[b,c]

[a]*Arba Minch Institute of Technology, Arba Minch University, Ethiopia*

[b]*Geophysical Institute, University of Bergen, Norway*

[c]*Bjerknes Centre for Climate Research, University of Bergen, Norway*

Corresponding author address:

Dereje Tesfahun Mengistu

Arba Minch

P.O. Box, 21, Arba Minch University, Ethiopia

E-mail:dertes_24@yahoo.com;dme061@uib.no

* Corresponding author.
E-mail address: dertes_24@yahoo.com.

Abstract

The sensitivity of the Omo Gibe river basin in southern Ethiopia to climatic and land use changes have been simulated using the hydrological model SWAT. Almost 60% of the average annual rainfall is lost through evaporation in the basin and the average runoff-rainfall coefficient was 0.26. Around two thirds of the water yield were simulated to come from surface runoff, while groundwater is responsible for the last third.

The sensitivity of streamflow to precipitation changes was found to be high. On average 25% change in streamflow for a 10% change in precipitation. On the other hand, the response of streamflow to changes in temperature, holding the precipitation fixed is modest. A linear regression analysis of streamflow responses for the different temperature scenarios indicates that a 1˚C change in temperature will produce a 1.4 percent change in annual streamflow.

The simulated effect of land use changes resulting from various hypothetical land use modifications is secondary to the effect of precipitation changes on the annual streamflow. However, the seasonal changes in streamflow were in some cases strongly affected by land use. As an example, a deforestation scenario (entire forest area coverage changed to bare lands) increased the Jan-April (dry season) streamflow by 38%.

Results further indicate that the combined effect of land use and climate change differs slightly from the sum of the individual land use and climate change simulations. For example, in an increased precipitation scenario, changing land use to more bare land areas would increase streamflow and water yield less than from simple additions of the individual effects. This shows that according to the model, nonlinear interaction among the water balance components or feedbacks may occur when simultaneous changes in land use and climate change are imposed.

Keywords: SWAT; Land use; Climate; sensitivity; Streamflow; hydropower

1 Introduction

The effects of land use and climate change on streamflow responses are crucial for sustainable water resource planning and management. Several investigations have been conducted on the question of the impacts of these changes on streamflow response. For example, Pikounis et al. (2003) examined the hydrological effects of specific land use changes in a catchment of the river Pinios in Greece using monthly SWAT model outputs. He developed three land use change scenarios; expansion of agriculture, complete deforestation and expansion of urban areas. All these three scenarios resulted in an increase in streamflow during wet months and a reduction in dry periods (Pikounis et.al, 2003). Similarly, Fohrer et al., (2001) studied land use changes in Germany and found out that the total annual water budget is significantly affected if the land use change is affected by more than 20% of the basin area. The above two studies mainly focused on land use changes and did not consider the consequences of the likely changes in the climate. Guo et al. (2008) stated several studies showing some interdependence of climate and land use changes on different aspects of the water cycle. A major finding of their study was that the climate effect is dominant in annual streamflow (Guo et. al, 2008). While land cover changes had a moderate impact on annual streamflow it strongly influenced the seasonal streamflow and altered the annual hydrograph of the basin (Guo et al., 2008). In a study of the upper Mara river basin in Kenya, Mango et al., (2011) showed that a conversion of forests to agriculture and grassland in the basin reduced the dry season flows and increased peak flows, leading to greater scarcity of water at critical time of the year. In the same paper the simulated runoff responses to climate change scenarios were non-linear and suggested that the basin was very vulnerable under low (-3%) and high (+25%) extremes of projected rainfall changes. However, the impacts of land use are more shown in seasonal streamflow change than climate change effects where its influence is mainly during extreme storm events. The above two studies show that various catchments behave differently due to climate and land use change on annual and seasonal scales.

Omo Gibe river basin is a lifeline for hundreds of thousands of indigenous people in southwestern Ethiopia and northern Kenya and the construction of hydroelectric power

plants in the basin has been widely debated. According to the report made by Avery (2010) “Runoff patterns in the Omo River have changed in the last twenty years. Forests and vegetation have been cleared in the Omo Basin through human activity, and as a consequence, runoff has become more variable, with much more rapid response to rainfall. Without effective catchment management, the overall runoff volume can be expected to increase with catchment land use change.” On top of this, the key issue which was reported on by international media was “elimination of the riverine forest and woodland, due to the construction of hydroelectric power plant in the basin lead to at least a 50% to 60% reduction of river flow volume” (BBC, 2009) and (Avery, 2010).

Based on the controversy around the management of the basin this paper will focus on four basic research questions that may be useful for basin integrated management practices. 1) Does changing land use due to deforestation affect the streamflow volume to the amount specified in the report above (BBC, 2009 and Avery, 2010)? 2) What sensitive is the annual streamflow to land use change compared to climate change? 3) How will the emerging hydropower development be affected by individual and combined changes of land use and/or climate change? 4) Will the combined effects of land use and climate change on the streamflow generation process be the sum of the individual effects or are there non-linearities in the system? Moreover, the paper further aimed to quantify the effect of climate and land use changes on the water balance components of the Omo Gibe river basin.

2. Description of the Study Area

The Omo-Gibe basin is one of the significant surface water resources of Ethiopia. It is drained by two major rivers from the highlands, the Gibe River flowing southwards and Gojeb River flowing eastwards.

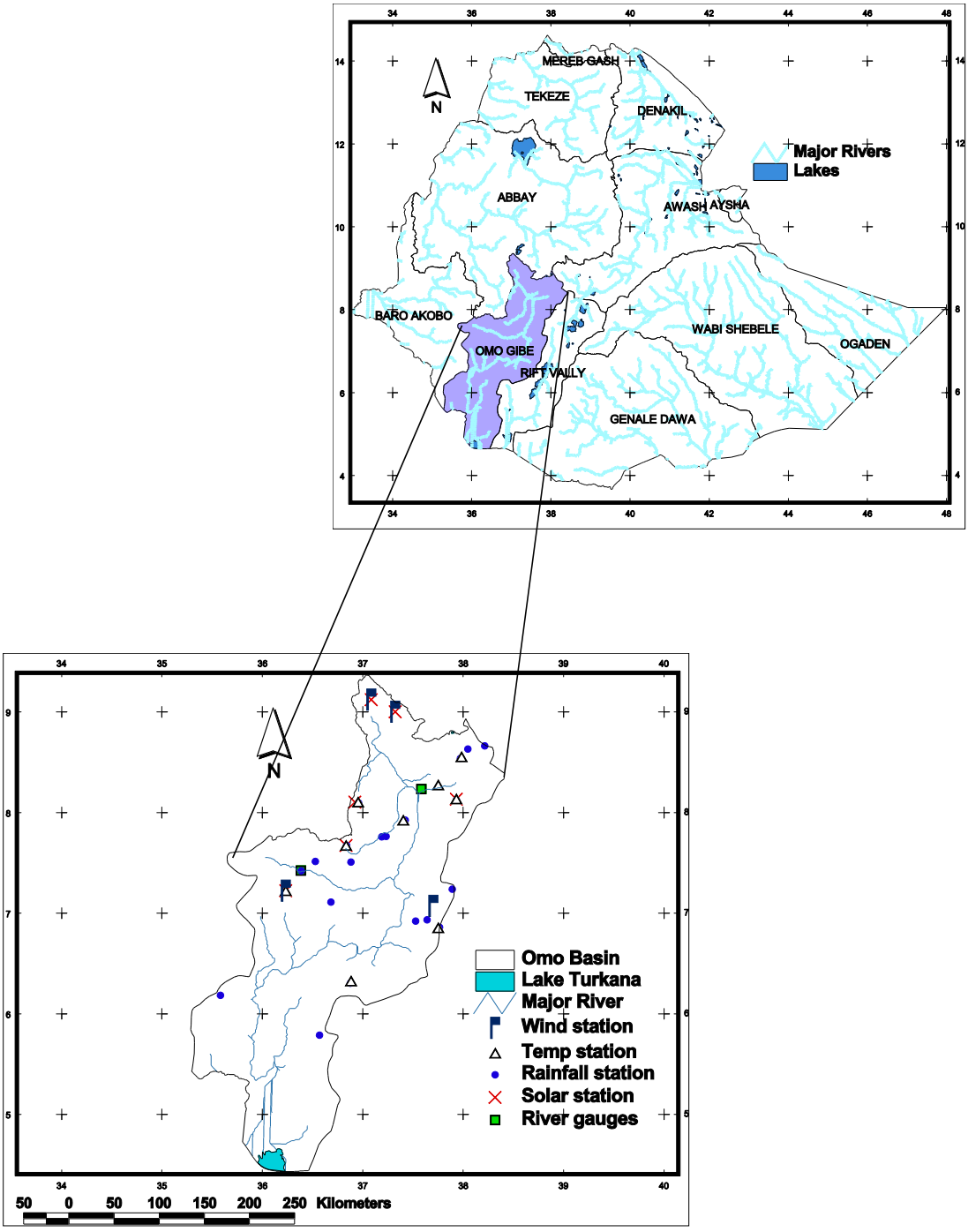

Figure 1: Map of the study area includes major River Networks, Meteorological stations and stream gauged used for calibration

Downstream of their confluence only minor tributaries join, as the river continues southwards where it empties into Lake Turkana at the border with Kenya (Avery, 2010)

(see figure 1). By volume Lake Turkana is the twenty-fourth largest lake and the world's largest permanent desert lake. The Lake Turkana catchment area is situated in both Ethiopia and Kenya and is 130860 km^2. Of which the Omo Gibe river basin covers 50 % (74300km^2) of the total drainage area and 90% of the inflow to Lake Turkana is contributed from the Omo Gibe river basin. However, 85% of the basin flow is originated from the upstream catchment where the Gibe III hydropower plant is situated (Avery, 2010). The Omo River has a total length of about 1200 kilometers with an average slope of 3.1 m/km. The long term mean flow is estimated to be 435m^3/s or 13.5 billion m^3 per annum (EEPCO, 2009) and seasonal variations are huge, with monthly mean flow ranging from 60 m^3/s in March to more than 1,500 m^3/s in August (EEPCO, 2009).

The annual rainfall within the Omo Gibe catchment decreases from north to south and with the decrease in elevation. It varies from a minimum of 1,200 mm in the lowlands to a maximum of about 1,900 mm high land areas (EEPCO, 2009). The average annual rainfall calculated over the whole basin is 1,426 mm with a mean annual temperature is 20.4°C. 75 to 80% of the annual rainfall occurs during a five months period from May to September (EEPCO, 2009).

3. Methods and Materials

3.1 Model Description

We use the physically based, distributed parameter model SWAT (Soil and Water Assessment tool, version SWAT2005) which operates on daily time step and uses physiographical data such as elevation, land use and soil properties as well as meteorological data and, streamflow data for calibration. It is computationally efficient for use in large watersheds, and is capable of simulating long-term yields for determining the impact of land management practices (Arnold and Allen, 1996).

Hydrological processes included in the model are evapotranspiration, surface runoff, infiltration, percolation, shallow and deep aquifers flow, and channel routing (Arnold

et al., 1998). The effects of spatial variations in topography, land use, soil and other characteristics of watershed hydrology is incorporated by dividing a basin into several subbasins based on drainage areas of tributaries and is further divided the subbasins into a number of hydrological response unit (HRUs) within each subbasin, based on land cover and soils. Each HRU is assumed spatially uniform in terms of land use, soil, topography and climate. The subdivision of the watershed enables the model to reflect differences in evapotranspiration for various crops and soils. All model computations are performed at the HRUs level.

The fundamental hydrology of a watershed in SWAT is based on the following water balance equation Arnold et al. (1998).

$$\frac{\partial SW}{\partial t} = R_{day} - Q_{surf} - ET_a - W_{seep} - Q_{gw} \quad (3.1)$$

Where SW is the soil water content (mm), R_{day} is the amount of precipitation on (mm), Q_{surf} is the amount of surface runoff/streamflow (mm), ET_a is the amount of actual evapotranspiration (mm), W_{seep} is the amount of water entering the vadose zone from the soil profile (mm), and Q_{gw} is the amount of ground flow (mm). Detail descriptions of the different model components can be found in Arnold et al. (1998) and Neitsch et al. (2002a).

3.2 Sensitivity of annual and seasonal streamflow to climate and land use change

The relative sensitivity of the streamflow ($\Delta Q_{\Delta P,\Delta T,\Delta L}$) to either a precipitation (ΔP), a temperature (ΔT) or a land use (ΔL) change or a combination of the three is calculated as:

$$\Delta Q_{\Delta P,\Delta T,\Delta L} = \frac{\left(Q_{\Delta P,\Delta T,\Delta L} - Q_{\Delta P=a,\Delta T=b,\Delta L=c}\right)}{Q_{\Delta P=0,\Delta T=0,\Delta L=0}} \cdot 100 \quad (3.2)$$

Where Q is the average annual or seasonal Qsurf which is calculated using equation (3.1) and a, b and c are the perturbations.

To be able to investigate if there is any nonlinearity in the streamflow change when precipitation, temperature and land use are changed we estimated the linear combination of the three changes as done in Mengistu and Sorteberg (2012).

$$\Delta Q_{\Delta T,\Delta P,\Delta L} = \left.\frac{\partial Q}{\partial P}\right|_{\Delta T=0,\Delta L=0} \Delta P + \left.\frac{\partial Q}{\partial T}\right|_{\Delta P=0,\Delta L=0} \Delta T + \left.\frac{\partial Q}{\partial L}\right|_{\Delta T=0,\Delta P=0} \Delta L \tag{3.3}$$

Where the local derivatives for each parameter is calculated as the mean response for the sensitivity test where the two other factors kept unchanged. For example, $(\partial Q/\partial P)|_{\Delta T=0,\Delta L=0}$ is the mean response in m^3/% of the four simulations covering the precipitation perturbations ±10-20%. Any deviation from this will indicate nonlinear effects that may arise as precipitation, temperature and land use changed simultaneously.

3.3 Input Data

Topographic features such as elevation, slope and aspect and soil types, land use and the stream network (optional) are needed for the model. A digital elevation (DEM) was created using a 90m*90m resolution topographic database obtained from the Ethiopian ministry of water resources. The DEM was used to delineate the watershed and the drainage patterns of the surface area analysis. Subbasin parameters such as slope gradient, slope length of the terrain, and the stream network characteristics such as channel slope, length, and width were derived from DEM (Fig.2a).

Land use is one of the main factors affecting surface erosion, and evapotranspiration in a watershed. The source of land use map of the study is the Ministry of water resources Ethiopia and land use/land cover map is taken from the global Hydro1K dataset a) en, 1998) and modified to correspond with tl b) AT predefined land uses classification (Fig. 2b). More than 40% of Omo Gibe river basin is covered by mixed forest whereas the rest is covered agriculture, pasture, grass, bush and shrubs. Table 1 summarizes the physical properties of land use of the study area used for SWAT simulation.

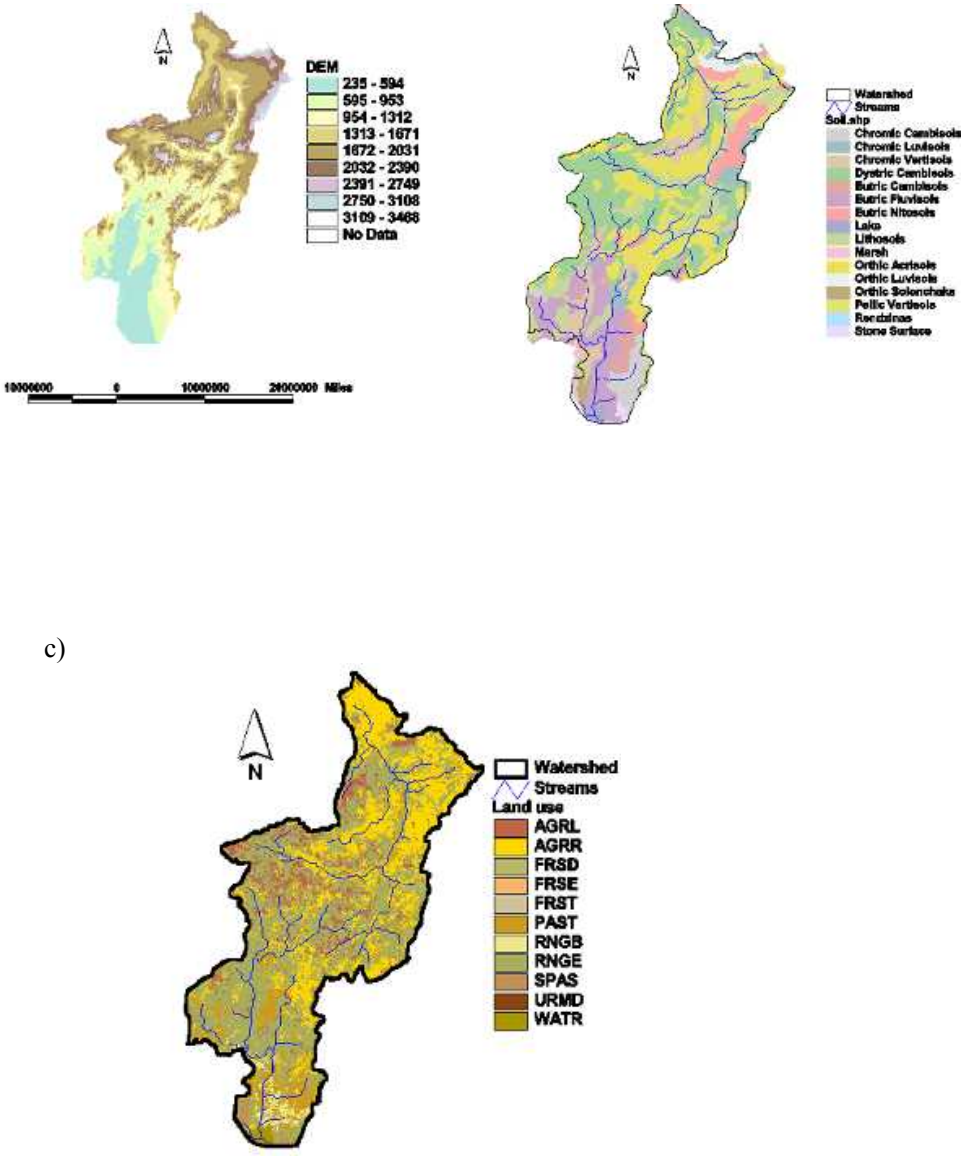

c)

Figure 2: Map for a) Digital Elevation Model, b) Land use and c) Soil

Table 1: Parameters for various land-use types

Land-use	*LAI*	*Maximum canopy height (m)*	*Maximum stomatal conductance (ms-1)*	*Maximum root depth (m)*
AGRL (Agricultural land Generic)	3.0	1.0	0..005	2.0
AGRR (Agricultural land-row crops	3.0	2.5	0.007	2.0
AGRC (Agricultural land close grown)	4.0	0.9	0.006	1.3
FRST (Mixed forest)	5.0	6.0	0.002	3.5
FRSD (Deciduous forest)	5.0	6.0	0.002	3.5
FRSE (Ever green forest)	5.0	10.0	0.002	3.5
RNGB (Range brush)	2.0	0.5	0.005	2.0
RNGE (Range grasses)	2.5	0.5	0.005	2.0
SPAS (summer pasture)	4.0	1.0	0.005	2.0
PAST (Pasture)	4.0	1.0	0.005	2.0

Different types of soil texture and physical-chemical properties are requirements for the SWAT model. These data were obtained from various sources. The soil map was obtained from ministry of water resources of Ethiopian at Water Resources Information and Metadata Base Centre department. But several properties like moisture bulk density, saturated hydraulic conductivity, percent clay content, percent silt content and percentage sand content of the soil which are required by SWAT model was not incorporated. This additional data was extracted from Wambeke, (2003); USDA, (1999) and FAO, (1995).As seen in Fig. 2c the major soil types of the Omo Gibe basin are Dystric cambisols and Lithosols.

SWAT requires daily meteorological data which were obtained from the Ethiopian National Meteorological Agency (NMSA) for the period 1987-2007. Twelve temperature and seventeen precipitation stations were used for the model input. Missing values were filled using the SWAT built-in weather generator developed by Nicks, (1974). The precipitation generator uses a first-order Markov chain model. The weather generator was developed based on observed precipitation data with a record length from 1967-2007 that was nearest the centroid of the basin. Given the wet-dry state, the model determines stochastically if precipitation occurs or not. When a precipitation event occurs, the amount is determined by generating from a skewed normal daily precipitation distribution or a modified exponential distribution. The amount of daily precipitation is partitioned between rainfalls using average daily air temperature. The average percentage of missing data in the observed datasets is less than 10% and 5% of precipitation and temperature, set respectively. For solar radiation and wind, we used the daily dataset of Sheffield et al. (2006) derived by combining reanalysis with observations. The data was interpolated to the meteorological stations within the region. Figure 1 shows the number and distribution of gauging stations applied in this study.

For hydrological streamflow data for two stations were collected from the Ministry of Water Resources of Ethiopia (Table 2).

Table 2: Stream gauge location, Monthly calibration and validation dates used for model simulation

Table 3: Calibrated values of adjusted parameters for flow calibration of the SWAT

Stream gauge	**Calibration date**[3]	**Validation date**
Great Gibe at Abelti	1/1/1987-12/12/1999	1/1/2000-12/12/2007
Gojeb	1/1/1987-12/12/1999	1/1/2000-12/12/2004

2005 model for the Omo Gibe river basin.

Id	*Parameter*	*Description*	*Range*	*Initial values*	*Calibrated value*
1	CN_2	Initial SCS CN II value	±25%	Default	-7.5
2	Sol_K	Saturated Hydraulic conductivity [mm/mm]	±25%	Default	-19.6
3	ESCO	Soil evaporation compensation factor	0.0-1.0	0.95	0.99

[3]Time period variation were due to differences in readily available measured flow data records

3.4 Model Setup

The Omo Gibe stream network and sub watersheds were delineated using ARCSAWT-X with the SWAT suggested minimum drainage area required to form the origin of the stream. 77 sub watersheds; and 633 HRUs of the Omo Gibe river basin as a function of 2% land use and 5% soil types within a given watershed, respectively were delineated up to the point of the outlet. This point constituents of total drainage area of 74300km^2 that drains about 95% of the entire Omo Gibe River basin (78213), which is located in Ethiopia.

The Soil Conservation Service (SCS) curve number procedure (USDA-SCS,1972) was applied to estimate surface runoff volumes due to the unavailability of sub daily rainfall data required for the Green and Ampt method that SWAT offers a different option to estimate surface runoff. The potential evapotranspiration (PET) estimates and channel routing were performed using Hargreaves and Muskingum methods, respectively.

Table 4: Land use scenarios with percentages of area changed. * Not 100% since 1.2% of the drainage area is covered by Lake Turkana, small water bodies and artificial reservoirs created due to hydroelectricity project dams

Scenario name	Land cover change	Area changed (%)
AG to FRST	Agricultural lands (AG) with slope greater than 25% changed into forest (FRST)	10.3
AAG to FRST	All Agricultural lands (AAG) change into forest	36.6
FRST to GRS	Forest to grass land (GRS)	48.1
FRST to BRLNDS	Forest to bare land (BRLNDS)	48.1

AAG to BRLNDS	All agricultural land changed to bare land	36.6
ALNDS to BRLNDS	All lands (ALNDS) charged to bare lands*	98.8

3.5 Model Implementation and Sensitivity Analysis

After pre-processing of the data and SWAT model set up, simulation was done for the period indicated in Table 2 for the basin. The built-in SWAT sensitivity analysis tool that uses the Latin Hypercube One- factor-AT-a –Time (LH-OAT) (Van Griensvenet al., 2002: Van Griensvenet, 2005) was used. Two outlets (Fig. 1) were selected for the sensitivity analysis.

According to Lenhart et al., (2002) the sensitivity of a flow to a parameter can be categorized into four classes. If the relative sensitivity lies between 0-0.05 and 0.05-0.2, then the parameter is classified as negligible and medium,

respectively, whereas if it is varying between 0.2-1.0 and greater than 1 then categorized as high and very high class, respectively. Out of 28 selected parameters the curve number, saturated hydraulic conductivity, soil evaporation compensation factor, available water capacity, maximum canopy storage, biological mixing efficiency, soil depth and deep aquifer percolation fraction, were identified as being parameters to which the flow has medium, high or very high sensitivity. The ranking of the parameters was different at the two outlets where sensitivity test was carried out. However, the curve number (CN_2) was the main sensitivity parameter for the two outlets. From the sensitivity test, eight parameters having a relative sensitivity greater than 0.05 (sensitivity of the flow to the parameter categorized as medium or higher) was selected for the calibration process.

Calibrations against available streamflow observations are often conducted to tune the model. Because automatic calibration relies heavily on the optimization algorithm and the specified objective function we follow the recommendations of Gan, (1988) to use both manual and automatic calibration procedures.We first conducted manual

calibration of monthly stream using the procedure developed by Santhi et al.,(2001).Parameters identified from the sensitivity analysis were varied in sequence of their relative sensitivity within their ranges (Table 2) until the volume is adjusted to the required quantity (Zeray et al.2007).This process continued till the volume simulated is within ±15% of the gauged volume. After each calibartion, the coefficient of determintation (R^2) and Nash-Sutcliffe effficeny value (E_{NS}) were checked ($R^2 > 0.6$ and $E_{NS} > 0.5$,Santhi et al.,2001). Finally, the automatic calibration algorithm in SWAT is used for fine tuning the calibration. This is based on the Shuffled Complex Evolution algorithm developed at the University of Arizona (SCE-UA) which is a global search algorithm that minimizes a single objective function for up to 16 model parameters (Duan et al., 1992).

3.6 Scenario Set up and Sensitivity Tests

Model tests were designed to evaluate effects of land use and climate changes on streamflow in the Omo Gibe river basin. To quantify these effects, the model was run with perturbed climatic and land use values from 1987-2007 and compared against the non-perturbed simulation (base run) using the average changes from 1987-2007 (equation 3.2).

3.6.1 Land use change scenarios

Due to the existing and ongoing hydroelectricity projects in the basin, people were exposed to resettlement *(Campagna per la Riformadella Banca Mondiale, CEE Bankwatch Network, 2008)*. In the process, lands which were formerly forest were turned into fields for agriculture.

On the other hand, in order to ensure the sustainability of the life of the dam, more trees were planted around the catchment of the dam area which has a direct impact in streamflow generation. We include several plausible land use change scenarios and in addition, some extreme land-cover change cases were also included, such as changing the entire land use in the basin to be either forested or left as bare ground (soil) to

identify the upper limit in water balance response that could be foreseen (Table 4). The changes in land use scenarios are summarized in Table 4 and Fig. 4.

3.6.2 Climate change scenarios

Several climate change sensitivity cases based on the 1987-2007 meteorological data has been developed in order to assess the impact of systematic meteorological changes on streamflow and other water balance components. Incremental changes in temperature, (0, +2 or +4 ˚C) and in precipitation (-20%, -10%, 0%, +10%, +20%) were imposed on the original meteorological data while solar radiation and wind speed were held at their reference values. A total of fourteen sensitivity test with possible climate change conditions were used.

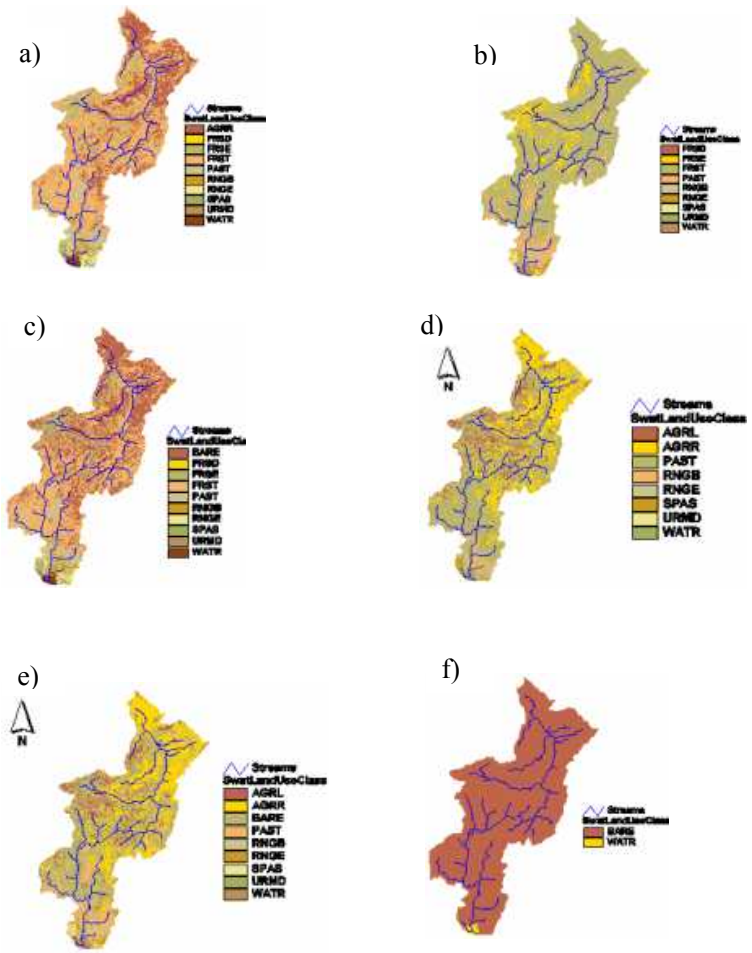

Figure 4: Land use in the different change scenarios **a)** AG to FRST **b)** AAG to FRST **c)** AAG to BRLNDS **d)** FRST to GRS **e)** FRST to BRLND **f)** ALNDS to BRLNDS for Omo Gibe River basin. See table 4 for a description of the Land use change scenarios.

3.6.3 Combined climate change and land use change scenarios

In order to investigate the combined effect of changes in both the land use and climatic conditions (e.g., Lahmer et al., 2001; Hu et al., 2004) a third group of sensitivity test were performed. However, since the model does not include interactive vegetation the climatic conditions are specified independent of the land use changes and vice versa, the full effect of interactions and feedbacks between the land use and climate changes on streamflow cannot be described in these tests. However, these tests are useful for investigating to what degree the changes in climate and land use are just the sum of the separate responses from the land use and climate change only runs or if there is a more subtle non-linear response.

4. Results and Discussion

4.1 Model Calibration and Validation

The model was calibrated at Great Gibe and Gojeb stream outlets which are the two major tributaries of the basin. The model slightly overestimates the flow during the calibration period with a bias (the mean difference between the simulation and observation) of 25% (Table 5). However, there was good agreement between simulated and observed flow variability on monthly time scale (see Figure 3a and c) for most of the years except 1992 where maximum simulation was seen, where relatively low rainfall was recorded in the year. The Nash-Sutcliffe effficeny value (E_{NS}) and coefficient of determintation (R^2) of the monthly values for the Great Gibe and Gojeb stations were 0.70 and 0.87 and 0.75 and 0.75, respectively (see Figure 3b and d).

a)

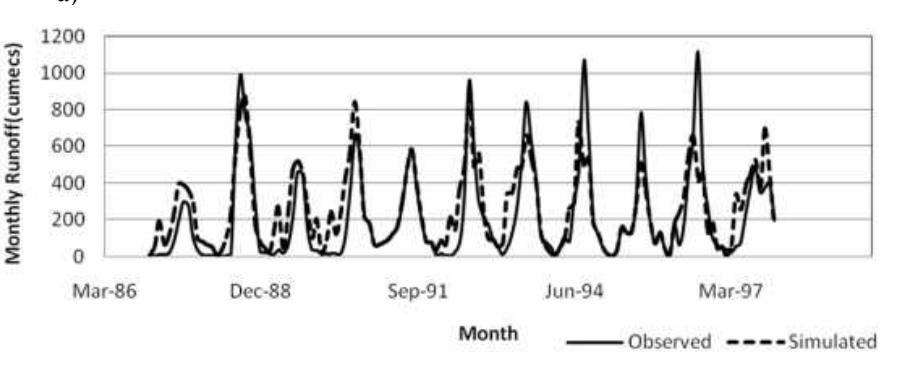
Monthly Runoff(cumecs)
1200
1000
800
600
400
200
0
Mar-86
Dec-88
Sep-91
Jun-94
Mar-97
Month
Observed
Simulated

b)

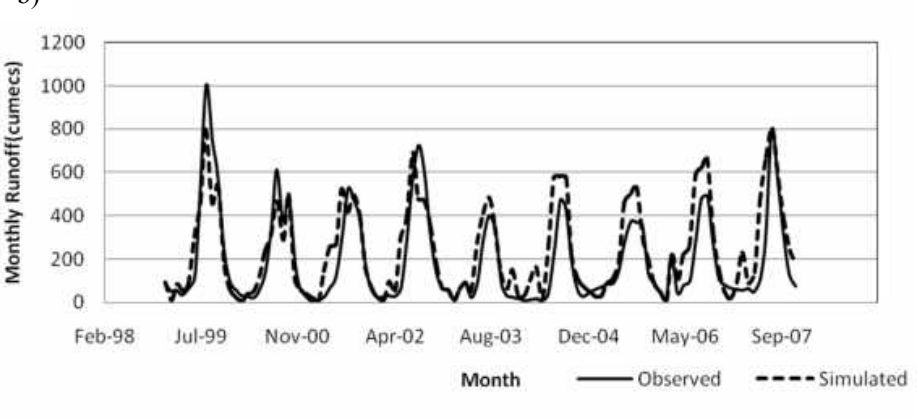
Monthly Runoff(cumecs)
1200
1000
800
600
400
200
0
Feb-98
Jul-99
Nov-00
Apr-02
Aug-03
Dec-04
May-06
Sep-07
Month
Observed
Simulated

c)

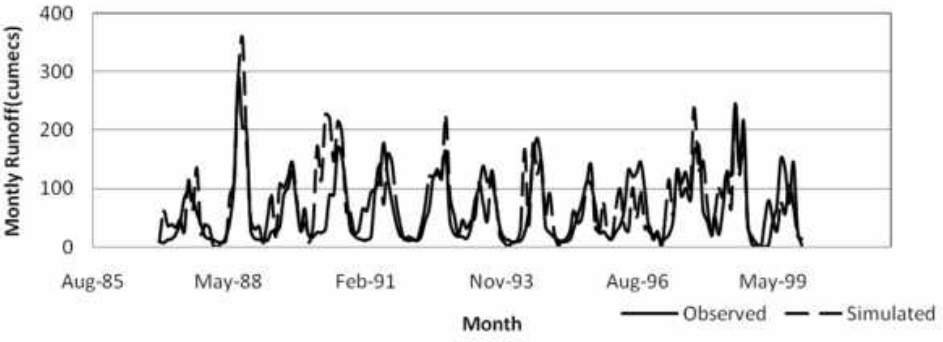
Montly Runoff(cumecs)
400
300
200
100
0
Aug-85
May-88
Feb-91
Nov-93
Aug-96
May-99
Month
Observed
Simulated

d)

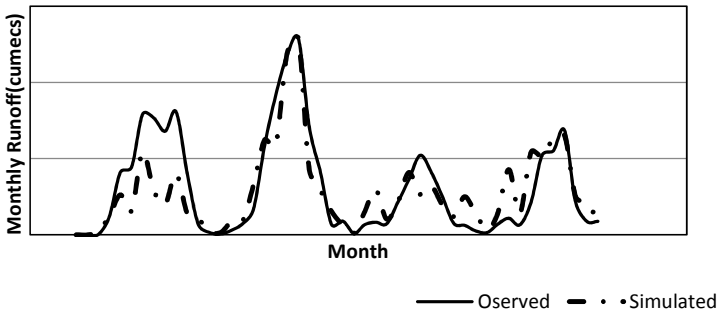

Figure 3: Streamflow calibration and validation at G. Gibe at Abelti (a and b) and Gojeb (c and d) stream gauges, respectively

In the validation period, the simulated flow at Great Gibe and Gojeb outlets showed a very good agreement for the year 2000-2007 and 2000-2004 respectively. The monthly E_{NS} and R^2 simulation efficiency were between 0.75 and 0.88 and 0.75 to 0.91 for the two stations, respectively. Other statistical analysis results are shown in Table 5.

4.1.1. Extreme land use change scenarios

In this section we test some extreme land use change scenarios in order to find the upper bound on the hydrological changes we can expect when changing the land use. In the fifth test (AAG to BRLNDS) in Table 7, the agricultural lands in the basin turned into bare lands. This change in land use from AAG to BRLNDS caused a nearly 20.5% and 23.5% increase in annual water yield and streamflow of the basin, respectively. This increase is due to reduced evapotranspiration of the surface in relation to more efficient evapotranspiration of the previously vegetated surfaces. Thus, more water is available for surface runoff (see Figure.5b) and less for the lateral flow (Figure.5b) and groundwater recharge (Figure.5b). These changes lead to a larger water yield (Figure.5b) and higher streamflow. Seasonal changes in water yield shown in Table 7 indicate that the large increase will occur in the wet period from May to September (25.2% increase). In the dry period from October to December and January to April, the water yield increased by 12.5% and 12.7%, respectively.

The ALNDS to BRLNDS case the entire basin was converted to bare land, an extended case of the FRST to BRLNDS scenario, where grasslands and croplands is also changed to bare land. This change causes the annual water yield and streamflow to increase by 24.3% and 16.8%, respectively compared to the base run. The largest increase of 29.2% is found in the May–September (wet) period. A relatively smaller increase of 14.2% occurs in the dry period. In the ALNDS to BRLNDS scenario one would expect a larger streamflow increase when all the land cover of the study area was altered to bare land (soil) compared to the FRST to BRLNDS scenario where only forested land was altered, but this was not the case, the streamflow change for the ALNDS to BRLNDS scenario is slightly smaller than the FRST to BRLNDS scenario (16.8 and 19.9%, respectively). This is mainly due to the fact that, in the ALNDS to BRLNDS case an increase of soil temperature in the basin lead to greater evapotranspiration loss and the soil dried out before producing streamflow. The effect of this was particularly large in the dry season (JFMA)

Table 5: Statistical evaluation of the simulated monthly streamflow for the Omo Gibe River basin at Great Gibe and Gojeb gauging stations compared to observations for the calibration and validation periods.STD is the standard deviation, r^2 is correlation coefficient. N_{ES} is Nash Sutcliff

	Great Gibe gauging station				*Gojeb gauging station*			
Statistical measure	Calibration (1987-1999) mmd^{-1}		Validation (2000-2007) mmd^{-1}		Calibration (1987-1999) mmd^{-1}		Validation (2000-2004) mmd^{-1}	
	Observed	Simulated	Observed	Simulated	Observed	Simulated	Observed	Simulated
MEAN	3.22	4.01	2.69	3.07	0.9	1.02	0.84	0.78
STD	0.88	0.79	0.63	0.41	0.21	0.29	0.31	0.27
r^2	0.75		0.79		0.70		0.91	
N_{ES}	0.70		0.75		0.87		0.88	
Bias (%)	-25		-14		13		7	

4.2 The Annual Water Balance

Table 6 summaries the simulated average annual water balance results for the calibration and validation periods. About 59/59% of the average annual rainfall is lost through evaporation in the calibration and validation periods respectively. The average surface runoff is 26/26% of the average annual rainfall. The groundwater contribution is about 14/13% of the average annual rainfall while percolation into the deep aquifers accounts about 15/14% in the calibration and validation periods respectively. Overall 67/68% of the total water yield is contributed from surface flow while 35/34% the total water yield is contributed from the shallow ground water flow. Not that the slight discrepancy in the total water balance is due to the unaccounted TLOSS in the system.

Table 6: Annual averaged calibrated/validated hydrological balances (mm) and percent contribution of the different water balance components for the Omo Gibe River Basin.SURQ[I]: surface runoff, LATQ[II]: lateral flow into stream, GW_Q[III]: groundwater in the shallow aquifer, ET[IV]: evapotranspiration, PET[V]: potential evapotranspiration (Hargreaves method is used), PERC[VI]: percolation below root zone (groundwater recharge),

Basin	**Period**	**Rainfall** (mm)	**SURQ[I]** (mm)	**LATQ[II]** (mm)	**GW_Q[III]** (mm)	**ET[IV]** (mm)	**PET[V]** (mm)	**PERC[V]** (mm)	**TLOSS[VII]** (mm)
Omo Gibe	Calibration /validation	1468/1467	386/385	1.5/1.4	199/191	863/869	1675/1694	218/210	11/12
	%	100/100	26/26	0.1/0.1	14/13	59/59		15/14	0.8/0.8

4.3 Effects of Land Use Change

Effects of land use change on streamflow and water yield are evaluated based on comparison between simulations using changes in land use (see Table 4 and Fig. 4) and the base run (base run land use as shown in Fig. 2b). The meteorological conditions in these tests are the same as in the base run, i.e., the simulations are based on the 1987-2007 meteorological data.

4.3.1 Increased forestation

The first two sensitivity tests (Table 7) show water yield and streamflow changes that may result from returning parts or all agricultural lands to forest lands (AG to FRST and AAG to FRST cases, Table 4). In the first case, farm lands of slope >25% are restored to forest (AG to FRST). This changes the land use in 10.3% of the basin area. The latter experiment (AAG to FRST) provides the upper boundary of forestation changes and changes the land use in 36.6% of the basin area. Both experiment reduced the annual streamflow with the AAG to FRST experiment resulting in a decrease of -25.2% compared to the base run (Table 7). The decrease in streamflow may be attributed to the fact that forest land has a higher rate of water loss by evapotranspiration than farm land does (an increase of 8.6% of ET_a in the AAG to FRST test). Deep roots of forest plants can draw moisture from soils faster than water being transpired by short rooted farm plants or bare soils during the operation. In addition, forest plants have larger leaf areas to transpire with a model leaf area index change from $3m^2/m^2$ for agricultural land to $5m^2/m^2$ for forested areas (Table 1).

The change in streamflow is around twice the change in water yield (table 7). As water yield is the sum of both streamflow and ground water, the impact of increased forestation is more significant in reducing streamflow amount than water yield. This is due to the available groundwater is less likely to be affected by evapotranspiration.

The reduction of streamflow by increased forest cover in the basin is particularly strong in the wet period from May to September (Table 7). The reason for this high sensitivity on May-September is that precipitation is abundant and temperatures are high enough to support evapotranspiration. Thus, a large change in evapotranspiration takes place (461.7 mm and 494.8 mm for the AG to FRST and AAG to FRST, respectively compared to 452mm in the base case). Consequently, as shown by the water budget in Figure 5a, the surface runoff decreased substantially in May– September, causing significant decrease of water yield (-18.6 %) and streamflow (-24.1%) for the period.

Table 7: Land use change scenarios with percent annual and seasonal basin discharge change $\left(\frac{Q^s_{wyld} - Q^b_{wyld}}{Q^b_{wyld}}\right) * 100\%$, streamflow changes $\left(\frac{Q^s_{surf} - Q^b_{surf}}{Q^b_{surf}}\right) * 100\%$ and evapotranspiration change $\left(\frac{ET^s_{Ea} - ET^b_{Ea}}{ET^b_{Ea}}\right) * 100\%$ Column 3a, 4a and 5a are percentage change in water yield, streamflow and evapotranspiration due to land use change to the total area land use, respectively; Column 3b, 4b and 5b are percentage change in water yield, streamflow and evapotranspiration per 10% change in land use, respectively.

Land cover change [1]	**Season [2]**	**Water yield Change (Q_{wyld}) [3]**		**Streamflow Change (Q_{surf}) [4]**		**Evapo-transipration Change (E_a) [5]**	
		(a)	**(b)**	**(a)**	**(b)**	**(a)**	**(b)**
AG to FRST	ANN	-3.0	-2.9	-6.3	-6.1	1.9	1.8
	MJJAS	-4.6	-4.5	-5.4	-5.2	2.1	2.0
	OND	1.0	1.0	-6.9	-6.7	-1.1	-1.1
	JFMA	-2.5	-2.4	- 10.1	-9.8	3.1	2.9
AAG to FRST	ANN	-13.0	-3.6	-25.2	-6.3	8.6	2.4
	MJJAS	-18.6	-5.1	-24.1	-6.6	9.5	2.6
	OND	3.8	1.0	-17.8	-4.9	-2.2	0.6
	JFMA	-17.7	-4.8	-38.3	-10.5	12.4	3.4
FRST to GRS	ANN	12.5	2.6	11.5	2.4	-8.5	-1.8
	MJJAS	17.5	3.6	13.8	2.9	-7.2	-1.5
	OND	-5.2	-1.1	-1.8	-0.4	4.4	0.9
	JFMA	21.9	4.6	13.7	2.8	-17.0	3.5
FRST to BRLNDS	ANN	19.7	4.1	19.9	4.1	-13.6	-2.8
	MJJAS	24.7	5.1	19.1	4.0	-15.3	-3.2
	OND	3.7	0.8	6.5	1.4	0.1	0.0
	JFMA	25.5	5.3	38.0	7.9	-17.5	-3.6
AAG to BRLNDS	ANN	20.5	5.6	23.2	6.3	-14.6	-4.0
	MJJAS	25.2	6.9	22.9	6.3	-19.5	-5.3
	OND	12.5	3.4	9.2	2.5	-0.6	-0.2
	JFMA	12.7	3.5	38.9	10.6	-13.5	-3.7
ALNDS to BRLNDS	ANN	24.3	2.5	16.8	1.7	-17.3	-1.8
	MJJAS	29.2	3.0	18.4	1.9	-22.0	-2.2
	OND	14.2	1.4	2.5	0.3	-2.3	-0.2
	JFMA	19.8	2.0	23.4	2.4	-17.0	-1.7

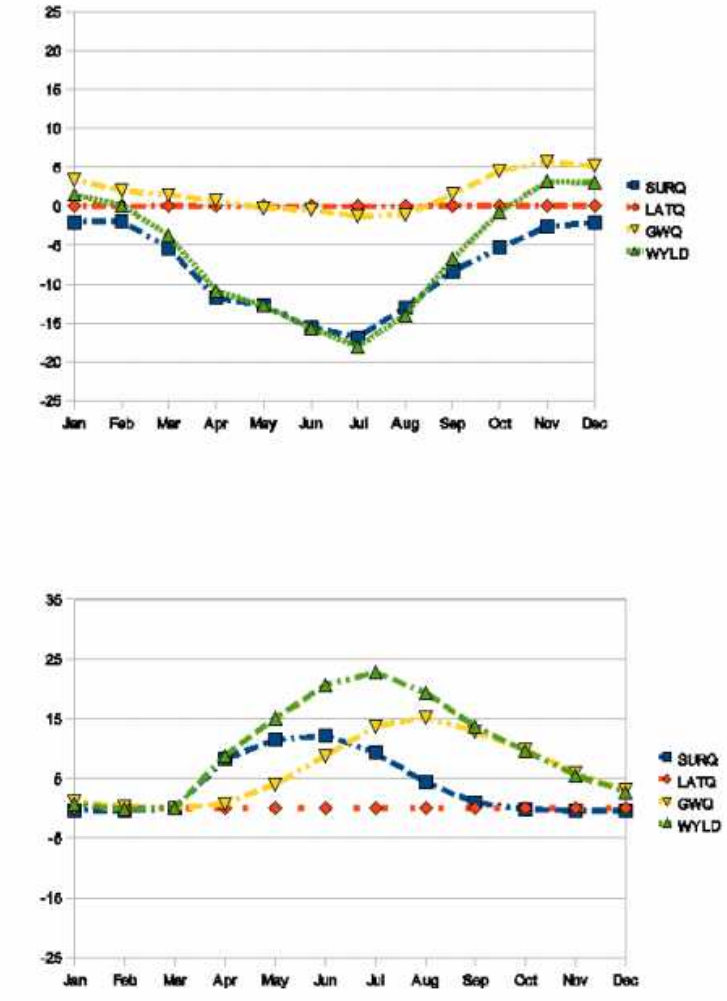

Figure 5: Anomalies (relative to the base run) of monthly contributions to surface streamflow from surface runoff (SURQ); lateral flow (LATQ); groundwater return flow (GWQ); water yield (WYLD). a) Upper panel shows AAG to FRST scenario which describes changes of streamflow when the agricultural land was changed to forest. b) Lower panel shows AAG to BRLNDS scenario which describes the monthly contributions to surface streamflow when agricultural land was changed to bare land. (Units are mm per unit area of the basin.

The larger decrease in streamflow in the January–April period resulting from the changes in land use may be attributed to the sharp decline of rainfall and warm

temperatures in these months. The combined effect causes the increase in evapotranspiration of the expanded forest areas. There is a slight increase in water yield during the dry period from October to December. This small increase in water yield is mainly due to the groundwater contribution (return flow) (Figure 5a). In fact, the contribution to water yield from the surface runoff decreased from the base run in the months from May (- 4.5 %) through July (-7.9 %). Most of the extra amount of surface water percolated into the shallow aquifer. And as indicated in Figure 5a, the increased groundwater for the period October - December due to return flow and surface runoff would increase the water yield.

4.3.2 Deforestation

FRST to GRS and FRST to BRLNDS scenarios in Table 7 represent two additional possible land use scenarios. In FRST to GRS, forest lands (48% of the basin area) are converted to grassland for grazing. This change resulted in an increase of 12.5% and 11.5% of the annual water yield and streamflow from the base run (Table 7), respectively. Seasonal changes of water yield and streamflow following these land use changes show increases from the wet (May-September; 17.5% and 13.8%) to dry seasons (January to April; 21.9% and 13.7%), respectively. As it is shown in table 3, these results were accompanied with the large decrease in evapotranspiration both in the wet and dry season. The water flow within soil profile that enters the main channel to replenish the small streams when grasses are entering the dormant in dry season (January to April; 21.9%) contributes larger water yield increment. A relatively small decrease in streamflow is shown in the dry season from October through December. This small decline in streamflow may be due to limited moisture in the soil during those months.

FRST to BRLNDS represents a deforestation scenario when basin forest (48% of the basin area) is cleared. This change causes an increase in annual water yield and streamflow of nearly 19.7% and 19.9%, respectively compared to the base run. The largest temporal increase of 24.7% of the seasonal water yield against the base run occurred in the period from May to September. These large increases in water yield resulting from deforestation (still keeping the crop lands and grasslands) are primarily

caused by larger surface runoff. This is because the contribution of forest transpiration to evapotranspiration is becoming minimized which in turn significantly increased water yield. However, groundwater (return flow) and lateral flow have minimum contribution for basin and streamflow due to reduced soil moisture. This implicitly shows the temporal increase followed by sharp decline in streamflow and water yield is mainly due to strong evaporation from the soil surface before recharging groundwater.

4.3.3 Comparing the different land use change scenarios

In order to compare the different land use change scenarios, we rescale the results of the different scenarios to look at the hydrological change per 10% change in land use area (see Table 7 and Figure 6). The basin is more sensitive to changing the land use from agricultural to bare lands (AAG to BRLNDS) or forest (AAG to FRST) than to the other scenarios. The annual streamflow increased and decreased by 6.3% per 10% area land use change, respectively. This is about three times greater than the change caused by changing all lands to bare lands (ALNDS to BRLNDS) (Table 7). Such difference may be due to the fact that in the ALNDS to BRLNDS scenarios,

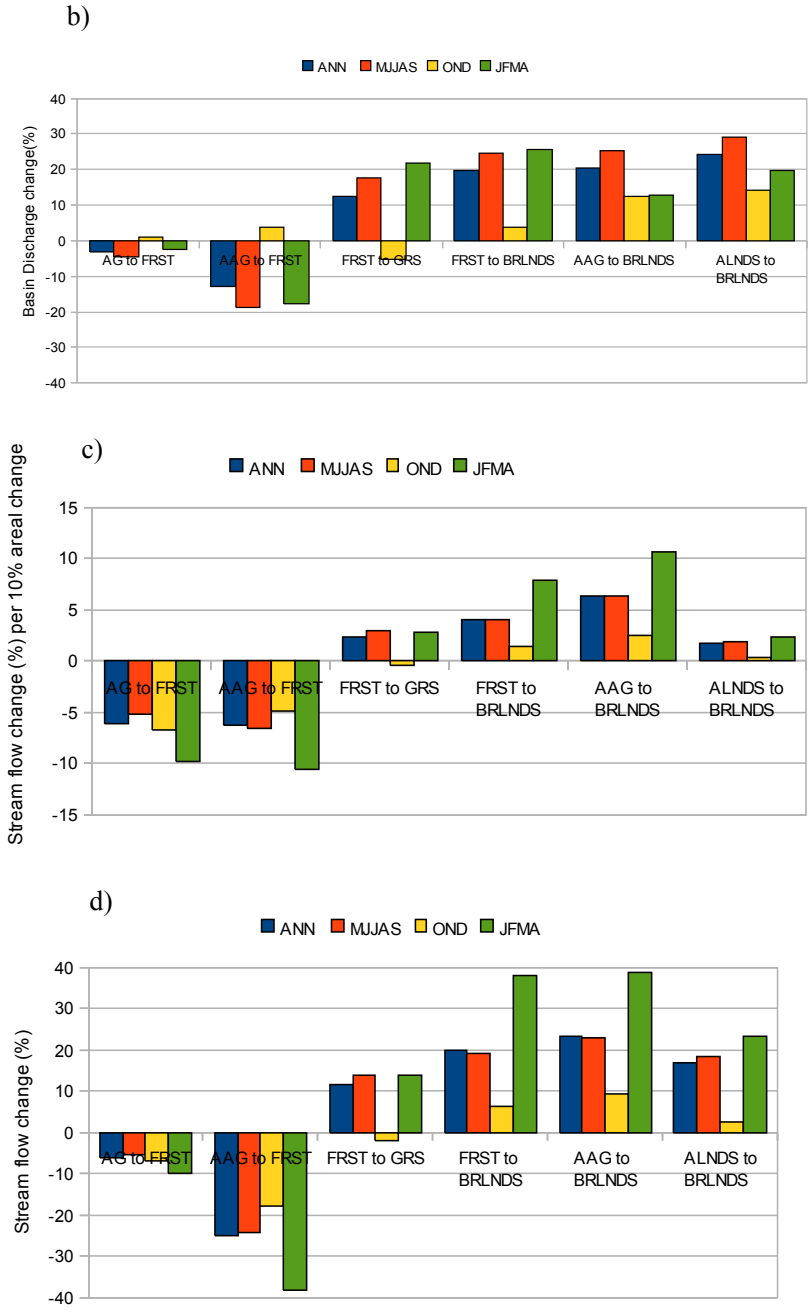

Figure 6: The upper two panels show the changes of annual and seasonal basin discharge (water yield) (a) per 10% area change in land use and (b) to the total area land use change. The lower two panels show changes in annual and seasonal streamflow (c) per 10% change in land use and (d) to the total area land use change.

the soil moisture is lost through evaporation before the soil gets saturated to generate streamflow. But, this was not true for the AAG to BRLNDS where there was strongly reduced evapotranspiration due to less transpiration and more soil moisture retained in the soil due to plant cover which later lead to increased streamflow. In contrast in the case of AAG to FRST, the soil moisture contributes significantly to reduce evaporation but there is strong transpiration due to plant cover. The overall effect results in decreased streamflow. This difference in sensitivity extends to the wet period (May-September) where the change in streamflow reaches at 6.3% and 1.9% for AAG to BRLNDS and ALNDS to BRLNDS scenarios, respectively. The sensitivity to land use change scenario in the dry seasons is different from the wet season response where a 10% change from agricultural to bare lands (AAG to BRLNDS) or forest (AAG to FRST) increased and decreased in the streamflow by10.6% and 10.5%, respectively (table 7) during January to April.

4.4 Effects of Climate Change on Streamflow

The effects of land use change on streamflow of the Omo Gibe River basin shown in table 7 were simulated under the same climate conditions; thus, they contained no contribution from climate variations. To estimate the various climate effects on streamflow or water yield, fourteen temperature and precipitation change scenarios were used (Table 8). Figure 7 (a) and (b) shows changes in annual and seasonal streamflow for different precipitation scenarios holding temperature fixed and various temperature scenarios at fixed precipitation, respectively.

Table 8: Percentage change in simulated average annual Streamflow for 14 scenarios compared with the baseline scenario

T change	Precipitation change (%)																			
	Annual					JFMA					MJJAS					OND				
	-20	-10	0.0	10	20	-20	-10	0.0	10	20	-20	-10	0.0	10	20	-20	-10	0.0	10	20
0	-42.2	-21.2	0.0	25.0	50.0	-51.5	-23.6	0.0	30.5	61.9	-41.1	-21.1	0.0	24.3	48.6	-38.4	-19.0	0.0	22.7	45.3
+2	-42.2	-22.2	-1.4	23.3	48.1	-51.5	-31.2	-9.1	19.7	49.7	-41.1	-20.9	0.1	24.4	48.7	-38.4	-19.8	-1.0	21.4	43.7
+4	-42.5	-22.8	-2.2	22.0	46.6	-55.9	-37.0	-16.2	11.2	39.9	-40.5	-20.3	0.7	24.7	49.0	-39.4	-21.1	-2.5	19.6	41.9

The most striking feature in Figure 7 is the strong change in the annual streamflow due to precipitation compared to those caused by land use changes discussed earlier. For example, the response of annual streamflow to a climate scenario of +20% precipitation and no temperature change resulted in an increase of about 50.0 %. In a 20% precipitation decrease scenario, the decrease of the streamflow was also substantial (over 42%). However, the sensitivity of streamflow to precipitation changes by holding temperature fixed and vice versa or combined changes in both may be rather different for the annual and seasonal streamflow estimation. The main results are given below:

a)

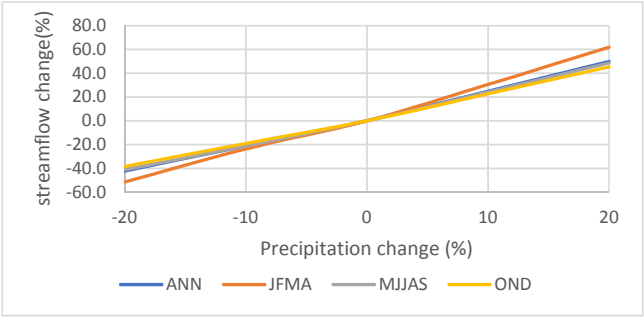

b)

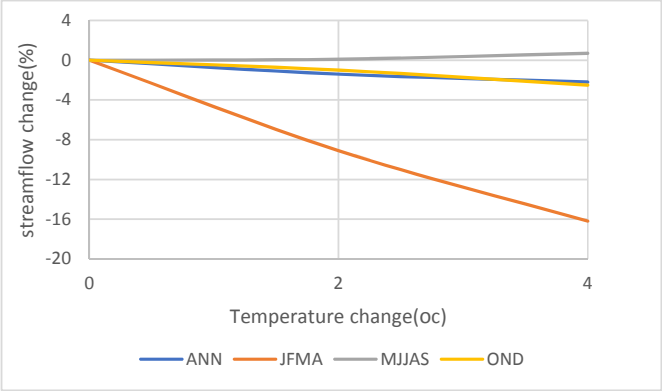

Figure 7: Climate change effects in annual and seasonal streamflow due to **a)** precipitation change by holding temperature fixed and **b)** temperature change by holding precipitation fixed.

4.4.1 The effect of precipitation changes

As a first approximation a linear regression analysis of the streamflow responses to the different scenarios indicates that a 10% change in precipitation and no temperature change will produce a 25% change in annual streamflow (Table 8). From the seasonal analysis, a 10% change in precipitation gives a 31%, 24% and 23% change in January-April (JFMA), May-September (MJJAS) and October-December (OND) streamflow, respectively (Table 8 and Figure 7a). The increase in streamflow in the JFMA is due to the reduction in evapotranspiration because of minimum vegetation cover during the dry period, whereas, in the MJJAS period when vegetation is in its peak growth, strong evapotranspiration reduces the impact of changes in precipitation on the streamflow, even though rainfall in absolute values increases considerably for those months.

Interestingly, the impact of increased precipitation influences the Omo basin streamflow more than a similar reduction in precipitation. This higher sensitivity to a precipitation increase can be explained by the soil physical properties (for instance; soil depth, soil moisture holding capacity, soil type and etc. and increased the water table to substantiate additional flow from subsurface as ground water flow. As the Omo Gibe catchment mainly covered by Dystric cambisols and Lithosols type with high soil moisture holding capacity, precipitation increase means increase in soil moisture and then as the soil moisture storage increases, the moisture gets a chance to percolate down to recharge groundwater.

4.4.2 The effect of temperature changes

The relative sensitivity of streamflow to changes in temperature, holding the precipitation fixed is modest in Omo Gibe river basin (Figure 7b). A linear regression analysis of streamflow responses for the different temperature scenarios indicates that a 1°C change in temperature will produce a 1.4% change in annual streamflow, 0.1% in MJJAS, 3.5% in JFMA and 1% in OND (Figure 7b). The JFMA (dry) season is more sensitivity to temperature change than the other two seasons. This is due to the fact that the soil is under moisture constraint in this period and an increased temperature will

dry out the soil via increased evapotranspiration which in turn results in the reduction of the streamflow.

4.4.3 Combined temperature and precipitation changes

Comparing the modelled relative streamflow sensitivity when both temperature and precipitation is changed with the linear combination of separate temperature and precipitation changes (equation 3.3), reveals that the Omo Gibe basin shows sensitivities that is a linear function of the temperature and precipitation changes for all seasons except JFMA where the combined effect of a strong precipitation reduction and temperature increase is smaller than the linear combination of the two (Figure 8). The reason for this is a large reduction in soil moisture and a declining in the water table due to significantly decreased precipitation result in reduced streamflow in the period.

a)

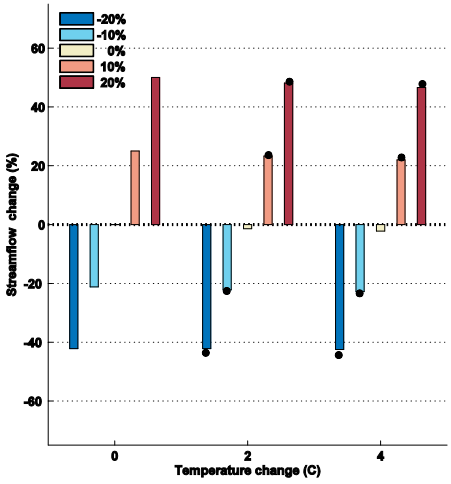

b)

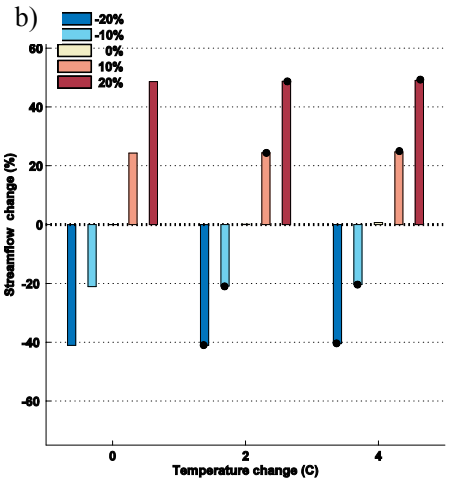

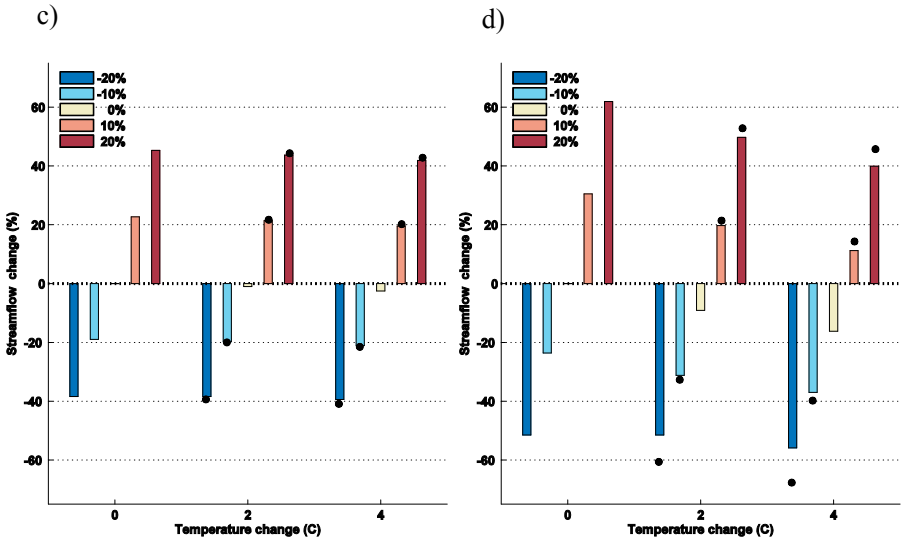

Figure 8: Change in annual (a) and seasonal (MJJAS (b), OND (c), JFMA (d)) streamflow (%) for different precipitation scenarios. Black dots indicate the linear sensitivity estimate based on equation 3.3

4.4.4 The Effects of Simultaneous Climate and Land Use Changes

In order to assess if the sensitivity of streamflow to simultaneously changes in land use and climate is just additive or if there is a more complex response integrated the model with various specified changes in both land use and climate, and compared the results to that of the base run where the land use is the present one (Fig. 2b), and the climate is given by the observed data.

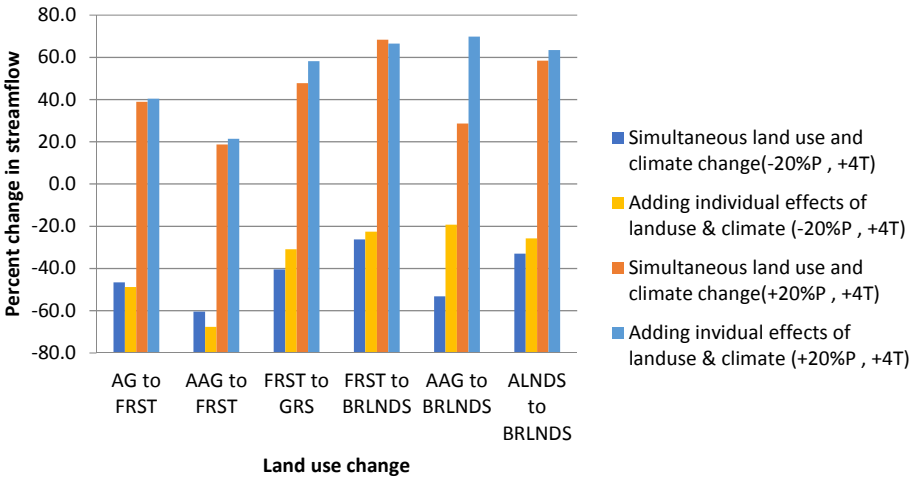

Figure 9: Annual streamflow change of the Omo Gibe river basin from simultaneous land use and climatic change and the sum of the individual effects of the changes.

As noted in the above sections a significant increase/reduction of the annual streamflow is happening under the increased temperature and simultaneously increased/reduced precipitation (+4°C and +20% or -20% precipitation change) scenarios (+46.6% and -42.5%, respectively, Table 8 and figure 9) compared to the simulation with the present climate. If scenarios with various land cover changes (given in Table 4) are imposed together with the climatic change of +4°C and +20% or -20% precipitation change the water budget response is changed. Figure 9 shows the annual water yield and streamflow change from six specific changes in land use scenarios and three climate conditions ([-20%, $+4^0$c]; [non-perturbed climate] and [+20%, $+4^0$c]) which with six land use changes gives a total of 18 possible combinations. In addition, the change from a simple addition of the effects from individual changes in climate and land use (equation 3.3) is shown. The general result from Figure 9 is that in many cases the nonlinear effects of both climate change and land use change are small. However, there are a few exceptions. According to Table 7 and Figure 6b and 6d the water yield and streamflow increased by 20.5% and 23.2% respectively when all lands changed to bare ground (AAG to BRLNDS scenario) under non-perturbed climate conditions. However, when both climate (+20%, $+4^0$C) and land use changes occurred at the same

time, annual streamflow increased by 28.4% (Figure 9) compared to the base run, this is smaller than the 69.8% change that would come from a simple addition of the effects from individual changes in climate (46.6%) and land use (23.2%) (See Fig.9). The change in simulated evapotranspiration (ET_a) varied from (5.3%), to (-14.6%) and 12.4%) for +4°C and +20% precipitation changes at reference land use, for non-perturbed climate at AAG to BRLNDS scenario and simultaneous change in the land use and climate scenario, respectively (Fig.10b). The effect of simultaneous land use and climate change on groundwater flow reached 59.2% which is slightly smaller than the sum of individual effects due to climate (27.5%) and land use (37.6%) change scenario.

Results in Figure 10a, b, c indicates the effects from land use and climate changes on water budget components (streamflow. ground water, lateral flow and evapotranspiration) and interactions among the components. The impacts of such changes may lead to either maximum or minimum streamflow under low or high evapotranspiration with big or small groundwater contribution in the basin. When the climate is becoming wetter (+20%, $+4^0$C) and land use changes that cause reduction of forest coverage in the basin (FRST to BRLNDS), for example, would magnify the wet climate effect and increase flow intensity and frequency (see Figure. 10b) even though the groundwater (Fig.10a) and lateral flow (Fig.10c) contribution is very low. On the other hand, if drier climate (-20%, $+4^0$C) is occurring in basin, the policy of returning agricultural land to forest (AAG to FRST) would further reduce streamflow and water yield and may enhance minimum flow impacts on water resources in the basin (see Fig.10a) because of increased losses via transpiration due to forest cover though there is relatively increase in groundwater and lateral flow contribution (Fig.10 b and c).

a

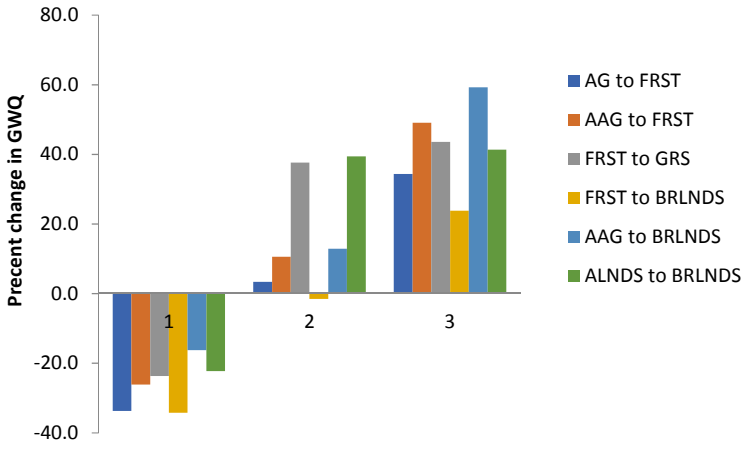
80.0
60.0
40.0
20.0
0.0
-20.0
-40.0
Precent change in GWQ
1
2
3
AG to FRST
AAG to FRST
FRST to GRS
FRST to BRLNDS
AAG to BRLNDS
ALNDS to BRLNDS

b)

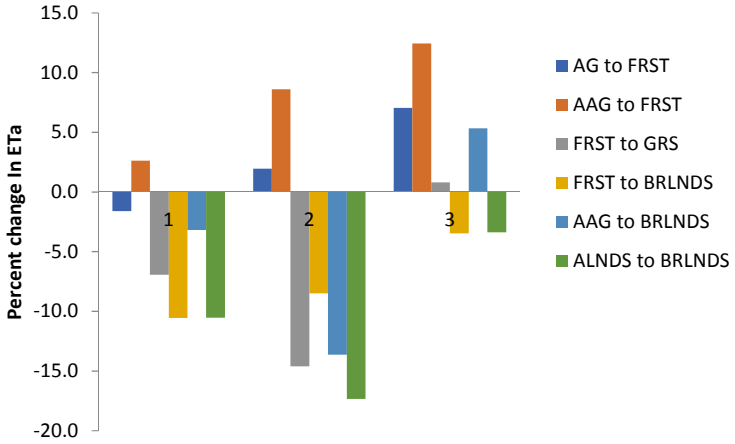
15.0
10.0
5.0
0.0
-5.0
-10.0
-15.0
-20.0
Percent change In ETa
1
2
3
AG to FRST
AAG to FRST
FRST to GRS
FRST to BRLNDS
AAG to BRLNDS
ALNDS to BRLNDS

c)

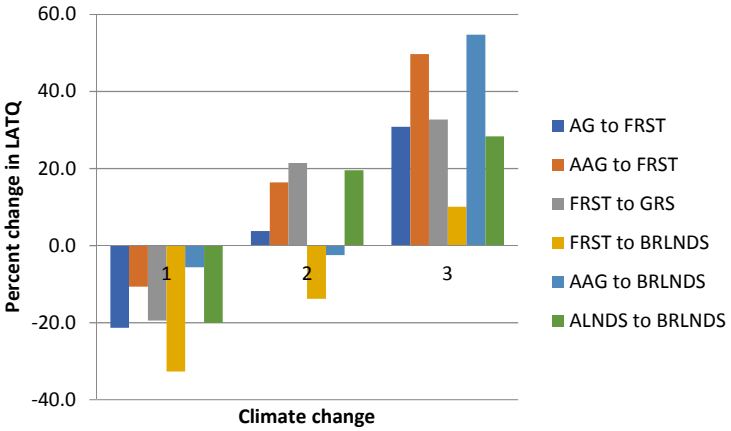

Figure10: Annual percent change in **(a)**base flow(GWQ), **(b)**evapotranspiration(ETa) and (c)lateral flow(LATQ) of the Omo Gibe river basin for various land use scenarios (**AG to FRST**: agricultural lands of slope > 25% changed into forest lands (10.3%) , **AAG to FRST:** All agricultural lands changed into forest lands (36.6%), **FRST to GRS:** Forest lands changed to grasslands (48.1%), **FRST to BRLNDS:** Forest lands changed to bare lands (48.1%), **AAG to BRLNDS:** All agricultural lands changed to bare ground (36.6%) and **ALNDS to BRLNDS** Change to a bare ground basin (98.8%) ,respectively) at -20% precipitation and $+4^0$C temperature change **(1),** non-perturbed**(2)** and at +20% precipitation and $+4^0$C temperature change**(3)** climate scenario**.**

5. Conclusions

The sensitivity of the Omo Gibe river basin to climate and land use change was modelled using the Soil Water Assessment Tool (SWAT) model. The model was successfully calibrated and validated at Great Gibe and Gojeb River gauges with good agreement between observed and simulated monthly streamflow. The monthly bias during the validation period was -14% and 7% Great Gibe and Gojeb River, respectively, while the Nash Sutclife efficiency factor was 0.75 and 0.88, respectively. Results indicate that modeling various changes in land use we found the change in streamflow to generally be below 10% per 10% change in land use. Deforestation of the entire region, through the change of the entire forest area coverage (48% of the

basin) to bare lands, increased the annual streamflow by 19.9% compared to the reference simulation. This result deviates from the report made by Avery (2010), where it was stated that the streamflow may decrease by 50-60%.

Streamflow sensitivity to land use change was largest when agricultural land was converted to either forest or bare lands. In the AAG to BRLNDS scenario where there is strongly reduced evapotranspiration due to less transpiration and more soil moisture retained in the soil due to plant cover which later lead to increased streamflow. In contrast in the case of AAG to FRST, the soil moisture contributes significantly to reduce evaporation but there is strong transpiration due to plant cover.

The overall effect results in decreased streamflow. For many of the simulations the relative streamflow sensitivity was largest in the dry period of JFMA because of changes in evapotranspiration as transpiration (component of evapotranspiration) was altered when the land use was altered. In addition, many of the simulations show the weakest streamflow response in the period of October- December. This is because the period is following the wet period (MJJAS) and evapotranspiration is dominated by evaporation and the soil moisture is large. Thus, changes in transpiration due to land use changes are less important. Sensitivity of streamflow to temperature and precipitation (14 hypothetical climate change scenarios) show that the basin streamflow is very sensitive to precipitation changes and moderately sensitive to temperature changes. The annual streamflow response to a 10% change in precipitation with no temperature change was on average 25%. While the streamflow sensitivity to temperature was relatively low. The average annual streamflow responses to a 1˚C change in temperature and no precipitation change was -1.4%.

The highest sensitivity to precipitation change was observed during dry period from JFMA with 31% change in streamflow from a 10% precipitation increase. This is because of relatively decreased evapotranspiration due to minimum transpiration from less vegetation cover during the period.

For all seasons except JFMA the combined effect of a precipitation changes and temperature increase was linear (the sum of the changes to precipitation and temperature individually). The non-linear behavior during JFMA was due to the interaction among various factors which are more pronounced in this season than in

other periods of the simulation. Some of the factors are the soil physical properties (in relation to limited soil moisture), less vegetation cover, minimum precipitation amount and high temperatures during the period.

The JFMA season is much more sensitivity to temperature change than the other two seasons (-3.5%/K). This is due to moisture constraint and an increased temperature to dry out moisture from the soil via evapotranspiration in the season which in turn results in the reduction of streamflow.

The large sensitivity of streamflow in JFMA may have serious implications for management of water supply for domestic and industrial use, power generation and agriculture, because a number of small streams which now are perennial may be altered to intermittent.

Results also indicate the effect of various land use changes, even some extreme land use changes, is secondary to plausible changes and variations in climate. These conclusions are consistent with some previous studies for different climatic regions around the world (e.g., Mimikou et al., 1999; Lahmer et al., 2001; Legesse et al., 2003; Tao et al., 2003; Hu et al., 2004; Guo et al., 2008).

In addition to describing the effects of individual land use or climate change on seasonal and annual streamflow, the effect of simultaneous changes in both land use and climate on the water cycle was investigated. Results indicate that the combined effects differ only slightly from the effect resulting from the sum total of individual land use and climate change. For example, in a wet scenario, changing land use to increase bare land areas would increase streamflow by 58.41% which is slightly less than the 63.4% from simple additions of the individual effects from changes of land use (16.8%) and climate (46.6%). However, there are exceptions to this near linear response showing that the model simulates some effects leading to nonlinear interactions among water balance components when simultaneous changes in land use and climate change would take place in the same basin.

Therefore, management of the emerging cascaded hydropower development will be daunting task given the high sensitivity of precipitation. This requires careful consideration of implementing seasonal flow forecasting models and reservoir operation management for sustainable upstream-downstream interaction.

Finally, we note that there are several uncertainties related to the above analysis, one is that it assumes the current streamflow-precipitation-temperature relationship is still valid under the future climate scenarios. As Liu et al. (2008) noted, in simulation of hydrological systems at the regional scale, many factors, such as model structure, parameters, and meteorological input, can lead to large uncertainty due to inherent multi-scale space-time heterogeneity. The limited number and spatial distribution of the meteorological and streamflow data is another big challenge. Most of the meteorological data located in the upper catchment. In our sensitivity studies we have multiplied the precipitation with a fraction. This means that we assume that the wet-day frequency is unchanged and the whole precipitation change is given as a change in intensity. For temperature we have added a constant for the whole year and thereby assuming that the change is not depending on season.

Acknowledgements

This work has been carried out with support from the Ethiopian Malaria Prediction System (EMaPS) project funded by the Norwegian Program for Development, Research and Education (NUFU). The authors would like to thank the Ministry of Water, Irrigation and Energy and the National Meteorology Agency of Ethiopia for providing the streamflow and meteorological data for the entire basin.

References

Arnold, J.G., and P.M. Allen. (1996). Estimating Hydrologic Budgets for three Illinois watersheds. Journal of Hydrology,176(1-4):57-77.

Arnold, J.G., Sirinivasan, R., Muttiah, R.S, Williams, J.R. (1998). Large Area hydrologic modelling and assessment, part 1: Model Development. Journal of the American water resources association, 7389.

Duan. (1992). Effective and efficient global optimisation for conceptual rainfall-runoff models. Water resources Engineering , 1015-1031.

Dunn, S.M., Mackay, R., 1995. Spatial variation in evapotranspiration and the influence of land use on catchment hydrology. J. Hydrol. 171, 49–73.

FAO. (1995). Soils of EAST Afica, SEA. Food and Agriculture organization of the United Nations.

Fohrer N, Eckhardt K, Haverkamp S, Frede H-G, 2001. Applying the SWAT model as decision supporting tool for land use concepts in peripheral regions in Germany. 994 -999. In: Stott D-E, Mohtar R-H, Steinhardt C-G (eds). Sustaining the Global Farm. 10th International Soil Conservation Organization Meeting, May 24-29, 1999, West Lafayette. http://topsoil.nserl.purdue.edu/nserlweb/isco99/pdf/isco99pdf.htm.

Fohrer N, Haverkamp S, Eckhardt K, Frede H-G, 2001. Hydrologic response to land use changes on the catchment scale. Phys Chem Earth B. 26: 577-582.

Fohrer, N., Haverkamp, S. and Frede, H.-G. (2005), Assessment of the effects of land use patterns on hydrologic landscape functions: development of sustainable land use concepts for low mountain range areas. Hydrol. Process. 19: 659–672. doi: 10.1002/hyp.5623

Gan T.Y., (1988). Application of scientific modelling of hydrological response from hypothetical small catchments to access a complex conceptual rainfall runoff model. Water Resources Series Technical reports, Department of Civil Engineering, University of Washington, Seattle,Washington.

Griensven, V. (2002). Sensitivity analysis and auto-calibration of an integral dynamic model for river water quality. *Water Science and Technology* , 321-328.

Guo, H., Hu Q., Jiang T. (2008). Annual and seasonal streamflow responses to climate and land-cover changes in the Poyang Lake basin, China, Science direct, *Journal of Hydrology*,355, pp 106-122.

Hansen, M.,R. Defries,J.R.G. Townshend,and R.Sohlberg (1998). UMD Global Land Cover Classification. specify 1 Degree, 8 Kilometer, or 1 Kilometer (1.0). Department of Geography, University of Maryland,College Park,Maryland,1981-1994.

Hu, Q., Willson, G.D., Chen, X., Akyuz, A., 2004. Effects of climate and landcover change on streamflow in the Ozark highlands, USA. Environ. Model. Assess. 10, 9–19.

Krause, P., 2002. Quantifying the impact of land use changes on the water balance of large catchments using the J2000 model. Phys. Chem. Earth 27, 663–673.

Lahmer, W., Pfiitzner, B., Becker, A., 2001.Assessment of land use and climate change impacts on the mesoscale. Phys. Chem. Earth (B) 26, 565–575.

Legesse, D., Vallet-Coulomb, C., Gasse, F., 2003. Hydrological response of a catchment to climate and land use changes in Tropical Africa: case study South Central Ethiopia. J. Hydrol. 275, 67–85.

Lenhart, T., Eckhardt, K., Fohrer, N., and Frede, H.G.: (2002). Comparison of two different approaches of sensitivity analysis, *Phys.Chem.Earth,27,* 645-654.

Mander, U., Kull, A., Tamm, V., Kuusemets, V., Karjus, R., 1998.Impact of climatic fluctuations and land use change on runoff and nutrient losses in rural landscapes. Landscape Urban Plan. 41, 229–238.

Mengistu, D. T. and Sorteberg, A. (2012): Sensitivity of SWAT simulated streamflow to climatic changes within the Eastern Nile River basin, Hydrol. Earth Syst. Sci., 16, 391-407, doi: 10.5194/hess-16-391-2012, 2012.

Mimikou, M.A., Kanellopoulou, S.P., Baltas, E.A., 1999. Human implication of changes in the hydrological regime due to climate change in Northern Greece. Global Environ. Change 9, 139–156.

MoWR. (2002). *Ethiopian water sector strategy.* Addis Abeba: Ministry of Water Resources.

Neitsch, S.L., Arnold, J.G., Kiniry, J.R., Williams, J.R., King, K.W., 2002a. Soil and Water Assessment Tool: Theoretical Documentation, version 2000 (available at http://www.brc.tamus.edu/swat/).

Neitsch, S.L., J.G. Amold, J.R. Kiniry, R.Srinivasan, and J.R. Williams. (2002). Soil and Water Assessment Tool User`s Manual, Version 2000.

Nicks, A.D. (1974). Stochastic generation of the occurrence, pattern and location of maximum amount of daily rainfall. Statistical hydrolgy (pp. 154-171). Washington,DC: U.S. Governmental print office.

Pikounis M., Verano E., Baltas E., Dassaklis A., Mimikou M., (2003). Application of the SWAT model in the Pinios River Basin under different land-use scenarios, Global Nest: the int.J.Vol.5, No.2, pp 71-79.

Ren, L., Wang, M., Li, C., Zhang, W., 2002.Impacts of human activity on river runoff in the northern area of China. J. Hydrol. 261, 204–217.

Santhi, C., Arnold, J. G., 5 Williams, J. R., Dugas, W. A., Srinivasan, R., and Hauck, L. M.: Validation of the SWAT Model on large River Basin with point and Nonpoint sources, J. Am. Water Res. Assoc., 37, 1169–1188, 2001.

Sheffield, J., G. Goteti, and E. F. Wood, 2006: Development of a 50-yr high-resolution global dataset of meteorological forcings for land surface modeling, J. Climate, 19 (13), 3088-3111

Tao, F., Yokozawa, M., Hayashi, Y., Lin, E., 2003.Future climate change, the agricultural water cycle, and agricultural production in China. Agri. Ecosys. Environ. 95, 203–215

Twine, T.E., Kucharik, C.J., Foley, J.A., 2004. Effects of land cover change on the energy and water balance of the Mississippi River basin. J. Hydrometeor. 5, 640–655

USDA. (1999). Soil Taxonomy (2nd edition ed.). (U. S. Agriculture, Ed.) Washington,Dc: U.S. Government Printinig office.

USDA-SCS. (1972). Hydrology. In *National Engineering Hand book section 4* . Washington ,Dc: USDA-SCS.

Wambeke. (2003). Properties and management of soils of the tropics. Rome: FAO Land and Water Digital Media Series.

Zeray, L. (2007). Calibration and Validation of SWAT Hydrologic Model for Meki Watershed,Ethiopia. Conference of International Agricultural Research for Development. University of Kassel-Wizenhausen and University of Gottingen.

Official documents, Media and independent Resources

Avery S. (2010): Hydrological impacts of Ethiopian Omo Basin on Kenya`s Lake Turkana water levels and Fisheries Final Report prepared for the African Development Bank Tunis.

Bank Information Center www.bicusa.org Campagna per la Riformadella Banca Mondiale.

BBC, "Ethiopia: Troubles Downstream," Crossing Continents (audio program), 2009. Available at: http://www.bbc.co.uk/iplayer/episode/b00j7txw/

BBC, "Ethiopia's Divisive Dam" (multimedia program), 2009.Available at: http://news.bbc.co.uk/2/hi/africa/7959444.stm.

Campagna per la Riformadella Banca Mondiale, "The Gilgel Gibe Affair," 2008.Available at: http://www.crbm.org/modules.php?name=browse&grpid=60/.

EEPCo, "Gibe 3 Environmental and Social Impact Assessment," 2009. Available at: http://www.eepco.gov.et/.

Friends of Lake Turkana: www.friendsoflaketurkana.org.

International Rivers, "Facing Gibe 3 Dam: Indigenous Peoples of Ethiopia's Lower Omo Valley," 2009. Available at: http://internationalrivers.org/en/ node/2794

Jones/www.nowater-nolife.org. Ethiopians Gibe III Dam. SOWING HUNGER AND CONFLICT. International Rivers | 2150 Allston Way, Suite 300, Berkeley, Available at www.friendsoflaketurkana.org/index.php?option=com_content&view

Revisiting Systems Type Black-box Rainfall-Runoff Models for Flow Forecasting Application

Dereje Tesfahun Mengistu[1,2], and Asgeir Sorteberg[2,3]

[1]Arba Minch Institute of Technology, Arba Minch University, Ethiopia

[2]Geophysical Institute, University of Bergen, Norway

[3]Bjerknes Centre for Climate Research, University of Bergen, Norway

Corresponding author address:

Dereje Tesfahun Mengistu

Arba Minch

P.O. Box, 21, Arba Minch, Ethiopia

E-mail:dertes_24@yahoo.com;dme061@uib.no

Abstract

Often, we tend to spend huge amount of time and resources to setup and use complex hydrological models for simple goal of flow estimation. Running complex models becomes even more difficult when the amount of available data is scarce as we usually face in many parts of Africa. The aim of this study is to evaluate and revitalize the systems type black box model against complex hydrological models for easy flow estimation application. Six systems type black box models, the Simple Linear Model (SLM), Non-Parametric Simple Linear Model (NP-SLM), Linear Perturbation Model (LPM), Non-Parametric Linear Perturbation Model (NP-LPM) and Linearly Varying Gain Factor Model (LVGFM), a non-linear black box type artificial Neural Network model (ANN) are compared with three complex hydrological models of those under SMAR, HBV and SWAT. The models are compared based on daily rainfall and stream flow data (1980–2000) on Gilgel Abbay watershed. Event -based analysis was also conducted using 100 selected runoff events.

In terms of the event rainfall-runoff relationship, it was indicated that the event runoff is largely a function of the amount of rainfall. The event rainfall-runoff relationships explained as much as 62% for the wet periods without the integration of the evaporating demands. Although rainfall intensity, duration and catchment characteristics play a role, in this watershed, rainfall amount affects substantial part of the runoff response consolidating a simple rainfall-runoff relationship can describe the runoff in this watershed.

Comparison of systems type black box and complex hydrological models in the study area indicates that the LPM and the ANN models perform better than the complex hydrological models such as SMARG, HBV and SWAT in terms of R^2 and Nash Sutcliffe Efficiency (NSE) criteria. This confirms that simpler models (that takes only rainfall as input) can surpass their complex counterparts in performance for continuous simulation and reproducing the hydrographs or flow estimation. There is a strong justification, therefore, for the claim that increasing the model complexity, thereby increasing the number of parameters, does not necessarily enhance the model performance. It is suggested that, in practical hydrology, the simpler models, may still play a significant role as effective simulation tools, and countries with scarce

hydrological data should revitalize application of such systems type black box modelling schemes that depend only on rainfall and runoff data sets which could be easily available.

Keywords
Black box models; distributed models; Rainfall-runoff relationships; event

1 Introduction

Rainfall-runoff relationships are complicated processes which may be highly non-linear and exhibits both temporal and spatial variations. Understanding their relationship is essential for practical basin management practices. Several hydrological models have been developed to simulate rainfall-runoff relationships across the world [1]. These can be classified as empirical black box models, conceptual and physically based distributed models [1]. Black box models are empirical, involving mathematical equations that have been assessed, not from the physical processes in the catchment, but from analysis of concurrent input and output time series. Conceptual (lumped) models treat the catchment as a single unit, with state variables that represent average values over the catchment area, such as storage in the saturated zone. Another approach to hydrological processes modeling is the attempt to construct models based on the governing equations describing all the surface and subsurface flow processes in the catchment called physically distributed models. Each of these types of models has their own advantages and limitations [1]. For instance, in areas where getting sufficient hydro-meteorological data are problematic or the purpose of hydrological modeling is limited to flow estimation, applications of linear systems theoretic models (black box models) are inevitably important for water related development. However, to choose between the various available hydrological models to suit a practical demand and find the most appropriate model for the specified basin is a big challenge. Many models are in practice simple linear system theoretic models (black box models) [1] which do often not represent the non-linear dynamics, which are inherent in the process of rainfall-runoff transformation.

[2] and [3] observed that the rainfall information alone is not sufficient to calculate the runoff from a catchment as the initial state (such as amount of soil moisture and orographic features) of the catchment plays an important role in determining the runoff rate behavior. The rainfall-runoff relationship in mountainous regions are influenced by the steep gradient profiles (i.e. inter flow and sheet flow) and less influenced by soil composition [4]. Nevertheless, soil composition in less steep environment plays a major role in runoff generation due to the presence of very to moderately drained soils [4] [5] [6] [7]. Therefore, higher streamflows and runoff coefficients (R/P, where R is runoff

and P precipitation) are usually associated with mountainous area [8], while smaller R/P ratios are expected for low-topographic gradient watersheds [8] - [9]. [10] argue that runoff in lower land plain watersheds have a much larger variability than upland watersheds because of a wider range of variable source areas, including ephemeral water storage in depressions in a low gradient terrain.

Evapotranspiration is another factor that affects the hydrological processes of the watershed in shallow water tables [11]. It is mainly influenced by humidity gradients, solar energy, wind speed, soil properties and vegetation type [12] [13]. Other studies have found that depending on the soil moisture status, lowland watersheds were highly responsive to rainfall by producing more frequent and greater amounts of runoff, with peak flow rates also depending on the surface depression storage [8]. Furthermore, some rainfall-runoff simulation models have demonstrated that the degree of water saturation in the soil prior to a precipitation event (the antecedent soil moisture condition, AMSC) correlates with the portioning of the event rainfall into infiltration and stream flow [14] [15] [16].

Seasonal climate variability affects both the soil moisture and the characteristics of the storm events that in turn affect the runoff generation pattern [11]. Some of these characteristics are rainfall intensity, frequency, duration, and direction [17]. Although the antecedence soil moisture condition of the watershed influences water available for runoff, evapotranspiration and infiltration via soil water storage, it is highly variable and difficult to measure [18].

The main objective of this study is to evaluate the performance of nine rainfall-runoff models (from simple to complex) whether model complexity is important for flow estimation in the context of data scarce areas in Africa. There is a tendency to use complex models such as SWAT for simple purpose of flow estimation in many African watersheds. The amount of spatial and temporal date sets required to calibrate complex models such as SWAT doesn't warranty the purpose if the purpose of the modeling is simply to estimate flow for water resources development application. Therefore, this study attempts to revitalize application of simple rainfall-runoff hydrological models

for use in water resources application. The study is conducted on Gilgel Abbay catchment of Blue Nile basin (Ethiopia) using 21 years (1980-2000) historical data of daily rainfall, temperature and stream flow. Finally, we compare the results from the individual rainfall-runoff models with several methods of combining the outputs to investigate if there is added value in making ensemble means.

2 The study area

The Gilgel Abbay catchment (4051km^2) is one of the largest among the four main sub-catchments in Lake Tana sub basin of the upper Blue Nile basin, Ethiopia (Figure 1), providing about 60% of the lake inflow. It is located at 10^0 44'N latitude and 37^0 23'E longitude. The catchment includes the two gauged sub-basins; Upper Gilgel Abbay (1664 km^2) and Koga (307 km^2), See Figure 1, with elevation ranging from 1787m to 3518 The topography is rugged in the southern part of the catchment and the periphery to the west and southeast, while the remaining part is a typical plateau with gentle slopes. The soil is dominated by clays and clay loams (Figure 1c). The dominant land use units are agricultural (65%) and agro-pastoral land (33%) [19], among this rainfed agriculture is the predominant cover of the Upper Gilgel Abbay (74%) and Koga (64%) sub-catchments (Figure 1b).

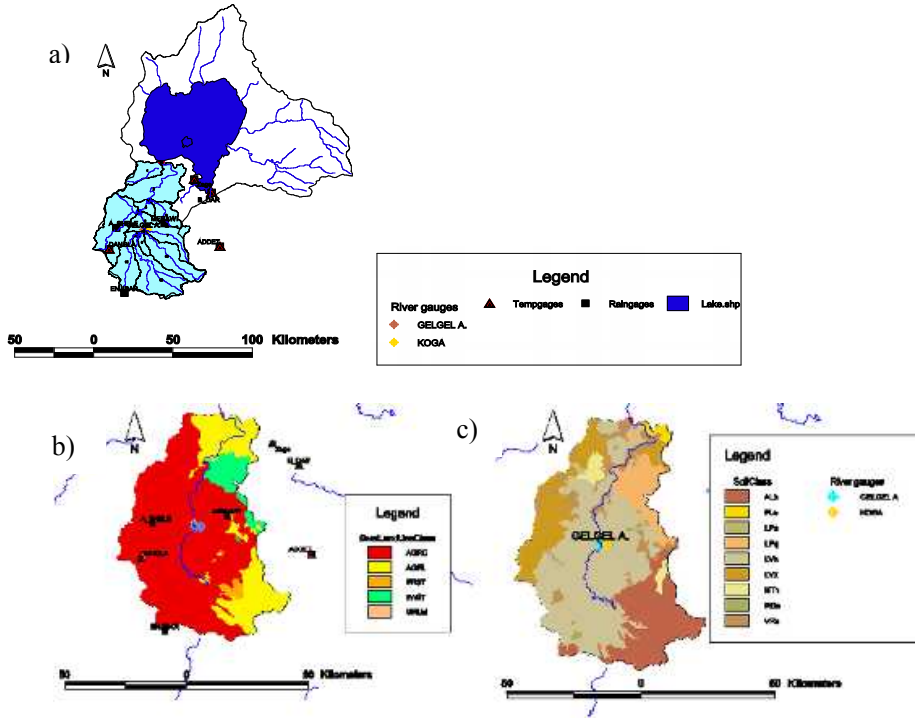

Figure 1.a) Distribution of meteorological stations and gauging station, b) land use and c) soil map in the Gilgal Abbay catchment

Upper Gilgel Abbay has its main rainy season between June and September, receiving about 70 to 90% of the annual rainfall during this season [20] [21] [22]. Annual area average rainfall (1964-2005) ranged from 834 to 2106 mm, with July representing the wettest month (356mm) and January representing the driest month (3mm) on average. Rainfall observations indicate significant spatial variability in rainfall following the topography, with decreasing amounts from south to north. Long-term (1980-2000) minimum and maximum annual air temperature values recorded at Merawi (2020m.a.s.l.) and Dangla (2180m.a.s.l.) stations ranged from 11^0C to 37.7^{o}C, respectively with temporal temperature variations being small throughout the year [19].

3 Data Assessments and Method

3.1 Historical Data

We used daily rainfall and temperature data (1980-2000) from seven and four stations, respectively (Figure 1a). Daily Stream flow data for Gilgel Abbay is taken from the then Ministry of Water and Energy (now Ministry of Water, Irrigation and Electricity). The meteorological data of rainfall and temperature is obtained from National Meteorological Agency (NMA). Missing values in rainfall and temperature were treated using the SWAT built-in weather generator developed by [23]. The daily area representative precipitation was calculated using thiessen polygon method.

3.2 Event selection

We selected storm events based on discharge rates greater than 1.84m^3/s (minimum mean discharge separated from base flow per day), where the base flow is calculated by using variable storage method, total mean daily area averaged rainfall values greater

than 2.3mm; and a period of 48 hours or more in between rain events (Table 1). A rain event is defined as the rainfall amount which contributes runoff event in a period of 48 hours [11]. These criteria were selected to identify detectable single peak events and minimize influence of prior rainfall on several peaks. Multiple peak events were excluded from this analysis in order not to complicate the identification of storm duration and total storm volume. The same method was used by [7] - [8] [24], [25], and [26]. Single event peak discharge can be modeled easier as described by [27]. The start of the runoff event is the rainfall available for runoff after infiltration and other abstractions have been accounted for.

The antecedent precipitation index (API) was calculated as a measure of the available soil moisture content (ASMC):

$$API_t = P_t + \sum_{i=1}^{N} K_{t-i} API_{t-i} \tag{3.1}$$

Where P_t is the area averaged precipitation at day *t, N* the number of days prior to the start of the runoff event and K_t is the recession constant calculated as the product for three individual constants, i.e. $K=K_s*K_i*K_g$ where $K_s=1.0$, $Kj=0.43$and $K_g=1.33$ are recession constants associated with surface storage, inflow and ground water flow respectively.

Total event runoff volume is calculated by dividing the daily runoff by the watershed area to obtain runoff depth in mm. The runoff volume was considered to be the area under the hydrograph from the start of the event (defined above) until it reaches base flow level or until the next rise starts. Using the above definition of an event, the average duration of the storm events was 12 days. Since the rainfall data was in daily basis, there was sometimes challenge to identify an exact amount of rainfall amounts resulting in a particular runoff event. The begin flow for each event was calculated as

the flow at which direct runoff starts. R/P was calculated using the accumulated runoff amount and corresponding accumulated area averaged rainfall over the runoff event.

Based on the above criteria, we selected 100 storm events with various parameters showing the hydrologic characteristic of the study area (table 1). [11] Used 51 storms for only a 10-year (1964-1973) period that included events with multiple peaks also. In other studies, [25] used 75 events, [28] used 29 events, [7] used 23 events, [26] used 4-9 events for each watershed, and [24] used 55 storm events for various study areas. We, therefore, believe that analysis of 100 storm events is adequate for testing event based rainfall runoff relationship.

3.3 Regression analysis

A simple linear regression analysis was used to determine the relationship between runoff and other variables. Equations of the linear regression lines and their parameters were tested for statistical significance at the 5% level (α=0.05) using a two-tailed t-test. In addition, a standard stepwise regression analysis was used to examine the effects of different factors on the runoff.

3.4 The Galway River Flow Forecasting System (GFMFS)

The Galway Flow Modeling Forecasting System (GFMFS) is software packages developed at Department of Engineering Hydrology, National University of Ireland, Galway [29]. A brief description of the GFMFS software package may be found in [30] [31] [32] [33] [34] - [35] [36] - [37] [38] - [39] [40] [41] - [42] [43] [44]. The GFMFS models may be run in *updating* mode or *simulation* mode, depending on the choice of model. In *updating* mode, the models use the lagged observed discharge along with precipitation input to simulate the streamflow simulation hydrograph to the corresponding observed hydrograph. In contrast, non-updating (*simulation*) mode uses

the input of precipitation and excluding the use of the recently observed discharge as model inputs.

The five major hydrological applications of the GFMFS packages are i) Modeling by calibration and validation for simulation of continuous river flow, ii) Estimation of river flow i.e. generation of synthetic flow series, using inflow data and a calibration model.iii) Modeling by calibration and verification, for lead-time forecasting in absence of QPF (quantitative precipitation forecasts), iv) Modeling by calibration and verification, for lead-time forecasting using QPFs, v) Real time flow forecasting using models and techniques chosen in step i. and/or iii or iv.

Modeling by calibration and validation for simulation of continuous river flow in step 1 was applied for this study. The models implemented in this study (from the GFMFS package) are six rainfall runoff models that depend only on rainfall and runoff relationships (single input) and one complex hydrological models that uses more than one rainfall input and several conceptual parameters in the model formulation. These models are the Simple Linear Model (SLM), Non-Parametric Simple Linear Model (NP-SLM), Linear Perturbation Model (LPM), Non-Parametric Linear Perturbation Model (NP-LPM) and Linearly Varying Gain Factor Model (LVGFM), a non-linear black box type artificial Neural Network model (ANN). The complex hydrological models accessed from GFMFS package include Soil Moisture Accounting and Routing Model conceptual model (SMAR, we tested the three variants, namely the SMARG, SMAR-NC1 and SMAR-NC2 versions, but only the SMARG is reported on here since the results were similar for the two other versions) (see Table 5).

3.5 Other Complex Hydrological Models

In addition to the above hydrological models we further apply a conceptual semi distributed (HBV) and a physically distributed (SWAT) model in the study. The HBV model [45] - [46] - [47]- [48] is a rainfall-runoff model, which includes conceptual

numerical descriptions of hydrological processes at the catchment scale. The general water balance can be described as:

$$R_{day} - ET_a - Q_{surf} = \frac{d}{dt}[SW + W_{seep} + Q_{gw}] \quad (3.2)$$

Where SW is the soil water content (mm), R_{day} is the daily precipitation, Q_{surf} is the amount of surface runoff/streamflow, ET_a is the amount of actual evapotranspiration, W_{seep} is the amount of water entering the vadose zone from the soil profile and Q_{gw} is the amount of ground flow.

The HBV model can be used as a semi-distributed model by dividing the catchment into sub basin. Each sub basin is then divided into zones according to altitudes and the elevation zones which are further divided into different vegetation zones (e.g. Lakes, forested and non-forested areas).

The model is normally run on daily values of rainfall and air temperature, and daily or monthly estimates of potential evaporation. Observed streamflow data were used for calibration of the model through optimizing the embedded parameters.

SWAT (Soil and Water Assessment tool, version SWAT2005) is a physically based, distributed parameter model which operates on daily time step and uses physiographical data such as elevation, land use and soil properties as well as meteorological data and, stream flow data for calibration. It is computationally efficient for use in large watersheds, and is capable of simulating the impact of land management practices [49].

The effects of spatial variations in topography, land use, soil and other characteristics of watershed hydrology is incorporated by dividing a basin into several sub-basins based on drainage areas of tributaries and is further divided the sub-basins into a number of hydrological response unit (HRUs) within each sub-basin, based on land cover and soils. Each HRU is assumed spatially uniform in terms of land use, soil, topography and climate. The subdivision of the watershed enables the model to reflect

differences in evapotranspiration for various crops and soils. All model computations are performed at the HRUs level [50].

The fundamental hydrology of a watershed in SWAT is based on the following water balance equation [50].

$$\frac{\partial SW}{\partial t} = R_{day} - Q_{surf} - ET_a - W_{seep} - Q_{gw} \tag{3.3}$$

Where SW is the soil water content (mm), R_{day} is the amount of precipitation on (mm), Q_{surf} is the amount of surface runoff/streamflow (mm), ET_a is the amount of actual evapotranspiration (mm), W_{seep} is the amount of water entering the vadose zone from the soil profile (mm), and Q_{gw} is the amount of ground flow (mm). Detail descriptions of the different model components can be found in [51] [52]. Like HBV model SWAT used observed streamflow data for calibration purpose to optimize high to very high sensitive parameters.

Table 5 rank the models according to complexity from simple to complex. SLM is the simplest followed by the LPM in their non-parametric and parametric forms and the LVGFM. Non-parametric and parametric assume the observations must be independent, the observations in non- parametric forms must be drawn from normally distributed populations, and these populations must have the same variances however in parametric form variable distributions have been.

The three models (SLM, LPM and LVGFM) are system-linear model in structure, and an ordinary least squares solution is used for estimation of the pulse response function except for the parametric forms where the parameters were optimised. HBV and SWAT models are the most complex with a complicated mathematical procedure to be processed during simulation.

3.6 Combination of Outputs

A particular rainfall-runoff model may have been selected from among a number of competing alternative models, based, perhaps, on its accuracy, its familiarity to the

user, its ease of use, the type of the catchment, and the available data. However, there may be a potentially danger in relying entirely on one substantive rainfall-runoff model (a sample of one) since it is unlikely to perform satisfactorily at all time or under all conditions (e.g. perhaps not all of its structural assumptions are valid or the conditions under which it is assumed to operate are not entirely fulfilled. The method of combination of outputs from each of the model applied for the study area are carried out in the concept that the individual model assumed to capture some physical characteristics of the study area. We use three different methods of combining outputs (MOCT): The Simple Average Method (SAM), the Weighted Average Method (WAM), and the Neural Network Method (NNM).

3.6.1 The Simple Average Method (SAM)

The simple average method (SAM) is the simplest method of combining the outputs of different individual models. Given the estimated discharges from N rainfall-runoff models, a combined estimate of the discharge of the i^{th} time period, using the SAM, is given by

$$\hat{Q}_{Ci} = \frac{1}{N}\sum_{j=1}^{N} \hat{Q}_{ji} \tag{3.4}$$

where $\hat{Q}_{Ci}$ is the combined estimate of the discharge of the i^{th} time period, N is the number of rainfall runoff models and $\hat{Q}_{ji}$ the average simulate discharge for time period *I* from rainfall-runoff model *j*.

3.6.2 The Weighted Average Method (WAM)

When some of the individual models selected for combination appear to be consistently more accurate than others, in which case the use of the simple average method for combination can be quite inefficient [53], the use of a weighted average would be considered.

The weighted average method (WAM) for combining the estimated model outputs, in the case of N rainfall-runoff models, may be expressed as [54]

$$Q_i = \sum_{j=1}^{N} a_j \hat{Q}_{ji} + e_i \tag{3.5}$$

Where Q_i is the combined discharge and a_m is the weight assigned to the j^{th} model estimated discharge. e_i is the combination error term.

The above equation may alternatively be expressed in matrix notation as

$$\mathbf{Q = PA + E} \qquad (3.6)$$

Where **P** is the input matrix defined by

$$\begin{bmatrix} \bar{Q}_{1,1}, \bar{Q}_{2,1} - - - \bar{Q}_{N-1,1}, \bar{Q}_{N,1} \\ \bar{Q}_{1,2}, \bar{Q}_{2,2} - - - \bar{Q}_{N-1,2}, \bar{Q}_{N,2} \\ , \\ , \\ , \\ , \\ , \\ , \\ \bar{Q}_{1,k-1}, \bar{Q}_{2,k-1} - - - \bar{Q}_{N-1,k-1}, \tilde{Q}_{N,k-1} \\ \bar{Q}_{1,k}, \bar{Q}_{2,k} - - - - - - \bar{Q}_{N-1,k}, \bar{Q}_{N,k} \end{bmatrix}$$

$Q = (Q_1, Q_2, Q_3, \ldots, Q_{k-1}, Q_k)^T$ is the output vector,

$A = (a_1, a_2, a_3, \ldots, a_{k-1}, a_k)$ is the weight vector and

$E = (e_1, e_2, e_3, \ldots, e_{k-1}, e_k)$ is the combination error vector, T denotes the transpose of the vector and *k* is the total number of observations.

The preceding equation can be perceived as a multiple linear regression model. Thus, it can be readily shown that the ordinary least squares estimate of the weight vector is given by;

$$A = (P^T P)^{-1} P^T Q \qquad (3.7)$$

In the **WAM**, the sum of the weights a_i is normally constrained to be equal to unity, that is

$$\sum_{i=1}^{N} a_i = 1 \qquad (3.8)$$

The main rationale behind constraining the sum of the weights to unity is that if the models included in the weighted average are unbiased, i.e. having a zero-mean output error term, then the weighted average combined forecast is likewise unbiased [53].

In the case where the sum of the weights is constrained to equal unity, it can be shown using the method of constrained least squares (CLS) that the estimate of the weights vector

$$\bar{A}_{cls} \tag{3.9}$$

is given by;

$$\bar{A}_{cls} = [p^T P]^{-1}\left(p^T Q + \frac{1}{2}bh\right) \tag{4.0}$$

where b is the unit vector (i.e. all of its scalar components are unity) having the same dimension as the parameters vector A and is the Lagrangian multiplier which is given by

$$A = 2(b^T(p^T p)^{-1}b)^{-1}(1 - b^T(p^T p)^{-1}p^T Q) \tag{3.10}$$

Alternative techniques, other than least squares, for estimating the weights a_i have also been used, e.g. by considering the covariance of the forecast errors of the individual models being considered [93].

3.6.3 The Neural Network Method (NNM)

The neural network method (NNM) provides an alternative to the simple average (SAM) and the weighted average methods (WAM) for combining outputs from different models. Neural networks are applied, in the GFMFS package, in the context of providing a non-linear function mapping of the simulated flows. Using a multi-layer feed forward neural network [44].

4 Results and Discussion

4.1 Relationship between Precipitation and Runoff

A linear regression analysis revealed a significant ($\alpha = 0.05$) correspondence between mean event runoff and mean event rainfall (Table 2). The coefficient of determination (R^2) was 0.62 and 0.33 for the wet (69 events) or dry (31 events) (Table 3). A dry event is defined as an event where precipitation is zero the day before the event started. Figure 3a and 3b shows the scatter plot between the mean event runoff and mean event rainfall for the wet and dry case. The average runoff coefficient (R/P) was 0.11 and 0.05 for the wet and dry events respectively. R/P ranged from 0.01 to 0.19 with a coefficient of variation (CV, which is the ratio of the standard deviation to the mean) of 0.97 for the dry events. This was almost three times higher than during the wet events. The higher relative variability observed during the dry period may be explained by the soil being close to saturation for the wet events, thus the relative variability between the different events will be small. Thus, event averaged precipitation is well correlated with event averaged runoff in the wet case, but not in the dry case. The mean monthly water balance plot for the study period for the Gilgel Abbay watershed shows the cycle of rainfall and runoff in relation to PET as estimated by the Penman Monteith method (Figure 2).

Table 2: Descriptive statistics results the run off coefficient for R/P for wet and dry events and wet and dry conditions on both 5- day prior rainfall-values correspond to the significant difference in periods and conditions.

Parameters	n. (no. Of events	R/P ratio ranges	Mean R/P	SD (±)	COV	P-value
Wet period	69	0.05-0.22	0.11	0.04	0.34	0.25
Dry Period	31	0.0-0.19	0.05	0.05	0.97	0.03
Wet condition (5-day prior)	73	0.0-0.22	0.1	0.05	0.44	0.01
Dry condition (5-day prior)	27	0.01-0.19	0.07	0.05	0.74	0.46

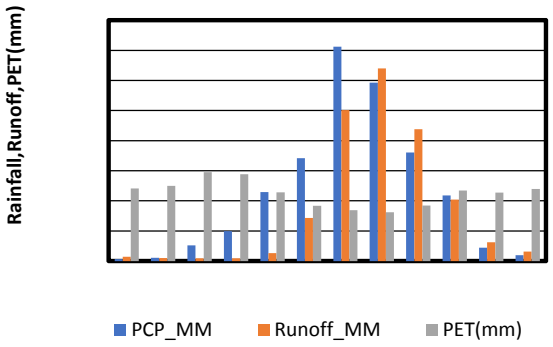

Figure 2: Mean monthly rainfall-runoff and PET for 1980-2000 period. PET was calculated using Penman monieth method.

a) b)

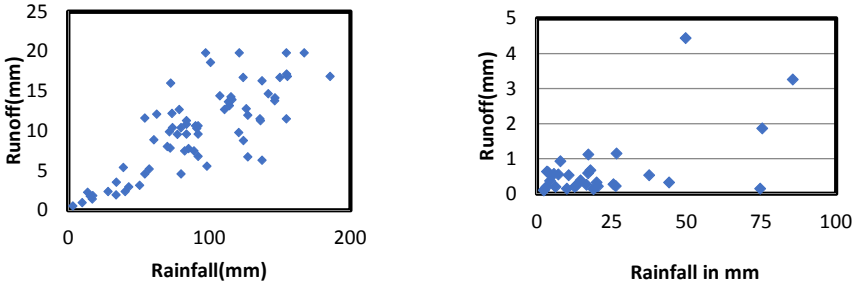

Figure 3: Event rainfall-runoff relationship for a) wet (May-October=69) and b) dry (November-April=31) periods

A seasonal cycle is also seen in PET rates which start increasing in September and peaks during the months of March. The plot in Figure 2 suggests that the difference between rainfall and runoff is close to the PET values during the wet periods with unlimited soil moisture calculated for the watershed (Figure 2). Thus, it is important to examine alternative relationships that include other important variables, such as PET

or water table depth as a surrogate for the ASMC, and their interactions for understanding rainfall–runoff dynamics.

4.2 Relationship between the Antecedent Precipitation Index (API) and Runoff

Using the precipitation information only on the day before the beginning of the event to classify the event into wet and dry may means that we are not taking into account information about the soil moisture content prior to the event. A crude way of getting information about this is to use the API (equation (3.1) to define wet and dry cases instead of the precipitation the day before the start of the event. Table 3 shows the regression between the runoff and the 5- day API.API 5-days prior to event are correlated with event averaged runoff both for dry (27 events) and wet (73 events) cases. Results shows a significant ($R^2 = 0.38$) relationship between runoff and 5-day API ($R^2 = 0.38$ and $R^2 = 0.31$ for the wet and dry conditions, respectively, Table 3 and Figure 4).

Table 3: Regression statistics results for runoff-rainfall relationships for wet and dry periods, and wet and dry conditions based on 5 prior rainfall.

Parameters	Regression equation	r^2	P-value	Intercept(p-value)	Slope(p-value)
Wet period	Runoff=1.853P+25.265	0.62	0.0	0.16	0.0
Dry period	Runoff=0.024P+0.15	0.33	0.0	0.45	0.0
Wet conditions (5-day prior)	Runoff=0.156P+4.026	0.38	0.0	0.0	0.0
Dry conditions (5-day prior)	Runoff=0.062P+0.463	0.31	0.0	0.0	0.0

Other factors such as rainfall intensity and its aerial variability, spatial distribution (for watershed of this scale) of soil type and their properties, and depth to water table (i.e. soil water storage volume) have been clearly examined through detail investigation of eight storm events among 100 ones.

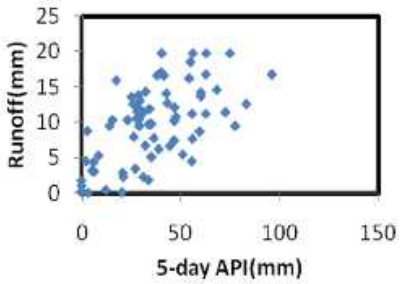

Figure 4: Rainfall-Runoff relationship for events wet (n=73) based on 5-day API.

Table 4: Results of stepwise regression analysis evaluated for all rainfall events (n=100), and wet and dry periods.

Variable	Begin flow	Rainfall	5-day rainfall
All storm events(n=100)			
Runoff	r^2=0.51, P=0.0	r^2=0.76, P=0.0	r^2=0.23, P=0.0
R/P	r^2=0.26, P=0.0	r^2=0.08, P=0.0	P>0.07
Wet Period			
Runoff	r^2=0.29, P=0.0	r^2=0.62, P=0.0	r^2=0.12, P=0.004
R/P	r^2=0.09, P=0.01	P>0.25	P>0.69
Dry period			
Runoff	r^2=0.41, P=0.0	r^2=0.33, P=0.0	P>0.57
R/P	P>0.10	r^2=0.13, P=0.05	P>0.30

Events selected either have very small or high R/P. For example, on day 17-Apr-80 a rainfall amount of 37.7 mm produced a runoff response of only 0.531 mm (R/P = 0.01), whereas for the storm event at day 2-Oct-94 17.3 mm produced 1.83 mm runoff (R/P = 0.11). The later event occurred directly following the return to base flow condition of the prior event and had a higher peak flow value, perhaps caused by surface runoff and shallow subsurface flow for a larger ASMC (already saturated conditions). For the event on day 17-Apr-80 with no previous rain 5 days prior, it is likely that the high ET rate during the dry period caused a large decrease in stream flow. Compare this with the event on day 2-Oct-94 where only 17.3 mm rain (5-days prior) produced a ratio of 0.11, whereas a ratio of 0.01 was generated for day 17-Apr-80 with no rain in the 5-day prior. Apparently, the near-term soil moisture condition played a larger role in

determining the runoff response during the dry period rather than a longer-term condition (30-day prior rainfall). The amount and rate of runoff will be dependent upon these key controlling factors (i.e. soil hydrologic properties, soil moisture storage, and rainfall) that vary spatially and temporarily [7]. However, we hypothesized that additional information on rainfall intensity, water table positions, and PET would help to more accurately determine the runoff and change in soil water storage processes.

4.3 Relationship between the Antecedent Precipitation Index (API) and begin flow

As described in Section 4.2 above, the equation of the simple linear regression model showed the 5-days API not significantly related to the begin flow during either the wet or dry period. Thus the 5-days API is unrelated to the begin flow as shown in table 4.

4.4 Multilinear Relationship between Begin Flow, API, Event Precipitation and Runoff

Results from the above analysis showed runoff was significantly related to rainfall amount and the API the initial flow rate (begin flow) (see Table 4). The 5-day API prior to the event had impact on runoff generation, but this was not strong. In the wet period, the runoff was correlated with initial flow due to previous rainfall condition and event rainfall amount. However, we did not find this was the case for the dry period at 5-day prior rainfall.

4.5 Model Results and Performance

In the above analysis, we had seasonal relationship using event based analysis. From the result, it has been noted a big difference in relationship of rainfall runoff which are explained by various variables such as mean begin flow, API and soil moisture. The importance of doing simulation of various models in this section is that to derive the advantage of individual model outputs from their particular consideration of the study area.

GFMFS software packages and other hydrological models have been applied to simulate rainfall- runoff relationship using observed daily rainfall and streamflow data for a period of 1980-2000.

Table 5: List of models ranking from simple to complex in terms of increased mathematical procedures involved in the model to be processed.

Model	Type	Complexity ranking	Mode	Description
NP-SLM	Empirical black-box	9	Simulation and non-parametric	Non-parametric simple linear model. A linear time-invariant relationship between the total rainfall R_i and the total discharge
P-SLM	Empirical black-box	8	Simulation and parametric	Parametric simple linear model. The linear transfer function type representation of the transformation process of the input series to the output series for discrete data intervals
NP-LPM	Empirical black-box	7	Simulation and non-parametric	Non-parametric linear perturbation model. The model uses the seasonal information of the observed rainfall and discharge series.
P-LPM	Empirical black-box	6	Simulation and non-parametric	Parametric linear perturbation model. The linear transfer function type representation of the transformation process of the departures of the values of the input series from their respective seasonal means to the departure of the values of the output series from their respective seasonal means for discrete data intervals
LVGFM	Empirical black-box	5	Simulation and non-parametric	Linearly varying gain factor model. The model is non-linear, can be viewed as a multiple linear regression model

ANN	Empirical black-box	4	Simulation	Artificial neural network model. The model is the multi-layer feed forward network consists of an input layer, an output layer and only one hidden layer between the input and the output layers.
SMAR	Physically inspired conceptual model	3	Simulation and non-parametric	Soil moisture accounting and routing model. It is rainfall-evaporation-runoff model with three variants; SMARG, SMAR-NC1, SMAR-NC2
HBV	Conceptual model	2	Simulation	HydrologiskaByransVattenbalans-Avedlning (Hydrological Bureau Water balance-section). It is considered as semi-distributed conceptual model and possible to run the mode separately for several sub basins and then add the contributions from all sub basins.
SWAT	Physical distributed model	1	Simulation	Soil and Water Assessment Tool. It is physically based distributed parameter model which operates on daily time step.

The comparison among each model output is made using three evaluators: The coefficient of variation (R^2), the Nash Sutcliffe Efficiency (NSE) and the bias (simulation minus observations divided by the observations in %). The 1980-1992 data were used for model calibration and the remaining data from 1993-2000 used for validation.

4.5.1 Simulation Mode

The performance of the SLM is inferior to that of all other models. The LVGFM, which is a modification of the SLM, incorporating an element of linear variation of the gain factor (G_t, see appendix) with the catchment wetness index at each time step, performs

consistently better than the SLM where the surface storage of the catchments might have affected the results.

As Gilgel Abbay is characterized by strong seasonality, the LPM in simulation mode, with its inherent component of seasonal variation, outperforms the LVGFM and SLM. From Table 6 and Figure 5(a-i), we see that in simulation mode, the performance of the ANN model is clearly the best followed by LPM during calibration and validation with R^2 of 87.8% and 76.3%, respectively. This implicitly shows the non-linearity of rainfall-runoff relationships can be well be handled by systems type black box models without using complex conceptual or physically based models. The performance of the

Table 6: The model efficiencies (%) in simulation mode

Model		Method	Calibration			Validation		
			R^2	Bias	ENS	R^2	Bias	ENS
NP-SLM		OLS	64.17	-7.81	0.65	51.00	-7.66	0.50
NP-LPM		OLS	86.94	0.02	0.87	77.98	-5.70	0.78
LVGFM		OLS	73.00	0.78	0.73	57.00	1.99	0.57
SMAR		OLS	80.49	-3.69	0.81	70.72	-4.44	0.71
ANN		OLS	89.70	2.35	0.90	85.00	3.44	0.85
HBV		Parametric	86.0	12.82	0.70	87.0	10.25	0.71
SWAT		Parametric	66.32	-0.02	0.62	59.4	-9.47	0.55
MOCT	SAM	Non-Parametric	83.37			79.16		
	WAW	Non-Parametric	90.41			85.53		
	NNM	Non-Parametric	90.42			84.82		

ANN model is R^2 89% and 85% during calibration and validation period, respectively. In the case of SMAR model, the parameter lumping applied to the study catchment which has diverse topographic variations may have influenced the performance of the model. Following LPM and ANN, the SMAR of SMARG variant explains the rainfall-evaporation-runoff relationships with 80.5% and 70.7% of R^2 during calibration and validation, respectively. As Table 5, the overall performance of the systems type black box models is comparable and in the case of ANN better than the conceptual or physically based hydrological models. Therefore, as far as estimation flow either in continuous or event based is concerned, systems type black box model with simple rainfall and runoff input can be adequate for water resources development purposes.

4.5.2 Updating Mode

In updating mode, LPM consistently performed the best of all other models. It accounted for more than 90% and 85% of the initial variance during calibration and validation period, respectively. Even, the simple models like P-SLM and P-LPM performs better than HBV and SWAT shown in Figure 5(a-i).

Generally, the updating models are better than the simulation mode models (with some exceptions) and the updating mode models has a lower reduction in R^2 and ENS in the validation period compared to the calibration period (Table 7).

a)

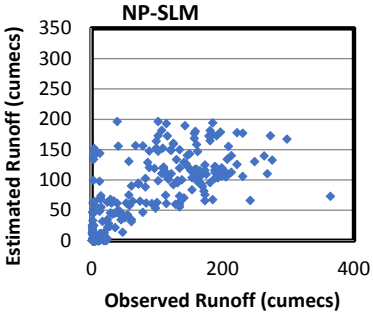
NP-SLM
Estimated Runoff (cumecs)
350
300
250
200
150
100
50
0
0
200
400
Observed Runoff (cumecs)

b)

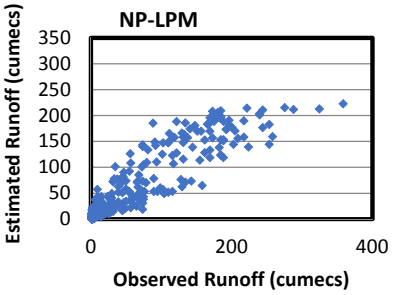
NP-LPM
Estimated Runoff (cumecs)
350
300
250
200
150
100
50
0
0
200
400
Observed Runoff (cumecs)

c)

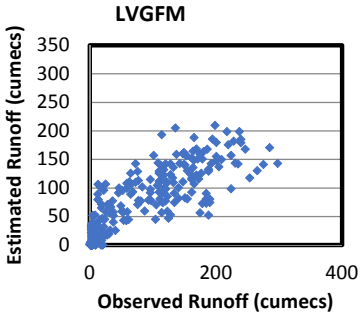
LVGFM
Estimated Runoff (cumecs)
350
300
250
200
150
100
50
0
0
200
400
Observed Runoff (cumecs)

d)

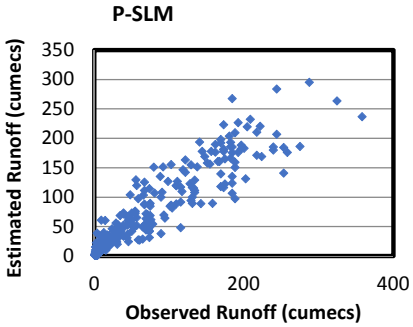
P-SLM
Estimated Runoff (cumecs)
350
300
250
200
150
100
50
0
0
200
400
Observed Runoff (cumecs)

e)

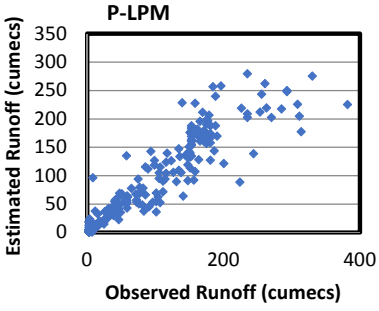
P-LPM
Estimated Runoff (cumecs)
350
300
250
200
150
100
50
0
0
200
400
Observed Runoff (cumecs)

f)

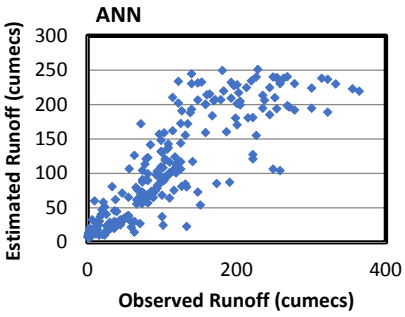
ANN
Estimated Runoff (cumecs)
300
250
200
150
100
50
0
0
200
400
Observed Runoff (cumecs)

g)

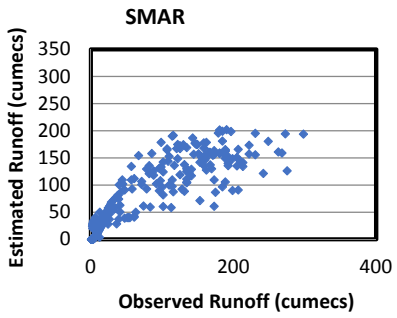

h)

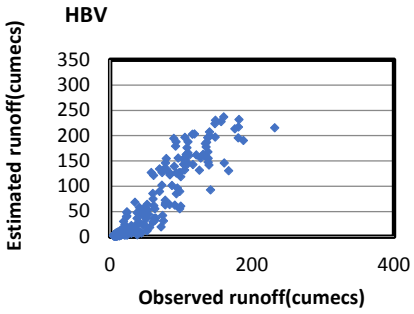

i)

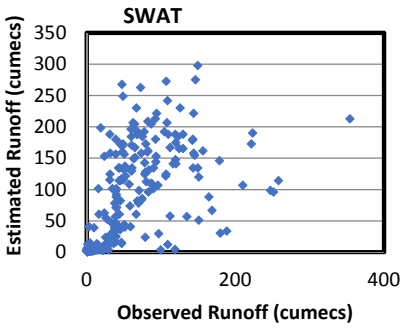

Figure 5: Scatter plots for various models [from (a) to (i)] for Upper Gilgel Abbay River basin

4.5.3 Combining Outputs from Different Models

The method of combined outputs was used to the results of the five substantive models included in GFMFS software packages, both in simulation and updating mode. Three techniques for combining the estimated outputs of different models were conducted namely, the simple average method (SAM), the weighted average method (WAM) and the neural network method (NNM).

SAM, WAM and NNM account with R^2 values of 83.4, 90.4 and 90.42 percent during calibration and 79, 85.5 and 84.8 percent during validation period, respectively in

simulation mode; and in the case of updating mode the values of R^2 are 90.2,91.5, and 91.4 percent during calibration and 85,85.3, and 85 percent during validation, respectively (table 6 and table 7). Therefore, combining the outputs of the systems type black box model has shown increased improvement in the accuracy of the results.

Table 7: The model efficiencies (%) in updating mode.

Model		**Method**	**Calibration**			**Validation**		
			R^2	Bias	ENS	R^2	Bias	ENS
P-SLM		Parametric	89.81	-0.91	0.898	85.33	-0.91	0.85
P-LPM		Parametric	91.35	0.00	0.91	84.90	-2.49	0.85
MOCT	SAM	Parametric	90.21			85.06		
	WAW	Parametric	91.46			85.32		
	NNM	Parametric	91.42			85.01		

5 SUMMARY AND CONCLUSIONS

We believe application of complex conceptual or physically based models for simple flow estimation may not be always feasible especially in scarcely gauged locations in Africa. On that basis, we compared systems type black box rainfall-runoff models and other complex models that require inputs beyond rainfall such as SMAR, HBV and SWAT. The models were compared on the basis of long-term rainfall and stream flow data (1980–2000) and for 100 selected runoff events for the Gilgel Abbay watershed Event runoff is largely a function of rainfall amount. The event rainfall-runoff relationships explained as much as 62% for the wet periods without incorporating the evaporative demands. Although the relationship between runoff and rainfall was significant ($\alpha = 0.05$) for wet and dry periods, it was not as strong as expected. This suggests that about 38% of the runoff response in this watershed is influenced by other factors such as its intensity and duration, and to the near-term soil moisture conditions created by accumulated evapotranspiration and precipitation balances. Event rainfall–runoff relationships were also affected by 5- day prior rainfall under wet conditions, suggesting that soil moisture condition is an important element dictating the hydrologic dynamics of this watershed. However, this was not the case for the dry period indicating that the rainfall–runoff dynamics was more complex and variable in this system with shallow moderately drain soil. We argued that this variability is most likely related to rainfall characteristics such as intensity and duration. We confirm that event R/P were significantly higher during the wet period than for the dry periods. Although peak flow rate relationships with rainfall for both wet and dry periods were also significant, the wet period relationship was found to be stronger. It was also concluded that the rainfall amount and ASMC represented by the initial base flow rate were the main controlling factors for event runoff. The results of this study showed that all event variables (runoff, R/P, and peak flow rates) were controlled by rainfall amounts and available soil water storage. Future studies should further investigate other hydrologic indicators that affect the runoff response, such as spatial and temporal water table dynamics determined by balances of rainfall and ET. Information on depth to water table along with soil

drainage porosity is necessary to determine available subsurface storage and, therefore, the ASMC at given times. Additionally, event rainfall intensity data are necessary not only to characterize the peak flow rates but also to accurately determine the rainfall amount responsible for event runoff regeneration and duration of storm events at different seasons and periods.

Using Continuous simulation models described in Section 3.5 and 3.6, we compared systems type black box and complex hydrological models in Gilgel Abbay catchment. Though the performance of the naïve SLM is clearly inferior to that of all other models (from systems type black box models), models such as the LPM and the ANN perform better than the complex hydrological models such as SMARG, HBV and SWAT. For instance, it is shown in Table 6 that the performance of LPM and ANN (both systems type black box) models evaluated with NSE criteria gives better hydrograph response than the complex models such as HBV and SWAT. Therefore, it confirms that simpler models (that takes only rainfall as input) can surpass their complex counterparts in performance for continuous simulation and reproducing of hydrographs or flow estimation. There is a strong justification, therefore, for the claim that increasing the model complexity, thereby increasing the number of parameters, does not necessarily enhance the model performance. It is suggested that, in practical hydrology, the simpler models, may still play a significant role as effective simulation tools, and countries with scarce hydrological data should revitalize application of such systems type black box modelling schemes that depend only on rainfall and runoff data sets which could be easily available.

As a concluding statement, results of this study site may be of great importance for regional water management and water quality studies, for that matter designing the water related structures such as detention ponds and restoration efforts. These data will also provide useful insight to explain the variability in storm runoff response observed for the dry period, for example. Additionally, future rainfall–runoff event analysis study at this site should take advantage of current monitoring of rainfall intensity data, water table depths, solar radiation, and other hydro meteorological data, as well as modeling studies for accurately estimating soil moisture and actual ET that would help to explain the variability in runoff generation.

Table 1: Basic hydrological characteristics for analyzed runoff events (n=100) and t-test results calculated for peak rate, runoff, rainfall, R/P, rain previous 5- and 30-days, SD=standard Deviation

Date	Begin flow(m3/s)	Rain in mm	Runoff(mm)	R/P	Q peak	Rain 5-day	Rain30 -Day
11-Feb-80	0.45	4.4	0.363	0.08	7.001	0.00	4.4
17-Apr-80	0.00	37.5	0.531	0.01	6.17	12.20	16.1
22-Jul-80	96.90	167.3	19.83	0.12	412.617	40.4	309
8-Aug-80	44.63	149.9	16.72	0.11	321.92	41.4	350.5
8-Oct-80	11.92	34	3.53	0.10	93.251	27.1	106.8
9-Jun-81	4.22	17	1.43	0.08	49.143	16	57.2
19-Aug-81	0.48	154.7	17.14	0.11	330.124	40.1	546.4
13-Sep-81	46.39	54.21	11.62	0.21	239.536	28.2	183.01
3-Oct-81	21.58	60.6	8.88	0.15	171.042	2.9	119.51
25-Nov-81	1.68	5.7	0.569	0.10	18.932	0.20	8
5-Jan-82	0.21	19.9	0.320	0.02	6.44	0.00	19.9
20-Aug-82	13.69	141.8	14.68	0.10	282.703	68.2	342.9
8-Sep-82	23.73	71.7	9.89	0.14	230.509	35.1	269.5
12-Oct-82	32.34	39	5.41	0.14	104.096	8.5	117.8
11-Mar-83	0.11	3.32	0.53	0.16	12.112	1.21	3.32
18-Jun-83	6.03	50.6	3.15	0.06	60.661	6.4	68.9
17-Jul-83	45.14	78.6	12.68	0.16	248.767	25.9	151.9
23-Aug-83	42.88	185.6	16.86	0.09	324.641	95.9	478.5
21-Mar-84	0.10	10	0.142	0.01	3.256	0.50	11.6
31-May-84	4.13	42.91	2.94	0.07	56.664	20.7	57.31
12-Jul-84	51.74	116	13.91	0.12	267.847	28.7	412.8
8-Aug-84	19.15	146.3	13.78	0.09	330.124	60.1	378.6
11-Sep-84	11.57	113.4	13.66	0.12	263	25.1	258.6
27-Mar-85	0.00	12.6	0.199	0.02	3.833	0.00	12.6
8-Sep-85	25.80	114.21	13.16	0.12	253.46	29.4	302.6
12-Nov-85	0.89	10.6	0.531	0.05	13.335	0.00	50.2
5-Apr-86	0.25	74.6	0.142	0.00	2.733	3.30	19.5
14-Jun-86	14.80	40.2	2.37	0.06	62.72	31.1	61.4
17-Jul-86	21.41	85.3	7.76	0.09	241.825	55.9	264.3
17-Aug-86	26.06	92	10.63	0.12	230.509	29.4	276.9
22-Oct-86	5.61	28.2	2.37	0.08	142.6	21.1	76.6
20-Nov-86	1.17	17.1	0.589	0.03	16.46	0.00	17.1
14-Jan-87	0.14	3.2	0.199	0.06	5.157	3.20	3.2
5-Mar-87	0.10	44.2	0.320	0.01	3.635	0.00	0
29-Apr-87	0.43	13.2	0.232	0.02	4.466	0.00	27.7
14-Jun-87	31.11	82.5	7.49	0.09	144.289	46.4	147.5

Date	Begin flow(m3/s)	Rain in mm	Runoff(mm)	R/P	Q peak	Rain 5-day	Rain30 -Day
1-Jul-87	41.68	89.1	7.49	0.08	253.46	46.7	172.5
19-Aug-87	25.90	127.2	11.97	0.09	234.997	34.2	264.9
15-Sep-87	53.33	73.4	12.20	0.17	234.997	46.8	224.7
24-Feb-88	0.17	25.6	0.268	0.01	5.157	0.00	30.3
12-Apr-88	0.08	2.3	0.096	0.04	2.118	0.00	2.3
12-Aug-88	46.81	107.4	14.42	0.13	277.699	32.4	357.5
11-Sep-88	11.95	83.8	10.84	0.13	219.511	47.6	235.9
9-Oct-88	3.62	98.2	5.55	0.06	140.922	51	197.4
13-Mar-89	0.00	16.6	0.255	0.02	3.442	0.00	2.8
17-Jul-89	27.75	97.4	19.83	0.20	406.365	62.8	161.9
13-Aug-89	17.98	137.3	16.30	0.12	438.188	54.2	441.6
7-Sep-89	25.72	62.6	12.09	0.19	234.997	28.4	226.7
7-Nov-89	4.23	7.8	0.930	0.12	26.332	3.10	6.7
15-Mar-90	0.20	18.9	0.133	0.01	2.901	12.80	19.9
14-Jun-90	0.35	9.9	0.96	0.10	90.648	0.8	24.1
22-Jul-90	38.67	136.3	11.29	0.08	248.767	55.7	255.8
13-Sep-90	20.90	70.1	8.03	0.11	277.699	26.3	171
7-Oct-90	22.55	54.2	4.57	0.08	121.692	2.3	133.9
11-Aug-91	23.44	155.3	16.86	0.11	341.251	62.6	416
22-Sep-91	13.15	110.7	12.68	0.11	352.596	83	265.4
6-Oct-91	7.55	79.9	4.57	0.06	101.319	55.6	254.1
12-May-92	0.16	13.7	2.28	0.17	43.911	13.7	152.4
7-Jul-92	56.32	80	10.41	0.13	200.503	15.6	93.4
14-Oct-92	13.94	72.2	7.85	0.11	151.163	36.5	183.4
8-Nov-92	6.89	49.7	4.443	0.09	85.573	6.10	75.9
7-Dec-92	2.00	17.9	0.671	0.04	19.451	0.00	20.6
5-Sep-93	18.47	121.2	19.83	0.16	381.915	74.8	198.3
9-Oct-93	49.80	73.9	10.41	0.14	200.503	23.2	136.3
7-Nov-93	8.98	75.3	1.867	0.02	40.613	0.00	38.7
27-Feb-94	0.21	20.4	0.210	0.01	4.038	20.40	20.4
11-Aug-94	32.74	72.5	16.02	0.22	308.515	17.5	333.7
5-Oct-94	9.75	17.3	1.83	0.11	44.759	4.2	85.2
10-Dec-94	1.51	3.8	0.609	0.16	11.72	0.00	13
25-May-95	0.15	15.5	1.79	0.12	66.96	13.1	76.7
7-Jun-95	26.23	92	6.81	0.07	131.1	32.1	148.5
7-Sep-95	0.00	77.3	9.58	0.12	290.308	14.1	278
17-Oct-95	3.00	33.8	1.94	0.06	50.964	33.8	90.9
3-Nov-95	2.72	17.2	1.122	0.07	21.609	1.50	18.7
23-Jan-96	0.43	6.2	0.199	0.03	4.69	0.00	6.2
3-Feb-96	0.44	2.5	0.125	0.05	3.076	0.00	2.5
6-Jun-96	5.18	57.4	5.19	0.09	190.377	35.1	224.2

Date	Begin flow(m3/s)	Rain in mm	Runoff(mm)	R/P	Q peak	Rain 5-day	Rain30 -Day
3-Aug-96	60.60	124	16.72	0.13	355.466	38.1	324.7
11-Sep-96	18.51	135.8	11.51	0.08	253.46	31.2	273.6
28-Nov-96	0.00	85.5	3.257	0.04	97.236	5.30	108.3
20-Jun-97	8.65	127.2	6.72	0.05	142.6	44.4	253.7
9-Jul-97	3.77	92	9.58	0.10	258.204	77.5	233.4
15-Aug-97	33.47	100.8	18.61	0.18	358.35	54.9	263.2
22-Sep-97	29.26	124.2	8.78	0.07	202.565	59.5	180.1
4-Aug-98	20.95	146.5	14.16	0.10	298.031	42.7	358.1
6-Sep-98	47.86	90.1	10.63	0.12	241.825	27.7	227
12-Oct-98	28.68	154.5	11.51	0.07	221.685	72.5	269.31
5-Jan-99	0.38	26.3	0.221	0.01	4.466	0.00	26.3
27-Apr-99	0.00	14.6	0.379	0.03	7.291	12.30	16.5
12-Jun-99	16.60	137.3	6.32	0.05	174.812	38.9	127.21
11-Jul-99	19.92	126.2	12.80	0.10	285.225	43.2	188.9
30-Aug-99	20.56	115.3	14.29	0.12	298.031	60.1	264.6
5-Sep-99	18.44	120.9	9.78	0.08	190.377	33.9	260.9
4-Oct-99	36.74	83.8	9.58	0.11	234.997	29.1	140.8
20-Nov-99	3.43	26.6	1.151	0.04	40.613	0.00	26.6
11-Dec-99	1.57	3.3	0.629	0.19	12.112	0.60	16.4
23-Jul-00	14.51	83.7	11.29	0.13	223.872	62.6	255.5
17-Aug-00	26.63	154.5	19.83	0.13	381.915	56.1	314.6
10-Oct-00	15.02	91.1	10.30	0.11	251.107	46.7	179.1
14-Dec-00	2.04	7.11	0.550	0.08	13.335	0.00	9.11
Mean		69.77	7.18	0.09	157.80	26.90	159.12
Median		72.95	6.77	0.09	147.73	26.70	148.00
Standard Deviation		49.76	6.21	0.05	128.55	24.00	131.89
Skewness		0.28	0.39	0.20	0.25	0.58	0.57
Range		183.30	19.73	0.22	436.07	95.90	546.40
Minimum		2.30	0.10	0.00	2.12	0.00	0.00
Maximum		185.60	19.83	0.22	438.19	95.90	546.40
Confidence interval (95.0%)		9.87	1.23	0.01	25.51	4.76	26.17

REFERENCES

[1] Rajurkar, M.P., Kothyari, U.C. & Chaube, U.C. (2004) Modeling of the Daily Rainfall-Runoff Relationship with Artificial Neural Network. J. Hydrol., 285, 96-113.http://dx.doi.org/10.1016/j.jhydrol.2003.08.011.

[2] A. W. MINNS & M. J. HALL (1996) Artificial neural networks as rainfall-runoff models, Hydrological Sciences Journal, 41:3, 399-417, DOI: 10.1080/02626669609491511http://dx.doi.org/10.1080/02626669609491511

[3] Campolo, M., P. Andreussi, and A. Soldati (1999), River flood forecasting with a neural network model, Water Resour. Res., 35(4), 1191–1197, doi:10.1029/1998WR900086.http://dx.doi.org/10.1029/1998WR900086

[4] Markewich H, Pavich M, Buell G. 1990. Contrasting soils and landscapes of the Piedmont and Coastal Plain, Eastern United States.Geomorphology3 (3–4): 417–447.

[5] Skaggs R, Gilliam J, Evans R. 1991. A computer simulation study of pocosinhydrology. Wetlands11: 399–416. Amatya D, Chescheir G, Skaggs R, Fernandez G. 2002. Hydrology of poorly drained coastal watersheds in Eastern North Carolina. In ASAE/CIGR Congress Annual Intl Meeting, Chicago, IL, 27–29 July 2002, Paper No. 022034. St. Joseph, Mich: ASABE.

[6] Amatya D, Chescheir G, Skaggs R, Fernandez G. 2002. Hydrology of poorly drained coastal watersheds in Eastern North Carolina. In ASAE/CIGR Congress Annual Intl Meeting, Chicago, IL, 27–29 July 2002, Paper No. 022034. St. Joseph, Mich: ASABE.

[7] Slattery C, Gares A, Phillips D. 2006.Multiple models of storm runoff generation in a North Carolina coastal plain watershed. Hydrological Processes 20: 2953–2969.http://dx.doi.org/10.1002/hyp.6144

[8] Amatya D, Skagss R, Gregory J, Hermann R. 1997. Hydrology of a drained forested pocosinwatershed. Journal of the American Water Resources Association 33(3): 535–546. http://dx.doi.org/10.1111/j.1752-1688.1997.tb03530.x

[9] Amatya D, Gregory J, Skaggs R. 2000. Effects of controlled drainage on storm event hydrology in a loblolly pine plantation. Journal of the American Water Resources Association 36(1): 175–190. http://dx.doi.org/10.1111/j.1752-1688.2000.tb04258.x

[10] Sun G, Boggs J, McNulty S, Amatya D, Trettin C, Dai Z, Vose J, La Torre Torres I, Callahan T. 2008b. Hydrologic processes of forested headwater watersheds across a physiographic gradient in the southeastern United States. In Proceedings of the South Carolina Water Resources Conference, Charleston, SC, 14–15 October 2008.

[11] La Torre Torres I, AmatyaDevendraM., Sun G., and Callahan Timothy J. 2011. Seasonal rainfall–runoff relationships in a lowland forested watershed in the southeastern USA, Hydrol. Process.25, 2032–2045 (2011), DOI: 10.1002/hyp.7955,2011http://dx.doi.org/10.1002/hyp.7955

[12] Amatya D, Trettin C. 2007. Annual evapotranspiration of a forested wetland watershed, SC. In ASABE Annual International Meeting, Minneapolis, MN, 17–20 June 2007, Paper No. 072222. St. Joseph, Mich: ASABE.

[13] Sun G, Noormets A, Gavazzi1 MJ, McNulty SG, Chen J, Domec J-C, King JS, Amatya DM, Skaggs RW. 2010. Energy and water balance of two contrasting Loblolly pine plantations on the lower coastal plain of North Carolina, USA. Forest Ecology and Management 259: 1299 1310. http://dx.doi.org/10.1016/j.foreco.2009.09.016

[14] Ye W, Bates BC, Viney NR, Sivapalan N, Jakeman AJ. 1997. Performance of conceptual rainfall-runoff models in low-yielding ephemeral catchments. Water Resources Research 33(1): 153–166.http://dx.doi.org/10.1029/96WR02840

[15] Wei L, Zhang B, Wang M. 2007. Effects of antecedent soil moisture on runoff and soil erosion in alley cropping systems. Agricultural Water Management 94: 54–62.http://dx.doi.org/10.1016/j.agwat.2007.08.007

[16] Tramblay Y, Bouvier C, Martin C, Didon-Liscot J, Todorovik D, Domergue J. 2010. Assessment of initial soil moisture conditions for event-based rainfall-runoff modeling. Journal of Hydrology 387(3–4): 176–187 http://dx.doi.org/10.1016/j.jhydrol.2010.04.006

[17] Singh V. 1997.Effect of spatial and temporal variability in rainfall and watershed characteristics on stream flow hydrograph.Hydrological Processes 11: 1649–1669.http://dx.doi.org/10.1002/(SICI)1099-1085(19971015)11:12<1649::AID-HYP495>3.0.CO;2-1

[18] Sun G, McNulty S, Amatya D, Skaggs R, Swift L Jr, Shepard J, Riekerk H. 2002. A comparison of the watershed hydrology of coastal forested wetlands and the mountainous uplands in the Southern US. Journal of Hydrology 263: 92–104.http://dx.doi.org/10.1016/S0022-1694(02)00064-1

[19] BCEOM: Abay River Basin integrated master plan, main report, MoWR, Addis Ababa, Ethiopia, 1999.

[20] Tarekegn, D. and Tadege, A.: Assessing the impact of climate change on the water resources of the Lake Tana sub-basin using the WATBAL model, CEEPA, Republic of South Africa, 2005.

[21] Kebede, S., Travi, Y., Alemayehu, T., and Ayenew, T.: Water balance of Lake Tana and its sensitivity to fluctuations in rainfall, Blue Nile Basin, Ethiopia, J. Hydrol., 316, 233–247, 2006.http://dx.doi.org/10.1016/j.jhydrol.2005.05.011

[22] Abdo, K. S., Fiseha, B. M., Rientjes, T. H. M., Gieske, A. S. M., and Haile, A. T.: Assessment of climate change impacts on the hydrology of GilgelAbbay catchment in Lake Tana basin, Ethiopia, Hydrol. Process., 23(26), 3661–3669, 2009.

[23] Nicks, A.D. (1974). Stochastic generation of the occurrence, pattern and location of maximum amount of daily rainfall. Statistical hydrolgy (pp. 154-171). Washington, DC: U.S. Governmental print office.

[24] Swindel B, Lassiter C, Riekerk H. 1983. Effects of different harvesting and site preparation operations on the peak flows of streams in Pinuselliottiiflatwoodsforests.Forest Ecology and Management 5: 77–86.http://dx.doi.org/10.1016/0378-1127(83)90059-2

[25] Swank W, Vose J, Elliott K. 2001. Long-term hydrologic and water quality responses following commercial clearcutting of mixed hardwoods on a southern Appalachian catchment. Forest Ecology and Management 143: 163–178.http://dx.doi.org/10.1016/S0378-1127(00)00515-6

[26] Sheridan. 2002. Peak flow estimates for coastal plain watersheds. Transactions of the ASAE 45(5): 1319–1326.http://dx.doi.org/10.13031/2013.11069

[27] Descroix L, Nouvelot J-F, Vauclin M. 2002. Evaluation of an antecedent precipitation index to model runoff yield in western Sierra Madre (North-west Mexico). Journal of Hydrology 263: 114–130.http://dx.doi.org/10.1016/S0022-1694(02)00047-1

[28] Amatya D, Callahan T, Trettin C, Radecki-Pawlik A. 2009.Hydrologic and water quality monitoring on Turkey Creek watershed, Francis Marion National Forest, SC. In ASABE Annual International Meeting, Reno, Nevada, 21–24 June 2009, Paper No. 095999. St. Joseph, Mich: ASABE.

[29] O'Connor, K.M., M. Goswami, G.C. Liang, R.K. Kachroo and A.Y. Shamseldin, 2001. The Development of The 'Galway Real-Time River Flow Forecasting System (GFFS). In Subtopic 1: 'Minimisation of Impacts of Extreme Hydrological Events in Europe': Volume C of the Proceedings, Paper No. 035 (38 pages) of the 19th European Conference on 'Sustainable Use of Land and Water' of the International Commission on Irrigation and Drainage (ICID), Brno & Prague, Czech Republic, 4-8 June, 2001.

[30] O'Connell, P.E., Nash, J.E. and Farrell, J. P., 1970. River Flow forecasting through conceptual models. Part 2. The Brosna catchment at Ferbane. J. Hydrol., 10: 317-329 http://dx.doi.org/10.1016/0022-1694(70)90221-0

[31] Nash, J.E. and Foley, J.J., 1982. Linear models of rainfall-runoff systems. In: 'Rainfall-Runoff Relationship', Proceedings of the International Symposium on Rainfall-Runoff modelling. Mississippi State University, May 1981, USA. Edited by Singh, V.P., and Water Resources Publications pp.: 51-66.

[32] Nash, J.E. and Barsi, B.I., 1983. A hybrid model for flow forecasting on large catchments. J. Hydrol., 65: 125-137.http://dx.doi.org/10.1016/0022-1694(83)90213-5

[33] Kachroo, R.K., G.C. Liang & K.M. O'Connor (1988). Application of the linear perturbation model (LPM) to flood routing on the Mekong River. Journal of the International Association of Hydrological Sciences (IAHS), 33, 2, 4, pp. 193 - 224. (This paper had earlier been presented by K.M. O'Connor at the Workshop on "Recent Developments in Flood Routing", held during the 2nd IAHS Scientific Assembly, Budapest, Hungary, July 1986).http://dx.doi.org/10.1080/02626668809491238

[34] Kachroo, R.K. and Natale, 1992.Non-linear modelling of the rainfall-runoff transformation. J. Hydrol., 135: 341-369.http://dx.doi.org/10.1016/0022-1694(92)90095-D

[35] Kachroo, R.K., Sea, C.H., Warsi, M.S., Jemenez, H. and Saxena, R.P., 1992. River flow forecasting. Part 3. Applications of linear techniques in modelling rainfall-runoff transformations. J. Hydrol., 133: 41-97.http://dx.doi.org/10.1016/0022-1694(92)90148-O

[36] Liang, G.C. and Guo, Y.F., 1994. Observed seasonal hydrological behavior used in flow forecasting on the Yangtze River above Hankou. J. Hydrol., 154: 383-402 http://dx.doi.org/10.1016/0022-1694(94)90226-7

[37] Liang, G.C., O'Connor, K.M. and Kachroo, R.K., 1994. A multiple-input single-output variable gain factor model. J. Hydrol., 155, 185-198.http://dx.doi.org/10.1016/0022-1694(94)90164-3

[38] Ahsan, M.and O'Connor, K.M. 1994a. A reappraisal of the Kalman filtering technique as applied in river flow forecasting. J. of Hydrol., 161: 197-226.http://dx.doi.org/10.1016/0022-1694(94)90129-5

[39] Ahsan, Mainul and O'Connor, K.M., 1994b. A simple non-linear rainfall-runoff model with a variable gain factor. J. Hydrol., 155: 151-183.

[40] Tan, B.Q., O'Connor, K.M. and Z.C. Liu. 1996. Application of a distributed form of the SMAR Model. Proceedings: Volume 1, International Conference on Water Resources and Environment research: Towards the 21st Century (Oct. 29-31,'96). Water Resources Research Center, Kyoto University, Japan.

[41] Shamseldin, A. Y., 1997. Application of a neural network technique to rainfall-runoff modeling, J. Hydrol., 199, 272-294.http://dx.doi.org/10.1016/S0022-1694(96)03330-6

[42] Shamseldin, A.Y., O'Connor, K.M. and Liang, G.C., 1997. Methods for combining the outputs of different rainfall-runoff models. J. Hydrol, 197: 203-229.http://dx.doi.org/10.1016/S0022-1694(96)03259-3

[43] Xiong, L., Shamseldin, A. Y. and O'Connor, K. M., 2001. A non-linear combination of the forecasts of rainfall-runoff models by the first-order Takagi-Sugeno fuzzy system. Accepted for publication by the Journal of Hydrology.

[44] Goswami, M, O'Connor, K.M., 2005. Application of a conceptual rainfall-runoff simulation model to three European catchments characterized by non-conservative system behavior. Proc. Int. Conf. Hydrological perspectives for sustainable development, Roorkee, India, 1, 117-130.

[45] Bergstr¨om, S.: Development and application of a conceptual runoff model for Scandinavian catchments, Bull. Series A52, University of Lund, 134 pp., 1976.

[46] Bergstr¨om, S.: Development and test of the distributed HBV-96 hydrological model, J. Hydrol., 201, 272–288, 1997.http://dx.doi.org/10.1016/S0022-1694(97)00041-3

[47] Bergstr¨om, S.: The HBV model, in: Computer models of watershed hydrology, edited by: Singh, V. P., Water Resources Publications, Highlands Ranch, Colorado, USA, 443–476, 1995.

[48] Bergstr¨om, S.: The HBV-model – its structure and applications, SMHI Reports RH No. 4, Norrk¨oping, Sweden, 1992.

[49] Arnold, J. G. and Allen, P. M.: Estimating hydrologic budgets for three Illinois watersheds, J. Hydrol. 176(1–4), 57–77, 1996.http://dx.doi.org/10.1016/0022-1694(95)02782-3

[50] Mengistu, D. T. and Sorteberg, A. (2012): Sensitivity of SWAT simulated streamflow to climatic changes within the Eastern Nile River basin, Hydrol. Earth Syst. Sci., 16, 391-407, doi: 10.5194/hess-16-391-2012, 2012.http://dx.doi.org/10.5194/hess-16-391-2012

[51] Arnold, J. G., Srinivasan, R., Muttiah, R. S., and Williams, J. R.: Large area hydrologic modeling and assessment, Part 1: Model development, J. Am. Water Res. Assoc., 34(1), 73–89, 1998. http://dx.doi.org/10.1111/j.1752-1688.1998.tb05961.x

[52] Neitsch, S.L., Arnold, J.G., Kiniry, J.R., Williams, J.R., King, K.W., 2002a. Soil and Water Assessment Tool: Theoretical Documentation, version 2000 (available Granger, C.W.J. and Ramanathan, R., 1984.Improved methods of combining forecasts. J. of Forecasting, 3:197-204.at http://www.brc.tamus.edu/swat/).

[53] Granger, C.W.J. and Ramanathan, R., 1984.Improved methods of combining forecasts. J. of Forecasting, 3:197-204.http://dx.doi.org/10.1002/for.3980030207

[54] Armstrong, J.S., 1989. Combining forecasts: The end of the beginning or the beginning of the end? International J. of Forecasting, 5: 585-588.http://dx.doi.org/10.1016/0169-2070(89)90013-7

Appendix

Model Description

The Galway River Flow Forecasting System (GFMFS) is software packages developed at Department of Engineering Hydrology, National University of Ireland, Galway [61].

NP-SLM (NON-PARAMETRIC SIMPLE LINEAR MODEL)

The hypothesis of the **SLM** is introduced by [54], is the assumption of a linear time-invariant relationship between the total rainfall R_i and the total discharge Q_i. In discrete non-parametric form, the **NP-SLM**, is expressed by the convolution summation relation [37].

$$Q_i = \sum_{j=1}^{m} R_{i-j+1}\, h_i^{'} + e_t \qquad \text{(A.1)}$$

where *m* is the *memory length* of the system and $h_j^{'}$ is the j^{th} discrete pulse response ordinate.

The above equation can be envisaged as a multiple linear regression model of the observed discharge on the *m* previous observed rainfall values. Estimates of the pulse response ordinates can be obtained by the method of **O**rdinary **L**east **S**quares (**OLS**).

P-SLM (PARAMETRIC SIMPLE LINEAR MODEL)

In the **P**arametric form of the **S**imple **L**inear **M**odel (**P-SLM**), the Linear Transfer Function type representation of the transformation process of the input series *x* to the output series *y* for discrete data intervals is given by

$$\sum_{i=0}^{r} \alpha_i\, y_{t-j} = \sum_{i=1}^{s} \omega_j\, x_{t-b-j+1} \qquad \text{(A.2)}$$

where α_j are the autoregressive parameters, with $\alpha_0 = 1$, the ω_j are the moving average parameters and b is the pure time delay restricted to integer values only [35]. r and s are the order of the autoregressive and the moving average parts of the model.

Writing explicitly for y_t with the addition of an error term, the above expression becomes

$$y_t = \sum_{j=1}^{r} \alpha_j y_{t-j} + \sum_{j=1}^{s} \omega_j x_{t-b-j+1} + e_t \qquad \text{(A.3)}$$

where α_j and ω_j are the autoregressive and moving average parameters respectively obtained after modifying the equation (A.2). In this form, the current value of y depends linearly on previous values of y and x. The parameters of the model are estimated by the method of Ordinary Least Squares.

It may be shown that, after estimation of the model parameters, the pulse response ordinates can be obtained by applying the transfer function to a single pulse of unit input. The pulse response ordinates are given by

$h=0 \qquad\qquad j< b$

$h_j = \alpha_1 h_{j-1} + \alpha_2 h_{j-2} + \ldots + \alpha_r h_{j-r} + \omega_{j-b+1} \quad j = b, b+1, b+2, \ldots, b+s-1$

$h_j = \alpha_1 h_{j-1} + \alpha_2 h_{j-2} + \ldots + \alpha_r h_{j-r} \qquad j > b+s-1$

If the resulting shape of the pulse response is unsatisfactory, appropriate changes need to be made to the model structure and the model needs to be recalibrated. In the non-updating mode, past computed values of y are used on the right-hand side of the transfer function equation, instead of the past observed values. However, the model provides the facility for being used in updating mode also, in which past observed value of y are to be used as input.

NP-LPM (NON-PARAMETRIC LINEAR PERTURBATION MODEL)

This model uses the seasonal information of the observed rainfall and discharge series. It was originally introduced in the context of rainfall-runoff modelling [53]. Initially known as the *hybrid* model, in a series of subsequent publications it

was referred to as the **L**inear **P**erturbation **M**odel *(***LPM***)* (e.g. [38] [40] [46]), perhaps to distinguish it from other forms of hybrid models.

In the **LPM**, it is presumed that, during a year, in which the rainfall is identical to its seasonal expectation the corresponding discharge hydrograph is also identical to its seasonal expectation. However, in all other years, when the rainfall and the discharge values depart from their respective seasonal expectations, these departures are assumed to be related by a linear time invariant system. Undeniably, the **LPM** structure reduces the reliance on the linearity assumption and increases the reliance on the observed seasonal behaviour of the catchment [43]. For the discrete system with recorded data sampled at one-day interval or averaged over one-day interval, the discrete **LPM** may be described by the following assumptions:

1) If the inflow (or rainfall) on each date *d* in a particular year is exactly the inflow (or rainfall) seasonal mean for that date, R_d, the corresponding outflow would likewise be the outflow seasonal mean Q_d.

Denoting by notations,

$R_d \longrightarrow Q_d$

2) In any actual record, the series of departures of the inflow (or rainfall) and the outflow from their seasonal means are linearly related

$(R - R_d) \longrightarrow (Q - Q_d)$

or $R' \longrightarrow Q'$

where $R' = R - R_d$ and $Q' = Q - Q_d$.

The relationship between the input departure series, the output departure series and the discrete pulse response relating to the departure series can then be expressed as

$$Q_i' = \sum_{j=1}^{m} R_{i-j+1}' h_j' + e_i \qquad \text{(A.4)}$$

where R_i' and Q_i' are the input (or rainfall) departures and the corresponding discharge departures from their seasonal expectations at the i^{th} instant, respectively, h_j' is the j^{th} ordinate of the discrete pulse response relating to the departure series of input and the output, e_i is the error term and m is the memory length. As in the case of the **SLM**, the

Ordinary **L**east **S**quares (**OLS**) method can also be used to give estimates of the pulse response ordinates of the **LPM**, provided that the values of these departures are known. For a multiple input case, the equation for the discharge *Qi* can be generalised to the form as given below.

$$Q_i^{'} = \sum_{k=1}^{k} \sum_{j=1}^{m(k)} R_{i-j+1}^{'(k)} h_j^{'(k)} + e_i \qquad \text{(A.5)}$$

i = 1, 2, …, N

where Q'_i is the output series,

K is the total number of input departure series,

$R'^{(k)}_i$ is the k^{th} input departure series,

$H'^{(k)}$ is the pulse response ordinates corresponding to the k^{th} input departure series,

$m^{(k)}$ is the memory length (defined later) of the system corresponding to the k^{th} input series,

e_i is the disturbance term and

N is the length of the output series.

In the application of the **LPM**, it is necessary to obtain an estimate of the expected values of the input (or rainfall) and discharge for each date, i.e. day of the year 1 - 365. These are referred to as the seasonal mean values. If n is the number of years of sample data, such an estimate can be obtained for each date d by taking mean of the values on that date among the years of record

$$x_d = \frac{1}{n} \sum_{r=1}^{n} x_{d,r} \qquad \text{(A.6)}$$

where *r* indicates the year number and *x* denotes the sample input or discharge value. As *n* increases indefinitely x_d approaches the true population value X_d. However, for small *n*, the population and the sample differ, not due to the errors in the physical sense, but due to the sampling variance of x_d. Expressing algebraically,

$$x_d = X_d + e_d \qquad \text{(A.7)}$$

While x_d normally varies unsmoothly with d, X_d might be expected to vary smoothly, reflecting the effects of smoothly and continuously varying climatic elements. X_d is however unknown.

If one were to disregard the information provided by any value of x_d concerning neighbouring values information which depends on the persistence of x_d and which is therefore stronger in the context of discharge than of rainfall, and stronger on more sluggish catchments than on those which are relatively flashy it is probable that the best estimate of X_d would be that given by the equation,

$$x_d = \frac{1}{n}\sum_{r=1}^{n} x_{d,r} \qquad \text{(A.8)}$$

and the sample mean and estimate of the population mean would coincide. However, it is intuitively tempting to assume a high degree of persistence in seasonal means and indeed it would be difficult to account physically for the high frequency variation one finds in plots of x_d obtained from samples of a few year's duration. Assuming the absence of such components in X_d implies that those which are observed in the sample are due to sampling variance only and standard techniques for filtering out such high frequency components may be employed to obtain X_d from x_d. The validity of such techniques depends on:

1) the assumption that high frequency variation is absent in the population values of x_d and

2) the assumption that it is the population value of x_d rather than the sample values that are sought.

The Schematic representation of the Linear Perturbation Model (**LPM**) [37] is given below.

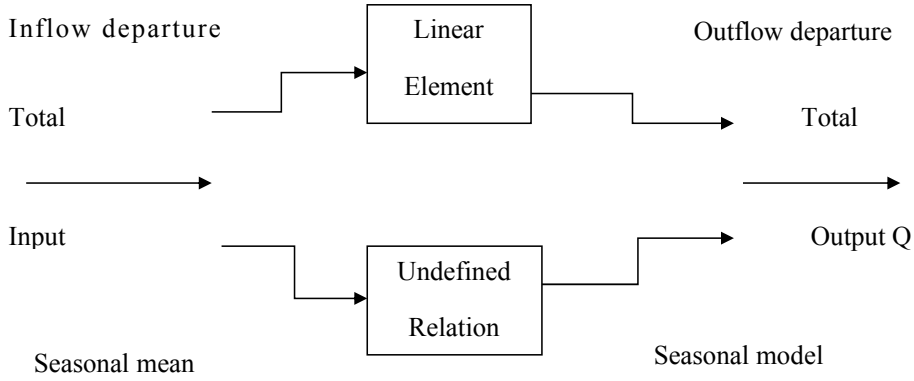

Schematic diagram of Linear Perturbation Model (**LPM**)

P-LPM (PARAMETRIC LINEAR PERTURBATION MODEL)

In the **P**arametric form of the **L**inear **P**erturbation **M**odel (**P-LPM**), the Linear Transfer Function type representation of the transformation process of the departures of the values of the input series from their respective seasonal means x to the departures of the values of the output series from their respective seasonal means y for discrete data intervals is given by

$$\sum_{j=0}^{r} \alpha_j y_{t-j} = \sum_{j=1}^{s} \omega_j x_{t-b-j+1} \tag{A.9}$$

where α_j are the autoregressive parameters, with $\alpha_0 = 1$, the ω_j are the moving average parameters and b is the pure time delay restricted to integer values only [37]. r and s are the order of the autoregressive and the moving average parts of the model.

Writing explicitly for y_t with the addition of an error term, the above expression becomes

$$y_t = \sum_{j=1}^{r} \alpha_j y_{t-j} + \sum_{j=1}^{s} \omega_j x_{t-b-j+1} + e_t \tag{A.10}$$

where α_j and ω_j are the autoregressive and moving average parameters respectively obtained after modifying the equation (3). In this form, the current value of output departure y depends linearly on previous values of output departures y and input departures x. The parameters of the model are estimated by the method of Ordinary Least Squares.

It may be shown that, after estimation of the model parameters, the pulse response ordinates can be obtained by applying the transfer function to a single pulse of unit input. The pulse response ordinates are given by

$$h_j = 0 \qquad j < b$$

$$h_j = \alpha_1 h_{j-1} + \alpha_2 h_{j-2} + \ldots + \alpha_r h_{j-r} + \omega_{j-b+1} \qquad j = b, b+1, b+2, \ldots, b+s-1$$

$$h_j = \alpha_1 h_{j-1} + \alpha_2 h_{j-2} + \ldots + \alpha_r h_{j-r} \qquad j > b+s-1$$

If the resulting shape of the pulse response is unsatisfactory, appropriate changes need to be made to the model structure and the model needs to be recalibrated. In the non-updating mode, past computed values of y are used on the right-hand side of the transfer function equation, instead of the past observed values. However, the model provides the facility for being used in updating mode also, in which past observed value of y are to be used as input.

The estimated departures are finally added to the seasonal means of the output series to obtain the estimated discharge values.

LVGFM (LINEARLY VARYING GAIN FACTOR MODEL)

The Constrained Linear System with Thresholds (**CLS-T**) and also the Multi-Linear Systems of [37] and [3]- [4] addressed the constant gain factor deficiency of the **SLM** by using a threshold concept to decompose the input rainfall vector into non-concurrent component input vectors, each of which are fitted to the rainfall-runoff data using separate linear time-invariant systems. However, an abrupt switch from one system response function to another whenever the threshold of the selected control variable (e.g. the antecedent precipitation or catchment wetness) is crossed, involving a substantial change both in the shape of the response function and in the magnitude of

its gain factor *G,* is physically unrealistic. Although a response function which varied gradually with the catchment wetness, both in scale *G* and in shape, would appear to be much more sensible, our experience of testing many models in the Galway workshops had indicated that getting the water balance (i.e. the volume of runoff) right is far more important in producing high model efficiency than the actual distribution of that volume over time. So, the **L**inearly **V**arying **G**ain **F**actor **M**odel (**LVGFM**), proposed by [3] - [4] for the single-input to single-output case, involves only the variation of the gain factor with the selected index of the prevailing catchment wetness, without varying the shape (i.e. the weights) of the response function. The model output has the familiar convolution summation structure (based on the concept of a time-varying gain factor G_i). The Schematic diagram of the Linearly Varying Gain Factor Model [3] - [4] is given below.

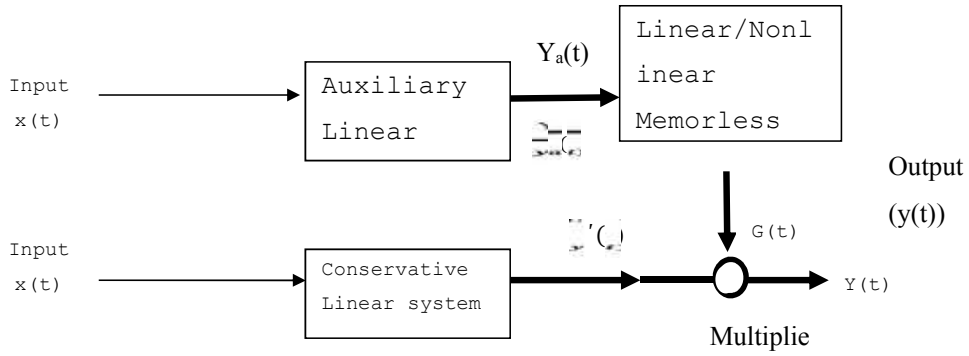

Schematic diagram of Linearly Varying Gain Factor Model (**LVGFM**)

A multiple-input linear system model is expressed as

$$y_t = \sum_{j=1}^{J} \sum_{k=1}^{m(j)} h_k^{(j)} x_{i-k+1}^{(j)} + e_t \qquad \text{(A.11)}$$

where, J is the total number of input time series (which is also equal to the total number of discharge components in the output time series), $x^{(j)}$ is the j^{th} input time series, $h^{(j)}$ is the pulse response (unit hydrograph) ordinate corresponding to the j^{th} input series, $m^{(j)}$ is the memory length of the system corresponding to the j^{th} input, yt is the output time series and e_t is the disturbance (i.e. the model error) term.

Introducing $G^{(j)}$ as the constant gain factor for the j^{th} input, the above equation may be written as

$$y_t = \sum_{j=1}^{J} G^{(j)} \sum_{k=1}^{m(j)} \beta_k^{(j)} x_{i-k+1}^{(j)} + e_t \tag{A.12}$$

where, $\beta^{(j)}$ are the standardised unit hydrograph ordinates corresponding to the j^{th} input defined by,

$$\beta_{jk}^{(j)} = \frac{h_k^{(j)}}{G^{(j)}} \tag{A.13}$$

In reality, however, the gain factor for each input is expected to change with respect to time depending on the degree of wetness of the catchment as characterised by the current outflow. The linearly varying gain factor model considers this variability of gain factor by assuming the gain factor $G^{(j)}$ as a function of the output component of an auxiliary elementary model (e.g. Simple Linear Model, **SLM**) corresponding to each input time series, i.e. a linear weighting of such outflow components having the form,

$$G_t^{(j)} = A_0^{(j)} + A_1^{(j)} \hat{y}_t^{(1)} / \overline{x}^{(1)} + \cdots . + A_j^{(j)} \hat{y}_t^{(J)} / \overline{x}^{(J)} \tag{A.14}$$

$$G_t^{(J)} = \sum_{s=0}^{J} A_s^{(j)} Z_t^{(s)} \tag{A.15}$$

where, $x^{(i)}$ is the mean of the j^{th} series in the calibration period,

$Z_t^{(t)} = \hat{y}_t^{(s)} / \overline{x}^{(s)}$

For s=1, 2, J and $Z_t^{(0)} = 1$

Substitution of the expression for $G_t^{(j)}$ in the expression for y_t gives,

$$y_t = \sum_{j=1}^{J} \sum_{s=0}^{J} A_s^{(j)} Z_t^{(s)} \sum_{k=1}^{m(j)} \beta_k^{(j)} x_{t-k+1}^{(j)} + e_t \quad \text{(A.16)}$$

This equation may also be written as,

$$y_t = \sum_{j=1}^{J} \sum_{s=0}^{J} \sum_{k=1}^{m(j)} A_s^{(j)} \beta_x^{(j)} x_{t-k+1}^{(j)} Z_t^{(s)} + e_t \quad \text{(A.17)}$$

Letting

$$H_{i,k}^{(j)} = A_K^{(j)} \beta_i^{(j)} \quad \text{(A.18)}$$

the above equation may be expressed as,

$$y_t = \sum_{j=1}^{J} \sum_{s=0}^{J} \sum_{k=1}^{m(j)} H_{k,s}^{(j)} x_{i-k+1}^{(j)} Z_t^{(s)} + e_t \quad \textbf{(A.19)}$$

ANNM (ARTIFICIAL NEURAL NETWORK MODEL)

A typical neural network consists of a number of elements (nodes) and connection pathways linking these. The nodes are the computational elements of the network and are usually known as neurons, thus reflecting the origin of the neural network method in modelling the biological neural networks of the human brain. The connection pathways transfer information between the various neurons. Each connection pathway between any pair of neurons has an associated value called the connection weight.

A neuron usually receives an array of inputs, but it has a single output. The input elements constituting a neuron input array can either be external inputs to the network or outputs of other neurons. The neuron accumulates these inputs and using a mathematical transformation formula known as a transfer function it transforms these

accumulated inputs to the neuron output. This output is generally distributed to (but not divided up among) a number of connection pathways to provide inputs to the other neurons, with each of these connection pathways transmitting the full value of the contributing neuron output.

There are various types of neural networks. However, the type chosen for use in the **GFMFS** package is the "multi-layer feed forward network" which is very powerful in function modelling (Nielsen, 1991, p. 131).

The multi-layer feed forward neural network used in the **GFMFS** consists of an input layer, an output layer and only one "hidden" layer between the input and the output layers. A layer is usually a group of neurons having the same pattern of connection pathways to the other neurons of adjacent layers. Each neuron in a particular layer has connection pathways to all the neurons in the next adjacent layer, but none to those of the same layer.

There is only one neuron, for the single output, in the output layer. For the input layer, the neurons are to be from the input series. As the neural network, itself does not incorporate storage effects, storage may either be implicitly accounted for by the use of the output series of the naïve **SLM** or any other substantive model, or by considering as many neurons of the input series as is adequate to account for the system response (i.e. equal to the memory length of the system). Number of neurons for the input layer is to be determined after a number of trial runs of the program for the **A**rtificial **N**eural **N**etwork (**ANN**) model considering different numbers of input neurons in each run, and observing the model efficiency values each time. The schematic diagram of the Artificial Neural Network (**ANN**) model is given below.

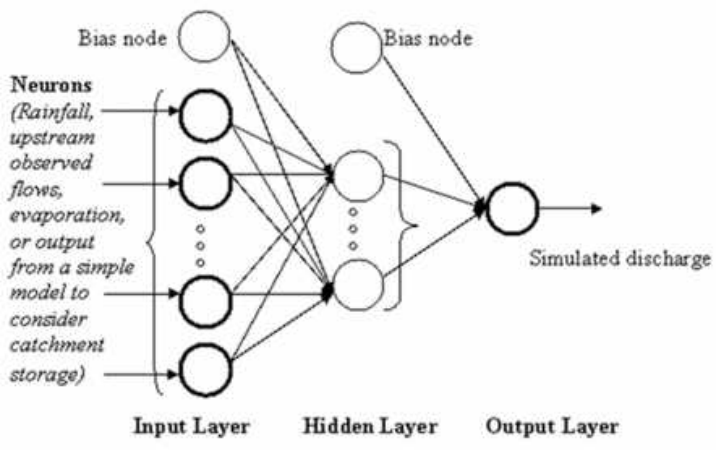

Schematic diagram of Artificial Neural Network (**ANN**) model

For a neuron either in the hidden or in the output layer, the received inputs y_i are transformed to its output y_{out} by a mathematical transfer function of the form

$$y_{out} = f\left(\sum_{i=1}^{M} \omega_i y_i + \omega_0\right) \quad \text{(A.20)}$$

where f () denotes the transfer function, w_i is the input connection pathway weight, *M* is the total number of inputs (which usually equals the number of neurons in the preceding layer), and w_o is the neuron threshold (or bias), i.e. a base-line value independent of the input. The non-linear transfer function adopted for the neurons of the hidden layer and also that of the output layer is the widely-used logistic function, i.e. a form of sigmoid function, given by

$$f\left(\sum_{i=1}^{M} \omega_i y_i + \omega_0\right) = \frac{1}{1+e^{-\alpha\left(\sum_{i=1}^{\sigma} \omega_{i=1} y_{i+\omega_0}\right)}} \quad \text{(A.21)}$$

which is bounded in the range [0,1]. The weights w_i, the threshold w_o and the σ of different neurons can be interpreted as parameters of the selected network configuration.

SMAR (SOIL MOISTURE ACCOUNTING & ROUTING) MODEL

The **SMAR** model is a simple lumped conceptual rainfall-evaporation-runoff model. It is designed to incorporate within its structure an approximate representation of some of those physical processes known to have an important role in the generation of stream flow by a number of interconnected conceptual storage sub-systems. **SMAR** is an abbreviation of the **S**oil **M**oisture **A**ccounting and **R**outing procedure [37]. This model was originally known as the *layers model* [60], its water-balance component being based on the 'Layers Water Balance Model' proposed in 1969 by [53]. In the **GFMFS**, a modified version of the **SMAR** layers model, called **SMARG** version, due to both [43], is used.

Although hydrological systems, in mathematical modelling exercise, are generally considered to be conservative, characterised by a dynamic balance between precipitation (rainfall and/or snowfall), evapotranspiration, runoff (discharge at the catchment outlet), and moisture storage within the system, and the **SMARG** variant of the model is designed for application to catchments with conservative system behaviour, some systems may deviate from the characteristics of conservative systems. Examples of such catchments are those with some physiographical peculiarities or those characterised by inconsistencies in the data sets. Physiographic features may be i) the existence of karstic formations — with a significant fraction of flow being lost in sub-surface processes through fissures, solution channels, sinkholes, underground streams and reservoirs etc., or ii) the existence of sandy deposits at the discharge gauging site of the river — flow through which is unaccounted for at the gauging site, etc. Data inconsistencies are manifested in i) inadequacy of recorded data, or ii) non-representativeness of the data record due to failure to capture information on significant loss or gain components affecting the system under consideration. The system response to precipitation may not be consistent with that of a conservative system in such typical cases. The term '*apparently non-conservative*' may be used to denote such a system.

For use in catchments characterised by non-conservative system behaviour, two variants called **SMAR-NC1** and **SMAR-NC2** are also included in the **GFMFS**. The

term **NC** in the names of these variants indicates '**N**on-**C**onservative', and numbers 1 and 2 refer to minor differences in one of these model forms from the other.

For a gauged catchment, the balance between the inputs and the output may be assessed from simple calculations based on long-term averages of precipitation, discharge, evaporation etc. so that the appropriateness of applying a model based on the assumption of the system being conservative may be determined *a priori*. However, even for systems that do not conform to near-conservative behaviour, the usual practice is that standard models are applied to simulate the flows. System-theoretic and conceptual quasi-physical models designed for conservative systems fail to recognise the dynamics of all the major flow-producing components, and the performance levels of these models drop down to unacceptably low values. Such model structures are, therefore, inappropriate for non-conservative systems, and they must be adapted to incorporate an element of loss or gain in the flow functions.

In the structure of the **SMAR** model, two distinct complementary components can be identified. The first is the non-linear water balance (soil moisture accounting procedure) component that keeps account of the balance between rainfall, evaporation, runoff and soil storage using a number of empirical and assumed functions which are physically realistic or at least physically plausible. The second is the routing component which simulates the attenuation and the diffusive effects of the catchment by routing through linear time invariant storage systems the different generated runoff components which are the outputs from the water balance part.

SMARG VERSION OF THE SMAR MODEL

The schematic diagram below shows the structure of the **SMAR** model incorporating [43] - [44] modifications (the **SMARG** version in the **GFMFS**).

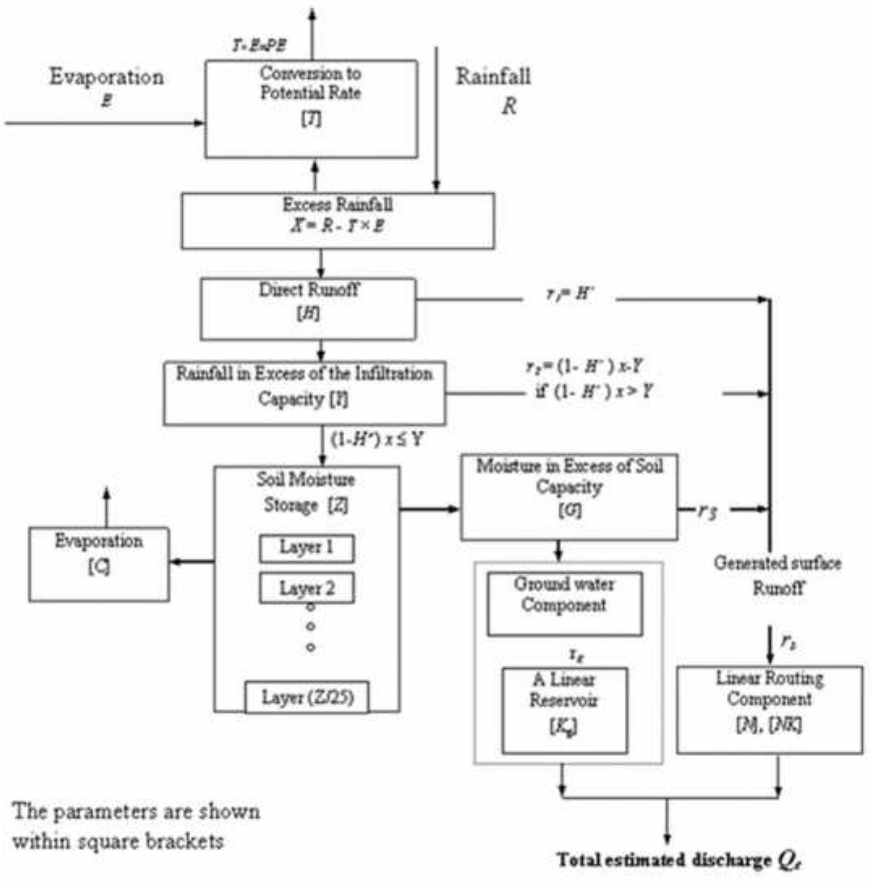

Schematic diagram of [43] - [44] version of the **SMAR** Model

The essence of the **SMAR** model is the concept of the soil layers. The catchment is visualised as being composed of a set of horizontal soil layers, each of which may contain water up to a maximum depth of *25 mm* except for the last (i.e. bottom) layer which may have a maximum depth less than *25 mm*. The total combined water storage depth of these layers is a parameter of the model, which is usually denoted by *Z*. In original structures of the **SMAR** model, maximum number of such layers was restricted to five with the total combined water storage depth of 125 mm. However, in the

GFMFS, value of *Z* other than 125 mm may also be adopted. Default maximum value of *Z* is kept at 125 mm.

The evaporation input (*E*) to the **SMAR** model is either the Pan evaporation depth or that obtained from Penman's equation, which when multiplied by a parameter *T* (less than unity), is converted to an estimate of the potential evaporation depth over the catchment.

Evaporation only occurs from the layers when there is no rainfall or when the rainfall is not sufficient to satisfy the potential evaporation demand (T×E). Any evaporation from the first layer occurs at the potential rate. On the depletion of the water depth in the first layer, any evaporation from the second layer occurs at the potential rate multiplied by a parameter *C* having a value less than unity. On the depletion of the water depth of the second layer, any subsequent evaporation from the third layer occurs at rate of C^2 and so on. Hence, if the all layers were full and there was no subsequent rainfall, then a constant potential evaporation applied to the catchment would reduce the soil moisture storage in, approximately, an exponential manner. Such evaporation would continue until either the storage of all the layers was depleted or the potential evaporation demand was fully satisfied.

In rainy days, provided the rainfall exceeds the potential evaporation (T×E) depth, runoff takes place. A fraction *H'* of the excess rainfall, i.e. the rainfall less than the potential evaporation, contributes to the generated runoff by producing the direct generated runoff component r_1. *H'* is considered to be directly proportional to the ratio of the available water depth to the maximum depth in the top five layers, or in the total set of layers if the number of the layers is less than five, i.e. $H'=H\times(W_{act}/W_{cap})$.
The constant of proportionality *H* is a parameter of the model, with *H'* having a value between zero and *H*.

Allowing the direct generated runoff to vary as a function of the available water in the top five layers (or if $Z < 125\ mm$ in the whole stack of layers) is a modification, due to Khan (1986), of the original version of the **SMAR** model presented by O'Connell et al. (1970) in which the direct generated runoff occurs without any consideration of the available soil moisture depth in the layers.

Any remainder of the excess rainfall, after the subtraction of r_1, which exceeds the maximum infiltration capacity *Y mm/day*, also contributes to the generated runoff as r_2, the component of runoff in excess of the infiltration capacity. The remaining rainfall, after subtraction of both the direct runoff r_1 and the runoff in excess on infiltration capacity r_2 (if any), replenishes each soil layer in turn beginning from the first (i.e. the top) layer downwards, until either the rainfall is exhausted or all layers are full. Any still remaining surplus is further divided into two portions, the first portion being envisaged as a groundwater runoff component r_g while the second is considered as a subsurface runoff component r_3. This r_3 component is added to the direct runoff r_1 and to that in excess of infiltration capacity r_2 to produce the total generated surface runoff r_s as $r_s = r_1+r_2+r_3$. The division of the final surplus exiting from the layers into two parts is controlled by a weight parameter *g*. This division was introduced by [54] as a further refinement to Khan's (1986) version of the **SMAR** model in which the whole surplus is directly added to other generated surface runoff components to give a single composite generated runoff.

The total generated surface runoff (i.e. $r_s=r_1+r_2+r_3$) is routed through a two-parameter distribution function. In the **GFMFS**, three two-parameter distribution options are available for routing the generated '*surface runoff*' component of the **SMAR** model, namely, the classic gamma distribution (Nash-cascade) model [54] having the shape parameter *n* and the *lag nK*, its discrete counterpart, the Negative Binomial distribution [61] having parameters *n* (number of linear reservoirs in the cascade) and *K* (storage coefficient of each linear reservoir), and the sharp-peaked Inverse Gaussian distribution for flashy catchments having parameters Ψ and μ.

The groundwater runoff component r_g is routed through a single linear reservoir with a storage coefficient parameter K_g.

The sum of the outputs of these two routing components is the **SMAR** model estimated outflow. Thus, the **SMARG** version of the **SMAR** model has nine parameters, five of which control the overall operation of the water-budget component, while the remaining four parameters (including a weighting parameter which determines the amount of generated '*groundwater runoff")* control the operation of the routing

component. Some of the parameters may be fixed at appropriately chosen values while the values of the rest are usually estimated empirically by optimisation to minimise the selected measure of error between the observed and the model estimated discharges. The parameters of the **SMARG** model at a glance are provided in the table below.

Parameter	Description
Z	The combined water storage depth capacity of the layers (mm)
T	A parameter (less than unity) that converts the given evaporation series to the model-estimated potential evaporation series.
C	The evaporation decay parameter, facilitating lower evaporation rates from the deeper soil moisture storage layers
H	The generated *'direct runoff'* coefficient
Y	The maximum infiltration capacity depth (mm)
n	The shape parameter of the Nash gamma function 'surface runoff' routing element; a routing parameter
nK	The scale (lag) parameter of the Nash gamma function 'surface runoff' routing element; a routing parameter
g	The weighting parameter, determining the amount of generated 'groundwater' used as input to the 'groundwater' routing element.
Kg	The storage coefficient of the 'groundwater' (linear reservoir) routing element; a routing parameter

SMAR-NC1 AND SMAR-NC2 VERSIONS OF THE SMAR MODEL

The **SMAR-NC1** and the **SMAR-NC2** models incorporate an additional parameter $F \leq 1$ to replicate, in different ways, any gain or loss component to or from a non-conservative system. These are, therefore, 10-parameter models. The structure of the **SMAR-NC1** model is shown below.

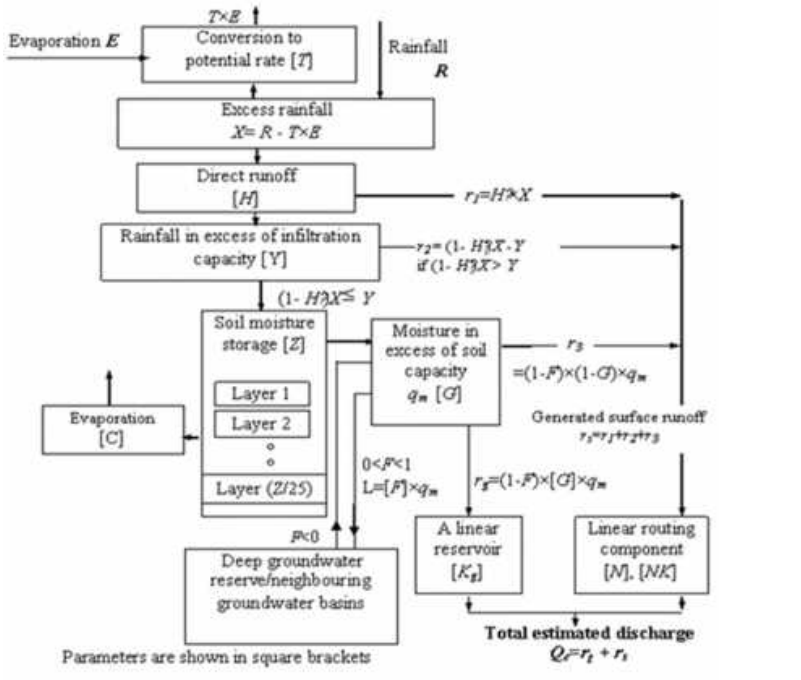

Schematic diagram of **SMAR-NC1** model

In the **SMAR-NC1** model, the parameter F comes into play just in advance of the application of the G parameter of the **SMARG** model. Thus, in case of the SMAR-NC1 model, the product $(F \times q_m)$ becomes the loss function L, the product $\{(1\text{-}F) \times q_m \times G\}$ becomes the groundwater component r_g, and the product $(1\text{-}F) \times q_m \times (1\text{-}G)$ becomes the 3rd surface runoff component r_3, the other parameters of the model being similar in operation to that of the **SMARG** model. The loss component L defines that part of the rainfall that does not evaporate and yet does not subsequently contribute to the estimated discharge at the outflow gauging station.

For $0 < F < 1$, and for $q_i > 0$, there is a positive loss function L from the system which is not available as input to the routing component of the model. For $F = 1$ and $q_m > 0$, we have $L = q_m$ and hence $r_g = r_3 = 0$, in which case the linear reservoir routing process (and parameter K_g) becomes redundant and the simulated outflow Q_e is produced solely by the routing of the surface component r_s, where $r_s=(r_1+r_2)$. For $F = 0$ and $q_m > 0$, the SMAR-NC1 version reverts to the **SMARG** model, the F parameter becoming redundant, i.e. there is neither loss from nor gain to the layer-overflow depth q_m before the routing takes place. An optimised value of $F < 0$, for $q_m > 0$, suggests a contribution to the simulated discharge Q_e from adjoining basins or groundwater reserves, with $(r_g+r_3) =[(1-F) \times q_m] > q_m$, i.e. a negative loss function L.

In the **SMAR-NC1** model, only a fraction of the moisture in excess of the storage capacity (Z) of soil layers (i.e. the overflow) can become the loss function, a scenario that might be quite rare. As an alternative structure, suggested as a more realistic scenario, provision is made in the **SMAR-NC2** model for a continuous loss function, regardless of whether the soil layers are full or not, by allowing a fraction of the storage content in the layers immediately following infiltration (if any), (which content may be >, =, or < the capacity depth Z, but may not = 0), to become the loss function. In the structure of **SMAR-NC2**, the operation of the parameter F in producing a positive loss function (for loss from the system) or a negative loss function (for gain to the system) is similar to that in the **SMAR-NC1** form.

The **SMAR-NC** model forms have ten parameters (Z, T, H, Y, C, F, G, N, NK and K_g). The objective function for model calibration and the model performance evaluation criteria for these models are the same as those for the **SMARG** model. The schematic diagram of the SMAR-NC2 is given below.

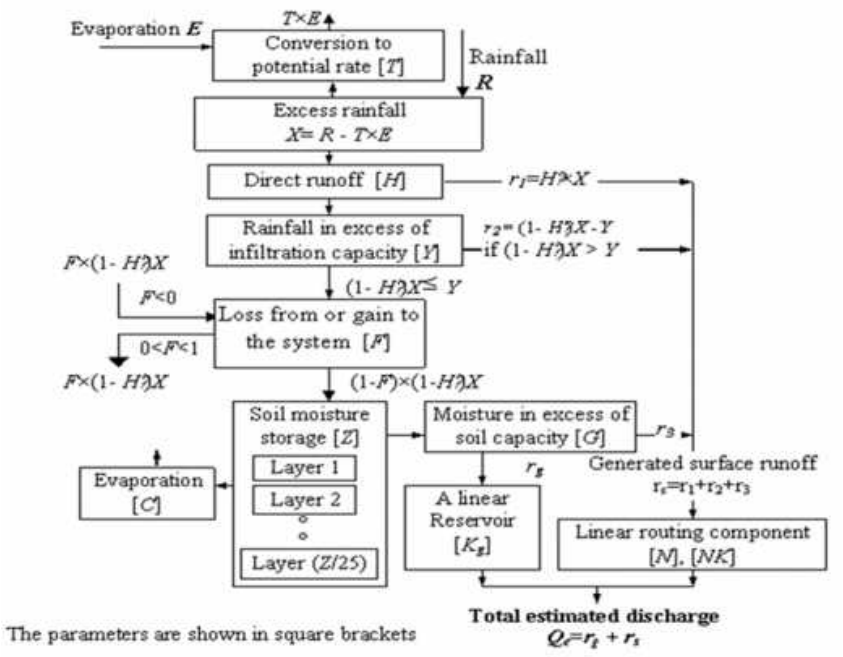

Schematic diagram of **SMAR-NC2** model

MOCT (MODEL OUTPUTS COMBINATION TECHNIQUES)

MODELS FOR COMBINING OUTPUTS FROM A NUMBER OF SUBSTANTIVE MODELS

Substantive rainfall-runoff models are normally used as components in real-time river flow forecasting systems. In such systems, a particular rainfall-runoff model may have been selected from among a number of competing alternative models, based, perhaps, on its accuracy, its familiarity to the user, its ease of use, the type of the catchment, and the available data. In such a case, the forecaster, or the forecast user, may depend exclusively on the forecasts of the selected model, although a more primitive auxiliary model may also be used simultaneously to provide an independent back-up forecast in the event of perceived short-term failure of the substantive model. However, there may be a potential danger in relying entirely on one substantive rainfall-runoff model (i.e. a sample of one) since it is unlikely to perform satisfactorily at all times or under all conditions (e.g. perhaps not all of its structural assumptions are valid or the conditions

under which it is assumed to operate are not entirely fulfilled). As a consequence, the failure of the model to yield consistently reasonable forecasts may undermine the credibility of the model and the faith of the user in such systems.

Instead of relying on one individual rainfall-runoff model, or even of switching from one to another, an alternative approach would be applied to generate discharges simultaneously from a number of different rainfall-runoff models and to combine the forecasts in an optimum manner. Thus, inferior models having low individual performance may also be significant in improving the overall performance of simulation, when included in an **MOCT** [71].

A combined estimate of discharge of N runoff simulation models for the i^{th} period of time may be defined as a function $F()$ of the estimated discharges of the N models for that time period, that is,

$$\hat{Q}_{Cj} = F(\hat{Q}_{1i}, \hat{Q}_{2i}, \dots, \hat{Q}_{N-1i}, \hat{Q}_{Ni}) \qquad \text{(A.22)}$$

$$\hat{Q}_{ji} \qquad \text{(A.23)}$$

being the estimated discharge of the j^{th} model for the i^{th} time period.

The essence of the concept is that each model output captures certain important aspects of the information available about the process being modelled, thereby providing a source of information which may be different from that of other models. Combining these various sources of output information may enable the user to avail of all the input information. Furthermore, the judicious combination of the outputs of different models has the additional merit that it may assist in understanding the underlying physical processes involved and thus in building better individual models.

Three techniques for combining the estimated outputs of different models are included in the **GFMFS** package, namely, the Simple Average Method (**SAM**), the Weighted Average Method (**WAM**), and the **N**eural **N**etwork **M**ethod (**NNM**). In a purely regression framework, viewing the actual observed outputs as the response (i.e. dependent) variable and the individual outputs of the models as explanatory (i.e. independent) variables, the assumption made in the first two methods (i.e. the **SAM**

and the **WAM**) is that the actual observed outputs are functionally related to the estimated outputs of the individual models by linear regression relationships.

The Neural Network method (**NNM**), as the name implies, utilises the model structure of a neural network, which is a very powerful computational technique for modelling complex non-linear relationships particularly in situations where the explicit form of the relation between the variables involved is unknown.

THE SIMPLE AVERAGE METHOD (SAM)

The simple average method (**SAM**), is the simplest method of combining the outputs of different individual models. Given the estimated discharges of N rainfall-runoff models, a combined estimate of the discharge of the i^{th} time period, using the **SAM**, is given by

$$\hat{Q}_{Ci} = \frac{1}{N}\sum_{j=1}^{N} \hat{Q}_{ji} \qquad \text{(A.24)}$$

This equation illustrates that the computation of the **SAM** combined output is very trivial, requiring very little effort and without any empirical curve fitting, once the estimated discharges of the N models have been calculated. Moreover, it highlights that equal emphasis (i.e. weight) is assigned to the outputs of all of the models being considered.

The **SAM** can produce forecasts that are better than those of the individual models and its accuracy depends mainly on the number of the models involved and on the actual forecasting ability of the specific models included in the simple average.

THE WEIGHTED AVERAGE METHOD (WAM)

When some of the individual models selected for combination appear to be consistently more accurate than others, in which case the use of the simple average method for combination can be quite inefficient), the use of a weighted average would be considered.

The weighted average method (**WAM**) for combining the estimated model outputs, in the case of N rainfall-runoff models, may be expressed as [33]

$$Q_i = \sum_{j=1}^{N} a_j \hat{Q}_{ji} + e_i \qquad \text{(A.25)}$$

where Q_i is the observed discharge of the i^{th} time period, a_j is the weight assigned to the j^{th} model estimated discharge

$$\hat{Q}_{ji} \qquad \text{(A.26)}$$

and e_i is the combination error term.

The above equation may alternatively be expressed in matrix notation as

$$\mathbf{Q} = \mathbf{PA} + \mathbf{E} \qquad \text{(A.27)}$$

where **P** is the input matrix defined by

$$\begin{bmatrix} \hat{Q}_{1,1} & \hat{Q}_{2,1} & \cdots & \hat{Q}_{N-1,1} & \hat{Q}_{N,1} \\ \vdots & & & \ddots & \vdots \\ \hat{Q}_{1,K} & \hat{Q}_{2,K} & \cdots & \hat{Q}_{N-LK} & \hat{Q}_{N.K} \end{bmatrix}$$

$Q = (Q_1, Q_2, Q_3, \ldots, Q_{k-1}, Q_k)^T$ is the output vector,

$A = (a_1, a_2, a_3, \ldots, a_{k-1}, a_k)$ is the weight vector and

$E = (e_1, e_2, e_3, \ldots, e_{k-1}, e_k)$ is the combination error vector, T denotes the transpose of the vector and *k* is the total number of observations.

The preceding equation can be perceived as a multiple linear regression model. Thus, it can be readily shown that the ordinary least squares estimate of the weight vector is given by

$$\hat{A} = (P^T P)^{-1} P^T Q \qquad \text{(A.28)}$$

In the **WAM**, the sum of the weights a_i is normally constrained to be equal to unity, that is

$$\sum_{i=1}^{N} a_j = 1 \qquad \text{(A.29)}$$

The main rationale behind constraining the sum of the weights to unity is that if the models included in the weighted average are unbiased, i.e. having a zero-mean output error term, then the weighted average combined forecast is likewise unbiased [33].
In the case where the sum of the weights is constrained to equal unity, it can be shown using the method of constrained least squares (CLS) that the estimate of the weights vector

$\hat{A}_{Cis}$ (A.30)

is given by

$$\hat{A}_{cis} = (P^T P)^{-1}\left(P^T Q + \frac{1}{2} b\lambda\right) \quad \text{(A.31)}$$

where b is the unit vector (i.e. all of its scalar components are unity) having the same dimension as the parameters vector A and is the Lagrangian multiplier which is given by

$$\lambda = 2(b^T (P^T P)^{-1} b)^{-1} (1 - b^T)(P^T P)^{-1} P^T Q \quad \text{(A.32)}$$

Alternative techniques, other than least squares, for estimating the weights a_i have also been used, e.g. by considering the covariances of the forecast errors of the individual models being considered.

The main disadvantage of the weighted average method (**WAM**) is that it may suffer from the problem of multi-collinearity which in turn may result in unstable estimates of the weights [93], thereby reducing the considerable advantages obtained from combining the different models' outputs. This applies especially in the present hydrological context, where the degree of multi-co linearity increases with the increase in the forecasting ability of the individual models, or even where the outputs of the various models used are very similar (without necessarily being good).

THE NEURAL NETWORK METHOD (NNM)

The neural network method provides an alternative to the simple average(**SAM**) and the weighted average methods (**WAM**) for combining outputs from different models, and indeed can be used to test whether or not a more complex relationship is needed for such combinations. Neural networks are applied, in the **GFMFS** package, in the context of providing a non-linear function mapping of a set of inputs (the inputs being the estimated outputs of the chosen rainfall-runoff models) into the network output (i.e. the combined discharge forecast). However, the specific mathematical form of the relationship is unspecified (i.e. it is a non-parametric method in that sense).

A typical neural network consists of a number of elements (nodes) and connection pathways linking these. The nodes are the computational elements of the network and are usually known as neurons, thus reflecting the origin of the neural network method in modelling the biological neural networks of the human brain. The connection pathways transfer information between the various neurons. Each connection pathway between any pair of neurons has an associated value called the connection weight.

A neuron usually receives an array of inputs, but it has a single output. The input elements constituting a neuron input array can either be external inputs to the network or outputs of other neurons. The neuron accumulates these inputs and using a mathematical transformation formula known as a transfer function it transforms these accumulated inputs to the neuron output. This output is generally distributed to (but not divided up among) a number of connection pathways to provide inputs to the other neurons, with each of these connection pathways transmitting the full value of the contributing neuron output.

There are various types of neural networks. However, the type chosen for use in the **GFMFS** package is the "multi-layer feed forward network" which is very powerful in function modelling.

The multi-layer feed forward neural network used in the **GFMFS** consists of an input layer, an output layer and only one "hidden" layer between the input and the output layers. A layer is usually a group of neurons having the same pattern of connection pathways to the other neurons of adjacent layers. Each neuron in a particular layer has

connection pathways to all the neurons in the next adjacent layer, but none to those of the same layer. The schematic diagram of Neural Network Model (**NNM**) for output combination is given below.

The input layer has a number of neurons equal to the number of the elements in the external input array to the network. These external inputs to the neurons in the input layer are transformed to outputs from these neurons using the identity function as a transfer function, according to $f(X_i) = X_i$; where X_i is the i^{th} external input to the i^{th} neuron of the input layer.

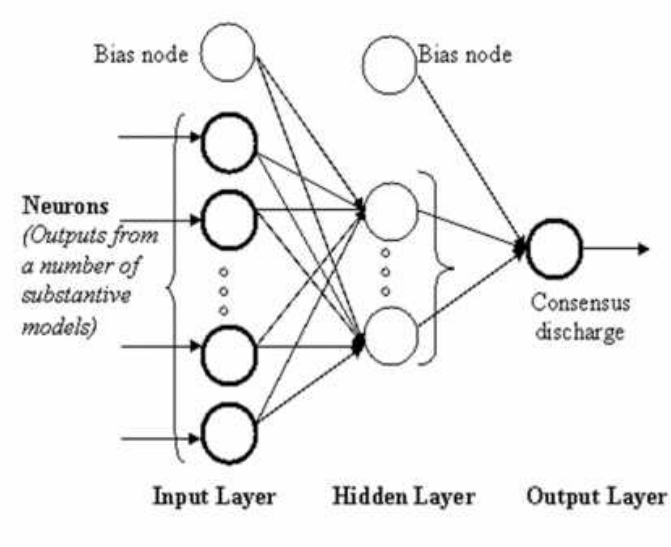

Schematic diagram of Neural Network Method (**NNM**) of **MOCT**

In the form of the network used in the **GFMFS** package, the neurons of the hidden layer have no direct connection with either the external inputs or the external output of the network. The inclusion of hidden layers generally enhances the performance of the network, enabling it to deal robustly and efficiently with complex non-linear problems but, for simplicity, only one hidden layer is used in the network considered in the **GFMFS** package. Each neuron of this hidden layer receives its inputs from the pathways connecting it to the neurons of the input layer, while its output is transmitted along connection pathways to all the neurons of the output layer.

The output-layer neurons accumulate the inputs transmitted by the hidden layer neurons and produce the network outputs. In general, the number of the neurons in the output layer depends on the number of outputs that the network is required to produce each time an input array is presented to the network. In the network chosen for the **GFMFS** package, the output layer consists of a single neuron, the output of which (after a suitable linear transformation yet to be defined) corresponds to the single overall output from the network (i.e. to the combined discharge forecast of the **NNM**).

For a neuron either in the hidden or in the output layer, received inputs are transformed to an output y_{out} by a mathematical transfer function of the form

$$y_{out} = f(\sum_{i=1}^{M} w_i y_i + w_0) \qquad \text{(A.33)}$$

where f () denotes the transfer function of the neuron, w_i is the input connection pathway weight, y_i is the input to the neuron, M is the total number of inputs which usually equals the number of neurons in the preceding layer, and w_o is the neuron threshold, i.e. a base-line value independent of the input.

The various weights w_i of the connection pathways between neurons and the thresholds w_o of the different neurons can be perceived as the parameters of the chosen network.

The transfer function of the neurons in the hidden and in the output layers of neural networks is usually a non-linear function. One of most widely used transfer functions, chosen also for the **GFMFS** package, is the logistic function) given by

$$f(\sum_{i=1}^{M} w_i y_i + w_0) = \frac{1}{1+e^{-\sum_{i=1}^{M} w_i y_i + w_0}} \qquad \text{(A.34)}$$

The logistic function is bounded in the range [0, 1], which implies that the network output is likewise bounded in the same range. In the context of the use in the **GFMFS** package, in order to facilitate the comparison between the actual observed discharges and the network estimated outputs, the following equation

$$Q_{si} = 0.1 + 0.75(Q_i/A_{max}) \qquad \text{(A.35)}$$

for which the Q_{si} series is bounded between 0.1 and 0.85, is adopted for rescaling the observed discharges for the purpose of calibration, where Q_{si} is the rescaled discharge

and Q_{max} is the maximum observed discharge of the calibration period. Thus, the linear transformation equation of the output of the neuron of the output layer to the combined overall network forecast is given by the inverse of preceding equation.

Graphic design: Communication Division, UiB / Print: Skipnes Kommunikasjon AS

uib.no

ISBN: 9788230860472 (print)
9788230863701 (PDF)